Max Planck Graduate Center

Johannes Gutenberg-Universität, Mainz

Proton Magnetic Resonance with Parahydrogen Induced Polarization:

Imaging Strategies and Continuous Generation

Dissertation zur Erlangung des Grades eines
„Doktor rerum naturalium“ der Fachbereiche:
08 - Physik, Mathematik und Informatik,
09 - Chemie, Pharmazie und Geowissenschaften,
10 - Biologie sowie
Universitätsmedizin

von Jan Falk Frederik Dechent

Mainz, den 17.12.2012

Dissertation im Rahmen des
Max Planck Graduate Center
Stipendiumsprogramm

unter der Betreung von

Abstract

A major challenge in imaging is the detection of small amounts of molecules of interest. In the case of magnetic resonance imaging (MRI) their signals are typically concealed by the large background signal of e.g. the tissue of the body. This problem can be tackled by hyperpolarization which increases the NMR signals up to several orders of magnitude. However, this strategy is limited for ^{1}H, the most widely used nucleus in NMR and MRI, because the enormous number of protons in the body screen the small amount of hyperpolarized ones.

Here, I describe a method giving rise to high ^{1}H MRI contrast for hyperpolarized molecules against a large background signal. The contrast is based on the J-coupling induced rephasing of the NMR signal of molecules hyperpolarized via parahydrogen induce polarization (PHIP) and it can easily be implemented in common pulse sequences.

Hyperpolarization methods typically require expensive technical equipment (e.g. lasers or microwaves) and most techniques work only in batch mode, thus the limited lifetime of the hyperpolarization is limiting its applications. Therefore, the second part of my thesis deals with the simple and efficient generation of an hyperpolarization.

These two achievements open up alternative opportunities to use the standard MRI nucleus ^{1}H for e.g. metabolic imaging in the future.

Nomenclature

ADC	Analog Digital Converter
ALTADENA	Adiabatic longitudinal Transport And Dissociation Engenders Nuclear Alignment
deFSE	dual echo time fast spin echo sequence
DNP	Dynamic Nuclear Polarization
FID	Free Induction Decay
GRE	Gradient Echo Sequence
hPHIP	hydrogenative PHIP (PASADENA or ALTADENA)
MRI	Magnetic Resonance Imaging
NMR	Nuclear Magnetic Resonance
PASADENA	Parahydrogen And Synthesis Allow Dramatic Enhancement of Nuclear Alignment
PHIP	ParaHydrogen Induced Polarization (hPHIP or SABRE)
RF	Radio Frequency
SABRE	Signal Amplification By Reversible Exchange
SE	Spin Echo sequence

Ingredients:
Hydrogen, Time

The Universal Label.[1]

Contents

Chapter 1

Introduction

Magnetic Resonance Imaging (MRI) is a non invasive method to obtain spatial information from within an object. Sir Peter Mansfield and Paul Lauterbur were awarded with the Nobel prize in medicine in 2003 "for their discoveries concerning magnetic resonance imaging".[2] Especially in health care this tool allows for diagnosis of diseases i.e. such as tumors.

Medical imaging comprises the fields of neurology, surgery and internal medicine (see figure 1.1 on the following page). In addition a variety of applications can be listed in biology, chemistry, physics or material sciences.

Modern Magnetic Resonance Imaging Scanners are not limited to the acquisition of static images. Sophisticated hardware and methods allow for the measurement of several images per second. Thus, dynamic measurements can be performed, such as tracking of a bolus of a contrast agent inside the body, representing a valuable tool for medical diagnosis. In many cases these contrast agents are required to improve the inherent contrast provided by the tissue itself.

Contrast Agents for improved diagnosis

Contrast agents are widely used in medical imaging to improve the contrast between healthy and pathological tissue. There are different classes of contrast agents such as positive ones which increase the MRI signal and negative contrast agents which decrease the signal compared to the situation without the contrast agents. Positive contrast agents are preferred, because they allow more reliable diagnosis. Paramagnetic materials such as Gadolinium shorten the T_1 time in their close surrounding. With proper concentration this shortening can be exploited to generate a positive contrast. If the concentration is increased not only T_1 but also T_2 is shortened leading to a negative MRI contrast. A different method of generating contrast is changing the nuclei, but here the sensitivity is

(a) Brain tumor [3] (b) Meniscus injury [4] (c) Liver tumors [5]

Figure 1.1: Magnetic Resonance Images from different medical applications: Diagnosis is based on evaluating a magnitude image from a complex-number data set.

even lower than for protons, thus this method is only used rarely in medical MRI.

However, all conventional contrast agents are limited in their efficiency by the available signal that can be generated from the thermal polarization level. Therefore the contrast always relies on a modification of inherent relaxation parameters such as T_1, T_2 or T_2^* or on the Boltzman polarization of the hetero nucleus.

Hyperpolarized contrast agents

Hyperpolarized contrast agents target a specific use: The observation of short processes where only a small signal is available in the thermally polarized case. For long processes or bigger signals convntional contrast agents in combination with averaging techniques are typically sufficient.

Thus, one way to increase the contrast between healthy and pathological tissue is the use of hyperpolarization in combination with hetero-nuclei imaging such as ^{13}C, ^{19}F or ^{15}N.[6–12] Here the low sensitivity of hetero nuclei is compensated by enhancing the signal by methods such as Dynamic Nuclear Polarization (DNP)[13,14] and Parahydrogen Induced Polarization (PHIP)[15–22].

In MR images, this methods allows a clear separation of the signal sources as presented by Mansson et al.[6]. Figure 1.2 on the next page presents a clear contrast between morphological thermally polarized proton image and the hyperpolarized ^{13}C features of interest, such as catheter tracking or heart perfusion.

Due to this excellent contrast mechanism, paired with long T_1 times (compared to proton relaxation times) and large chemical shift ranges, these hetero nuclei methods were investigated extensively in the last years. Interesting applications were developed, for instance, malignant tissue can be differentiated from healthy organs on the basis of different metabolic pathways within the citrate cycle. As a consequence, the NMR signal intensity of lactate after injection of hyperpolarized ^{13}C-pyruvate is significantly ele-

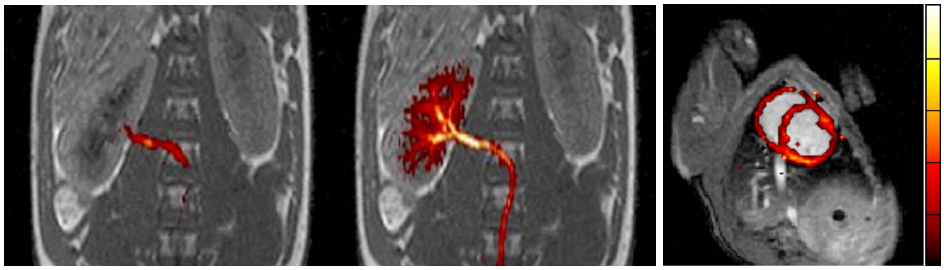

(a) Catheter tracking in a kidney (b) Myocardial perfusion

Figure 1.2: Hyperpolarized ^{13}C images (red) and morphological proton images (grayscale). The diagnostic relevant information can be extracted easily.[6]

vated in cancer when compared to normal tissue.[10,12,23] Recently, in vivo pH mapping after injection of hyperpolarized bicarbonate has been demonstrated for tumor visualization.[7]

All these advantages and developed methods allow hetero nuclei hyperpolarization to be favored over conventional proton MRI when short processes are to be observed.

Goals of this thesis

Nevertheless, hyperpolarized protons offer important advantages that make it worth working on the limits of this approach:

The PHIP hyperpolarization method has a huge advantage over other hyperpolarization methods: The most important technical equipment by far is a cryostat. By cooling hydrogen gas in the presence of a paramagnetic catalyst (e.g. charcoal), parahydrogen in excess of 90% compared to the ortho state can simply be generated. The conversion of parahydrogen into an exploitable hyperpolarization can happen in two ways either by a hydrogenation (hPHIP)[17] or by a reversible exchange (SABRE)[21]. Both methodologies simply require a mixing of a substrate, a catalyst and a solvent.

Proton imaging is the standard application of clinical MRI scanners, thus PHIP-imaging requires no additional hardware such as broadband amplifiers and additional hetero nuclei coils. Within a clinical environment a method relying on protons is much more likely to spread because of reduced costs and easier handling. Additionally new methods have been developed to prolong the T_1 with so called long lived singlet states.[24,25]

The work within my thesis will be centered around the question:

> Is it possible to perform proton MR-imaging experiments with PHIP hyperpolarized contrast agents, where a clear separation of ^1H background and ^1H contrast agent is possible and the hyperpolarization is available continuously and ready for application?

In order to answer these questions, different issues open up and have to be worked on:

If MR-imaging is performed on ^{1}H hyperpolarization generated by PHIP, imaging of antiphase signals is required. In case of hydrogenative PHIP these antiphase signals arise within the spectrum of the molecule whereas in SABRE experiments the whole spectrum is inverted by $180°$ compared to the thermal polarization. Despite the different features it is important to realize that hPHIP and SABRE can hyperpolarize different classes of molecules and therefore suppleemt each other. Their antiphase or phase relation characteristics have to be understood, to be able to find the optimal imaging sequence and optimal parameters for imaging. This will be dealt with in chapters 3.3 on page 35 and 3.4 on page 44.

Contrast agents have to allow for an unambiguously differentiation between areas with and without them. Since all images are acquired on the proton channel it might not be sufficient to rely on differences in signal strength only. Therefore a method exploiting the PHIP antiphase character for generating a contrast is presented. This will be presented in chapter 3.5 starting on page on page 51.

Continuous supply of the contrast agent will equip these methods with huge advantages compared to other methods. As stated before, hyperpolarization methods are preferred for the observation of short time processes, because typically other approaches (e.g. DNP) require significant built up times for the hyperpolarization. This results in the necessity to work in a batch mode providing only limited sample volumes. Continuous hyperpolarization will be dealt with in chapters 4 and 5 starting on page 57. This development will also help to overcome the limits due to short T_1 times by allowing to use averaging techniques.

Chapter 2

Basics of spin dynamics, hyperpolarization, MRI and signal enhancement

Contents

This chapter gibes a brief introduction to the basic knowledge needed to follow the scope of this thesis. All information presented in this chapter is extracted from the literature, and more detailed descriptions can be found in there.[26–30]

2.1 Spin Dynamics

2.1.1 Nulcear Magnetism

The intrinsic angular momentum of nuclei can be employed for NMR spectroscopy and imaging. The total spin angular momentum of a nucleus is determined by $\hbar\sqrt{I(I+1)}$:

$$I = 0, \frac{1}{2}, 1, \frac{3}{2}, \dots \tag{2.1}$$

The azimuthal quantum number may have the following values: $m_I = -I, -I+1, \dots, I-1, I$. In the absence of magnetic or electric fields this leads to a $2I+1$-fold degeneracy.

The source of signal for NMR is the magnetic moment that rises from the angular momentum. It is proportional to m_I and the gyromagnetic ratio γ, which is a unique constant for each isotope:

$$\mu = \hbar\gamma m_I \tag{2.2}$$

NMR spectroscopy makes use of the fact that this nuclear magnetic dipole interacts with the *local* magnetic field surrounding the nuclei, allowing for characterizing molecular structure and dynamics.

2.1.2 External magnetic Field

In the presence of a magnetic field B in z direction a splitting of the energy levels caused by the angular momentum occurs (Zeeman effect).

$$E = -\vec{\mu} \cdot B\hat{e}_z = -\hbar\gamma m_I B_{0z} = \pm\frac{1}{2}\hbar\gamma B_{0z} \qquad I = \frac{1}{2} \tag{2.3}$$

Due to the negative sign, the low energy state for a spin $\frac{1}{2}$ particle is given by $m_I = +\frac{1}{2}$ referring to the nuclear spin state that will be labeled by the notation $|\uparrow\rangle$ in the following. The high energy state is then given by $m_I = -\frac{1}{2}$ ($|\downarrow\rangle$).

$$\Delta E = \hbar\gamma B_0 = \hbar\omega \tag{2.4}$$

This energy splitting leads to the precession frequency $\omega = \gamma B_0$ and drives the equation of motion - the Schroedinger equation.

2.1.3 Schroedinger equation

The Schroedinger equation allows for a mathematical description of the equation of motion of a spin. Depending on the interaction different Hamilton operators are needed to include the effect in the calculations.

$$H\Psi = i\hbar\frac{d\Psi}{dt} \tag{2.5}$$

$$H_{\text{Zeeman}} = \sum_{i=1}^{N} \omega_i I_z^i \tag{2.6}$$

$$H_{\text{J}} = \sum_{i\neq j} \pi J_{ij}(2I_x^i I_x^j + 2I_y^i I_y^j + I_z^i I_z^j) \tag{2.7}$$

$$H_{\text{Rf}} = \gamma B_1 \sum_{i=1}^{N} \left(\cos(\phi) I_x^i + \sin(\phi) I_y^i\right) \tag{2.8}$$

The Zeeman interaction term describes the previously introduced interaction with an external magnetic field. H_{J} describes the coupling of the nuclear spin with electrons in the surrounding. The orientation of the spins can be manipulated by (oscillating) magnetic field orthogonal to the field causing the Zeeman interaction. This interaction is described by H_{Rf}. The dipolar coupling interaction is neglected because all experiments are performed in a fluids that are additionally heated or moving fast.

2.1.4 Macroscopic Magnetization

If a large number of spins is brought into a magnetic field ($B \cdot \hat{e}_z$) they start precessing around the z-axis initially without showing any preferred direction. After a the time constant ($5 \cdot T_1$) a thermal equilibrium is established due the Zeeman interaction. When measuring the difference in the populations of the states $|\uparrow\rangle$ and $|\downarrow\rangle$, which are $|\uparrow\rangle$ and $|\downarrow\rangle$ respectively the following equilibrium holds:

$$\frac{n_\uparrow}{n_\downarrow} = \exp\left(-\frac{\Delta E}{kT}\right) \approx 10^{-5} \tag{2.9}$$

This population differnce is very small, allowing only a a faction of the spins to contribute to the macroscopic magnetization. In medical imaging (e.g. 7 Tesla) the temperature is fixed to physiological values and the macroscopic magnetization results in

$$\vec{M}_0 \approx \rho \frac{(\hbar\gamma)^2 \cdot I(I+1)}{3kT} \cdot \vec{B}_0 = 3 \cdot 10^{-3}\,{}^{\mathrm{A}}/_{\mathrm{m}} \cdot \hat{e}_z \qquad \text{with } kT >> \hbar\gamma B_0$$

2.1.5 Equations of motion and NMR signal

The equations of motion result either from the Schrodinger equation or can be derived using a classical approach. Here, the Bloch equation for an ensemble of non-interacting spins is presented, neglecting, however, J-coupling between them.

$$\frac{d\vec{M}}{dt} = \underbrace{\vec{M} \times \gamma(B_0 \cdot \hat{e}_z + \vec{B}_1(t))}_{\text{precession + rf. pulses}} \underbrace{-\frac{\vec{M} \cdot (\hat{e}_x + \hat{e}_y)}{T_2}}_{\text{transv. relax.}} \underbrace{-\frac{\vec{M} \cdot \hat{e}_z}{T_1}}_{\text{long. relax.}} \tag{2.10}$$

With the help of B_1 the magnetization M_{0z} can be rotated away from the z-axis and it will start precessing with the Larmor frequency ω. Due to this precession the magnetic moment can be detected by the voltage it will induce in an appropriately oriented coil. This allows for acquisition of an FID. If an additional magnetic field gradient is applied, the detected frequency will differ from the Lamor frequency allowing for spatial encoding

.

2.2 Hyperpolarization Methods

The small difference in population of the two energy states $n_\uparrow$ and $n_\downarrow$ is the reason for exploring techniques to artificially enhance the polarization in order to gain more signal.

In this thesis hyperpolarization is generated by exploiting the spin order or parahydrogen. This spin order is transformed into a hyperpolarization on molecules by two different methods and can lead to a signal enhancement of up to 10^5.

2.2.1 Hydrogen and its isomeric forms

The hydrogen molecule is a system with two nuclear spin $\frac{1}{2}$ particles. The wave function of the hydrogen molecule must therefore be antisymmetric under the exchange of the nuclear spins (fermions).

$$\Psi_{\text{tot}}(A,B) = -\Psi_{\text{tot}}(B,A) \tag{2.11}$$

For hydrogen the total wavefunctin can be written as

$$\Psi\text{tot} = \underbrace{\psi_{\text{trans}}\psi_{\text{elec}}\psi_{\text{vib}}}_{\text{symmetric}} \cdot \underbrace{\psi_{\text{rot}}\psi_{\text{nuc.spin}}}_{\text{either way}} \tag{2.12}$$

This requires an adequate basis for the nuclear spin $\psi_{\text{nuc.spin}}$ that can be either symmetric or antisymmetric, depending on the rotational wave function:

$$|S_0\rangle_{\uparrow,\downarrow} = -|S_0\rangle_{\downarrow,\uparrow} \quad = \frac{1}{2}\left(|\uparrow\downarrow\rangle - |\downarrow\uparrow\rangle\right) \tag{2.13}$$

$$|T_0\rangle_{\uparrow,\downarrow} = +|T_0\rangle_{\downarrow,\uparrow} \quad = \frac{1}{2}\left(|\uparrow\downarrow\rangle + |\downarrow\uparrow\rangle\right) \tag{2.14}$$

$$|T_{+1}\rangle_{\uparrow,\downarrow} = +|T_{+1}\rangle_{\downarrow,\uparrow} = |\uparrow\uparrow\rangle \tag{2.15}$$

$$|T_{-1}\rangle_{\uparrow,\downarrow} = +|T_{-1}\rangle_{\downarrow,\uparrow} = |\downarrow\downarrow\rangle \tag{2.16}$$

$$\tag{2.17}$$

This allows for four different conformations of the spin system hydrogen. There are three conformations caractereized by the total spin $I = 1$ and the three states $m = -1, 0, 1$ (T_{-1}, T_0, T_{+1}), which are called orthohydrogen. The conformations with $I = 0$ (S) is called parahydrogen. These different conformations arise depending on the rotational state of the molecule.

The thermal equilibrium at room temperature leads to equally populated states: 75% orthohydrogen (consisting of tree sub states) and 25% parahydrogen (one state). When cooling hydrogen, the thermal equilibrium is shifted towards parahydrogen and under the precence of active char coal the spin transition $S \leftrightarrow T$ is possible. The cooling

process drains energy from the rotational states, forcing the molecules to populate the (symmetric) rotational ground state. This forces the nuclear spin wave function to be antisymmetric (parahydrogen). A enrichment of up to 95% parahydrogen can be acieved at $30\,\mathrm{K}$. When heating up to room temperature again, under absence of the active charcoal, the hydrogen can not relax back into the thermal equlibium at this temperature.

The manipulation of the rotational states is much easier than manipulating the nuclear spins directly. For a direct nuclear spin flip, temperatures down to mK would be required, while the rotational states can be manipulated with much higher temperatures (see figure 2.1).

When expressing hydrogen in the language of spin operators the following density matrix results:

$$\rho_{\mathrm{H}_2} = \frac{\mathbf{1}_4}{4} + \frac{1 - 4 \cdot [\%pH_2]}{3} \mathbf{I}_1 \mathbf{I}_2 \tag{2.18}$$

$$\rho_{\mathrm{pH}_2} = \frac{\mathbf{1}_4}{4} - \mathbf{I}_1 \mathbf{I}_2 \tag{2.19}$$

This 95% enriched parahydrogen is a system heavily out of equilibrium (at room temperature) and PHIP offers a possibilty to take advantage of this by separating the two protons. When these two protons don't form a $I = 0$ system anymore, it is possible to generate a hyperpolarization that is detectable by NMR experiments, before they can relax back to thermal equilibrium.

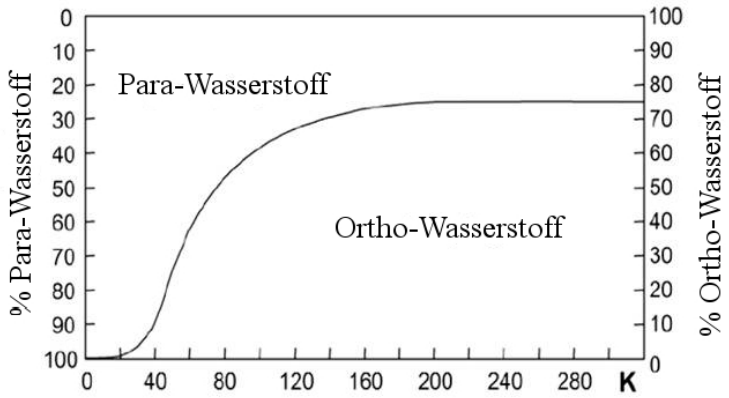

Figure 2.1: Thermal equilibrium of hydrogen as a function of temperature. At the temperature of liquid nitrogen 50% parahydrogen can be reached. At a temperature of $30K$ an enrichment up to 95% is possible.

2.2.2 Hydrogenative Parahydrogen Induced Polarization

Hydrogenative Parahydrogen Induced Polarization (hPHIP) was the first method to be discovered for producing a hyperpolarization originating from parahydrogen. Therefore

it is often only referred to as Parahydrogen Induced Polarization (PHIP). But meanwhile other method have been discovered (see next section), therefore it is important to clarify which kind of PHIP method is used.

hPHIP is based on a chemical reaction that hydrogenates both spins of the parahydrogen simultaneously into a molecule. It is important to transfer both protons at the same time, because otherwise the antiparallel orientation will not be preserved and the feature of hyperpolarization will be lost. After the transfer additional energy levels become accessible, but only those are populated, in which the spin conformation is antiparallel.

As an example consider an AX spin system in thermal equilibrium. The four energy levels $\uparrow\uparrow$, $\uparrow\downarrow$, $\downarrow\uparrow$, $\downarrow\downarrow$ are almost equally populated. Only small differences are present due to the Boltzmann polarization (see figure 2.2(a)).

PASADENA

When a reaction with parahydrogen is performed at high magnetic field, the energy diagram is populated according to to figure 2.2(b). This type of reaction is called a PASADENA (Parahydrogen And Synthesis Allow Dramatic Enhancement of Nuclear Alignment) hPHIP experiment. During the reaction the symmetry of parahydrogen is broken and sudden transition from a strongly coupled A_2 system into a weakly coupled AX spin system occurs. This sudden transition preserves the spin orientation and both antiparallel energy levels are populated. The resulting density matrix for PASADENA is then given by:

$$\rho_{\text{PASADENA}} = \frac{\mathbf{1}_4}{4} - \mathbf{I}_{1z}\mathbf{I}_{2z} \tag{2.20}$$

This density matrix is the same as for parahydrogen except the $\mathbf{I}_{1x}\mathbf{I}_{2x}$ and $\mathbf{I}_{1y}\mathbf{I}_{2y}$ coherences. This is a result of the chemical reaction that takes place a different time for each individual molecule. All these coherences overlap with slightly different phases canceling out each other.

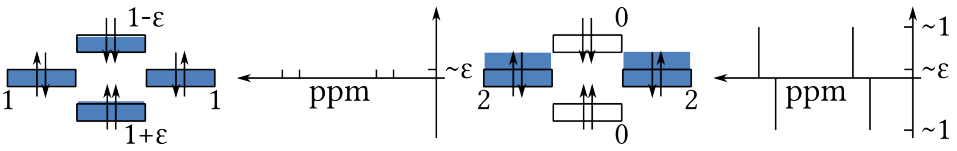

(a) Thermal equilibrium polarization: All energy levels are populated. The NMR signal arises from the small population differences described by the Boltzmann factor.

(b) Hyperpolarized: The spin system is out of thermal equilibrium, only antiparallel levels are populated.

Figure 2.2: Energy level diagram of a AX spin system. ϵ indicates the Boltzmann polarization level that gives rise to the thermal signal.

ALTADENA

A different experiment called ALTADENA (Adiabatic longitudinal Transport And Dissociation Engenders Nuclear Alignment) hPHIP can be performed by a reaction starting in low field. The protons are strongly coupled there and by an adiabatic transport to high field the system can adapt during the transport. By doing so, only the antiparallel energy level with the lower energy is populated. This leads to a different spectrum where only the outer peaks remain: Two antiphase peaks separated by the chemical shift are present.

The density operator after a ALTADENA experiment is given by:

$$\rho_{\text{ALTADENA}} = \frac{\mathbf{1}_4}{4} + \frac{1}{2}\left(\pm\mathbf{I}_{1z} \mp \mathbf{I}_{2z} - 2\mathbf{I}_{1z}\mathbf{I}_{2z}\right) \tag{2.21}$$

Features of hyperpolarization

It is important to understand the effect of radio frequency pulses on such a density operators. When considering a PASADENA experiment and a pulse of angle α the following density operator arises:

$$\rho = \cos^2(\alpha)\mathbf{I}_{1z}\mathbf{I}_{2z} + \sin(\alpha)\cos(\alpha)(\mathbf{I}_{1x}\mathbf{I}_{2z} + \mathbf{I}_{1z}\mathbf{I}_{2x}) + \sin^2(\alpha)\mathbf{I}_{1x}\mathbf{I}_{2x} \tag{2.22}$$

$$\rho = \begin{cases} \frac{1}{2}\left(\mathbf{I}_{1z}\mathbf{I}_{2z} + (\mathbf{I}_{1x}\mathbf{I}_{2z} + \mathbf{I}_{1z}\mathbf{I}_{2x}) + \mathbf{I}_{1x}\mathbf{I}_{2x}\right) & \vee\alpha = 45^\circ \\ \mathbf{I}_{1x}\mathbf{I}_{2x} & \vee\alpha = 90^\circ \\ \mathbf{I}_{1z}\mathbf{I}_{2z} & \vee\alpha = 180^\circ \end{cases} \tag{2.23}$$

The 45° pulse generates the best transversal magnetization when looking at single quantum terms. The 90° pulse generates a pure double quantum operator, and a 180° degree pulse has no effect on the magnetization at all.

The detectable transversal magnetization $\mathbf{I}_{1x}\mathbf{I}_{2z} + \mathbf{I}_{1z}\mathbf{I}_{2x}$ evolves under the chemical shift difference Ω and J coupling:

$$|M(t)| = \frac{1}{2}\left|\cos\left(\frac{t\Omega}{2}\right)\sin(J\pi t)\right| \tag{2.24}$$

The transversal magnetization at $t = 0$ is zero - or better to say in antiphase orientation and therefore not detectable. The time evolution of the J coupling cna then give rise to the observable magnetization. The chemical shift oscillations lie within this shape. By inserting this magnetization in formula 2.37 on page 14 the effects on MRI images can be predicted.[31]

The reaction is typically done in complex molecules, which adds extra complexity. The magnetization can be transferred to other spins via J coupling, which can lead to a hyperpolarization of the whole molecule - if the conditions match.

Sensitivity enhancement

The maximum sensitivity enhancement that can be reached if all the hydrogenations occur instantaneously. Then the fractions of available hyperpolarization towards thermal polarization are compared. First the density matrices are needed for the comparison:

$$\rho_{\text{th}} = \frac{\mathbf{1}_4}{4} - \frac{\epsilon}{2}(\mathbf{I}_{1z} + \mathbf{I}_{2z}) \qquad \text{with } \epsilon = \frac{\gamma\hbar B_0}{kT} \qquad \xrightarrow{\alpha=90^\circ} \tag{2.25}$$

$$\rho_{\text{th}}(t) = \cos(\pi J_{12} t)(\mathbf{I}_{1x} + \mathbf{I}_{2x}) \cdot \frac{\epsilon}{2} \tag{2.26}$$

$$\rho_{\text{PASADENA}}(t) = \sin(\pi J_{12} t)(\mathbf{I}_{1y} + \mathbf{I}_{2y}) \cdot \frac{1 - 4[\%pH_2]}{12} \tag{2.27}$$

$$\text{Enhancement} = \frac{\frac{1-4[\%pH_2]}{12}}{\frac{\epsilon}{2}} \tag{2.28}$$

$$= \frac{kT(1 - 4[\%pH_2])}{6\gamma\hbar B_0} \tag{2.29}$$

The enhancement depends on the enrichment of parahydrogen as well as the thermal equlibrium polarization. If exactly the same experiment is performed at different magnetic field strengths, different enhancement factors will be obtained even though the performance of the hyperpolarization did not change. Experiments in this thesis are performed at 1.5 Tesla allowing for the theoretical enhancements as depicted in figure 2.3. If the reaction is carried out with 25% parahydrogen theoretically no enhancemnt is observable, because the inserted spins orientations populate all energy levels equally. The experimental evaluation of enhancement factors can tricky (see 2.4.3 on page 20).

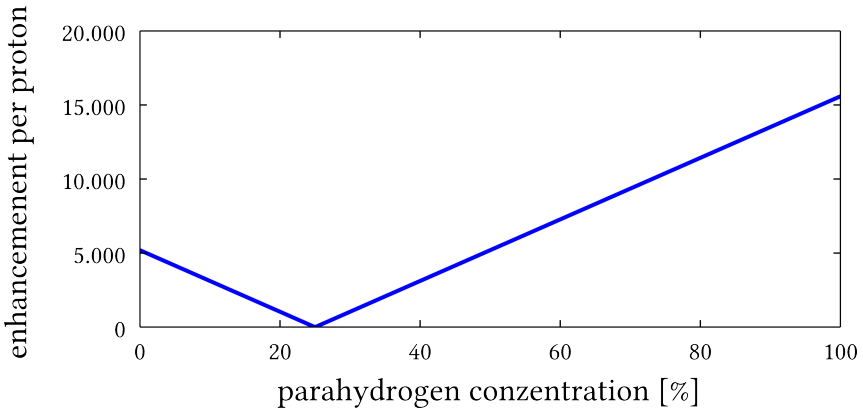

Figure 2.3: Maximum theoretical enhancement per proton at 1.5 Tesla as a function of the parahydrogen concentration. At a concentration of $90\,\%$ a enhancement of up to 14.000 can be achieved.

2.2.3 Signal Amplification By Reversible Exchange

Signal Amplification By Reversible Exchange (SABRE) exploits parahydrogen in a different way.[21] A catalyst is used to transfer the spin order onto a molecule without completing the hydrogenation. The target molecule is not consumed by the reaction and therefore the same molecule can be hyperpolarized over and over again.

The transfer of the spin order onto the substrate happens though a metal based catalyst - in this case an iridium catalyst is used. When both the parahydrogen (I and S) and the target protons T and R (substrate) are connected to the catalyst, a complex four spin system forms (see figure 2.4). A first theory model has been developed by Adams et al.[32] that allows for a first understanding of the process. Depending on the field strength (four chemical shift values) and the six J coupling constants, a certain amount of this spin order is transferred onto the substrate resulting in a hyperpolarization of the substrate.

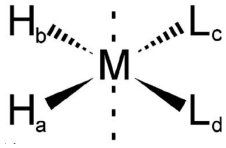

Figure 2.4: Spin system at the center of the catalyst. Parahydrogen (labeled as I and S for the calculations) are in contact with the metallic center M - as well as the two substrates ligands (labeled as T and R).[32]

At this center a initial density operator, consisting of the parahydrogen and the two ligands forms at low field, where their thermal polarization is omitted:

$$\rho_{\text{initial}} = \underbrace{\frac{1}{8}\begin{pmatrix} 0 & 0 & 0 & 0 \\ 0 & 1 & -1 & 0 \\ 0 & -1 & 1 & 0 \\ 0 & 0 & 0 & 0 \end{pmatrix}}_{\mathbf{I}_1 \cdot \mathbf{I}_2} \otimes \underbrace{\begin{pmatrix} 1 & 0 \\ 0 & 1 \end{pmatrix}}_{\text{for T}} \otimes \underbrace{\begin{pmatrix} 1 & 0 \\ 0 & 1 \end{pmatrix}}_{\text{for } R} \tag{2.30}$$

This initial state will evolve under the Hamiltonian operators for this four spin system:

$$\rho(t) = \exp(-iHt)\rho_{\text{initial}} \exp(+iHt) \tag{2.31}$$

The transfer depends critically on the lifetime of the temporary complex of parahydrogen and the substrates. Adams et al.[32] evaluated these terms and showed that after the lifetime of the complex the following density operator forms:

$$\rho = a_{ZZ}(2\mathbf{R}_z\mathbf{T}_z) + a_{ZQ_x}(2\mathbf{R}_x\mathbf{T}_x + 2\mathbf{R}_y\mathbf{T}_y) + a_Z(\mathbf{R}_z - \mathbf{T}_z) \tag{2.32}$$

During the transport of the sample into the spectrometer, the magnetic field strength increases continuously and chemical shift evolution is increased. Inside the spectrometer the system will be weakly coupled and the zero-quantum terms will average out. This leads to the formation of a time averaged density operator:

$$\bar{\rho} = a_{ZZ}(2\mathbf{R}_z\mathbf{T}_z) + a_Z(\mathbf{R}_z - \mathbf{T}_z) \tag{2.33}$$

The amplitudes of the factors a_{ZZ}, a_{ZQ_x} and a_Z are strongly dependent on the scalar coupling constants J and precession frequency differences in the four-spin system of the model complex. Additionally, due to the field dependency of the precession frequencies, polarization transfer rates and signal enhancements strongly depend on the field strength during the polarization step.

This model helps understanding the SABRE process but still the ligands are treated as one single spin. For a understanding of the complete picture, much more complex simulations have to be done, including all the interactions constants.

2.3 Magnetic Resonance Imaging

Magnetic Resonance Imaging relies on the encoding of spatial information by applying magnetic field gradients. These gradients are used to spatially change the resonance condition $\omega(\vec{x}) = -\gamma(B_{0z} + \vec{G} \cdot \vec{x})$. Usually, a frequency encoding gradient of strength G_x and length t is applied together with a phase encoding gradient (G_y, t_p), which is orthogonal to the frequency encoder. By variation of these gradients, the object with a spin density of ϱ (in protons per volume, and therefore magnetization M) is encoded into the frequency domain:

$$\tilde{I}(t, G_y) = \iint M(x, y) \cdot \exp(-i(\gamma G_x x t + \gamma G_y y t_p))dx\, dy \tag{2.34}$$

$$\tilde{I}(k_x, k_y) = \iint M(x, y) \cdot \exp(-i(k_x x + k_y y))dx\, dy \tag{2.35}$$

$$\text{with} \quad k_x = \gamma G_x t \quad \text{und} \quad k_y = \gamma G_y t_p \tag{2.36}$$

When spins with different chemical shifts and J coupling are involved the magnetization M will show oscillations over time because of the different frequencies involved.

$$\tilde{I}(t, G_y) = \iint M(x, y, t) \cdot \exp(-i(\gamma G_x x t + \gamma G_y y t_p))dx\, dy \tag{2.37}$$

Now two options arise: A very short time might be chosen for the frequency encoding time t. If this time is smaller than the shortest period in $M(t)$ the different frequencies can not be separated and the geometry of the phantom is preserved. The second option

is to increase t until a full period of the oscillation can be recorded. These additional oscillations separate the peaks in the image and for each peak in the spectrum a separate object appears. Therefore the inverse of time t is also referred to as the bandwidth per pixel, because it indicates which frequency range can be mapped onto one point. In clinical MRI this effect typically arises when water and fat are present and can lead to shifts between the water and the fat image.

2.3.1 Image reconstruction

When performing imaging experiments on hyperpolarized compounds an additional problem arises. The hyperpolarized compound will be subject to both T_1 relaxation and radio frequency pulses that diminish the available hyperpolarization exponentially. Eventually, the system will relay back to thermal equilibrium. Therefore, when hyperpolarization is present, it has to be controlled carefully, otherwise severe imaging artifacts can arise.

In MRI the image is reconstructed by a (inverse) 2D Fourier transform from the frequency domain (kSpace) into the image domain:

$$I(x, y) = \text{FFT}\left(\tilde{I}(k_x, k_y)\right) \tag{2.38}$$

2.3.2 Point spread function (PSF)

If the underlying transversal magnetization is not stable, distortions in the image will emerge. For example, if the transversal magnetization in phase encoding direction is not constant but is modulated by the function f(k_y) the image will be distorted in the following way:

$$I'(x, y) = \text{FFT}\left(\tilde{I}(k_x, k_y) \cdot \text{f}(k_y)\right) \tag{2.39}$$

$$= \text{FFT}\left(\tilde{I}(k_x, k_y)\right) * \text{FFT}\left(\text{k}(k_y)\right) \tag{2.40}$$

$$= I(x, y) * \text{FFT}\left(\text{k}\right) \tag{2.41}$$

The Fourier transform of the distortion ($f(k_y)$) is convoluted with the image. E.g. when the distortion has a Gaussian shape, each point of the image will be blurred in phase encoding direction with a Gaussian filter. When no distortion exists ($f(k_y) = 1$), then the Fourier transform of it will result in a Dirac delta function. In this case, each point is mapped exactly on its location. This leads to the introduction of the Point Spread Function PSF $= \text{FFT}\left(f(k_y)\right)$ that describes how a point in the original image is mapped in the resulting image.

The decrease of usable (longitudinal) magnetization due to radio frequency pulses

and T_1 can be incorporated in one formula where n is the line number of the kSpace lines that is acquired.

$$M(n) = M_0 \cdot \exp\left(-\frac{(n-1)\cdot \mathrm{TR}}{T_1}\right) \cdot \cos(\alpha)^{n-1} \tag{2.42}$$

$$= M_0 \cdot \exp\left((n-1)\cdot\left(-\frac{\mathrm{TR}}{T_1} + \ln(\cos\alpha)\right)\right) \tag{2.43}$$

$$= M_0 \cdot \exp\left((n-1)\cdot R\right) \tag{2.44}$$

The PSF of this exponential decay is a Lorentz distribution. Therefore the intensity of one point is spread along the phase encoding direction following the Lorentz distribution with a half-width at half-maximum (HWHM) of R. E.g. if relaxation is neglected and a very high flip angle is chosen, R becomes very big. In such a case the image will show a white stripe along the phase encoding direction because the each pixel is smeared along this direction. In figure 2.5 this is depicted, where the left image is undistorted and the right image shows the smearing in the horizontal direction.

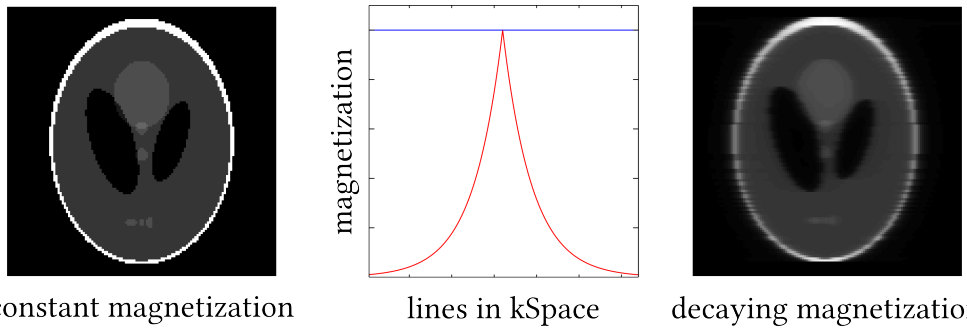

Figure 2.5: Example for strong kSpace weighting along the horizontal direction. When no weighting is present (blue), the kSpace is sampled with uniform magnetization along the horizontal direction and the image is presented without artifacts (left image). If a strong weighting is present (red), strong smearing along the horizontal direction is observed along with a reduction of image quality (right image).

2.3.3 Image evaluation and Signal-To-Noise (SNR)

The pixel values of the images in this thesis are presented as Signal to Noise Ratio (SNR). This allows a direct representation of the image quality, but it should be kept in mind that a image distorted by massive artifacts can still show very high SNR values. For the calculation of the SNR, each pixel of the magnitude image (I) is divided by the mean value of noise(N). Therefore a region of interest (ROI) in each image has to be chosen such that it covers as many pixels as possible, while only noise contributes to this region. In this

thesis regions in the corer of the images were chosen, preventing a contribution from artifacts from the centered phantom. A correction factor of $\sqrt{\frac{2}{\pi}}$ is needed to account for the Rayleigh distribution of the noise after calculating the magnitude image.

$$N = \sqrt{\frac{2}{\pi}} \cdot \frac{\sum_{x,y \in \text{ROI}} I(x,y)}{\sum_{x,y \in \text{ROI}} 1} \tag{2.45}$$

$$\text{SNR}(x,y) = \frac{I(x,y)}{N} \tag{2.46}$$

Especially when dealing with a hyperpolarization the calculation of the SNR has to be done carefully. Typically the signal high and so the receiver gain has to smaller to avoid a clipping of the signal. In such a scenario the noise values might only be mapped onto a small range of values and digitization errors can occur. This can be checked by calculating a histogram of the values in the noise region. If the histogram does not show a Rayleigh distribution no meaningful SNR can be calculated. Within this thesis all noise ROIs were checked and therefore the representation in SNR units is given.

2.3.4 Gradient echo sequence (GRE)

The gradient echo sequence or GRE sequence uses a small flip angle (α) to tip a small amount of magnetization into the transversal plane. The basic elements of a GRE sequence (figure 2.6 on the following page) are the slice selective excitation (RF and G_z) and the encoding in the first spatial direction via a phase encoding gradient (G_y). The frequency encoding gradient simultaneously encodes this spatial direction and generates the echo.

2.3.5 Spin echo sequence (SE)

The spin echo sequence uses a $180°$ inversion pulse at time ($\frac{\text{TE}}{2}$) that inverts the rotation of the magnetization in the transversal plane, thus refocusing the T_2^* relaxation. This leads to signal rise at the echo time TE and this signal is now subjected to the T_2 relaxation.

2.3.6 Dual echo time fast spin echo sequence (deFSE)

The Dual Echo time Fast Spin Echo sequence (deFSE) is a spin echo sequence where one excitation pulse is followed by a train of refocusing pulses. Two echo times are used where the first echo time describes the occurrence of the first echo after the excitation pulse. The second echo time describes the timing within the echo train. The reason for this timing can be understood when looking at spin system with J coupling: The refocusing pulses only affect the chemical shift differences but not the J coupling. So

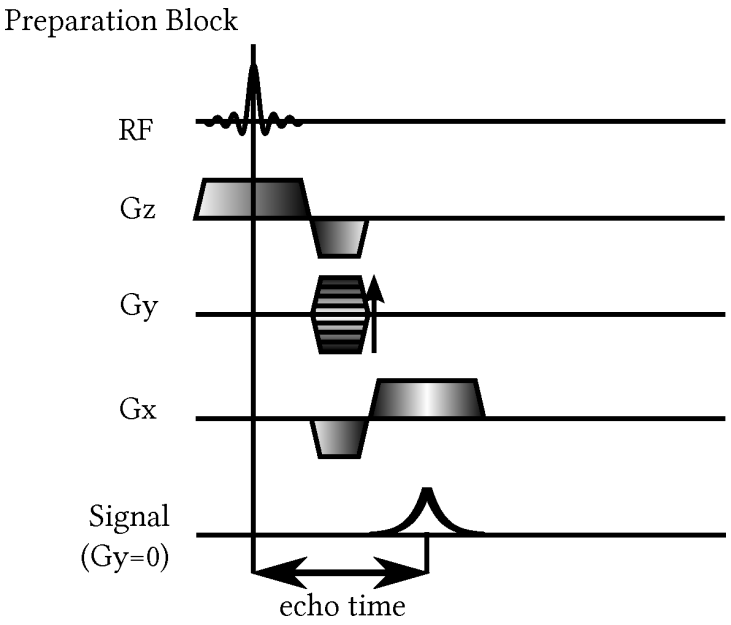

Figure 2.6: Pulse diagram for a GRE sequence. The preparation block contains the excitation by a soft radio frequency pulse (RF) combined with a slice selective magnetic field gradient (G_z) as well as the phase encoding gradient (G_y). The readout gradient (G_x) can be moved in order to increase or decrease the echo time. The color inside the gradient area indicates the amount of dephasing in this direction, where white means no dephasing.

when generating a spin echo train one can monitor the pure evolution due to J coupling. But when the time evolution due to J coupling is not wanted any more one can decrease the echo time in the train and thereby eliminate this time evolution (see Stables et al. [33]). This results in the two echo times, where the first one allows a time evolution of the J coupling and the second one where a signal without J modulation can be recorded.

2.4 Data analysis and image reconstruction

After the experiment are performed a chain of post processing steps is necessary before images and signal plots can be presented. These methods shall be presented in this section. It is followed by the calculation of enhancement factors, that are necessary to assess how good the performance of the hyperpolarization was.

2.4.1 Reconstruction algorithm for MR images

Within this thesis all images are acquired from the raw data that can be exported from the scanner prior to the vendors image reconstruction algorithms. This step is necessary, because the MRI internal algorithms maps the pixel intensities onto 4096 gray values.

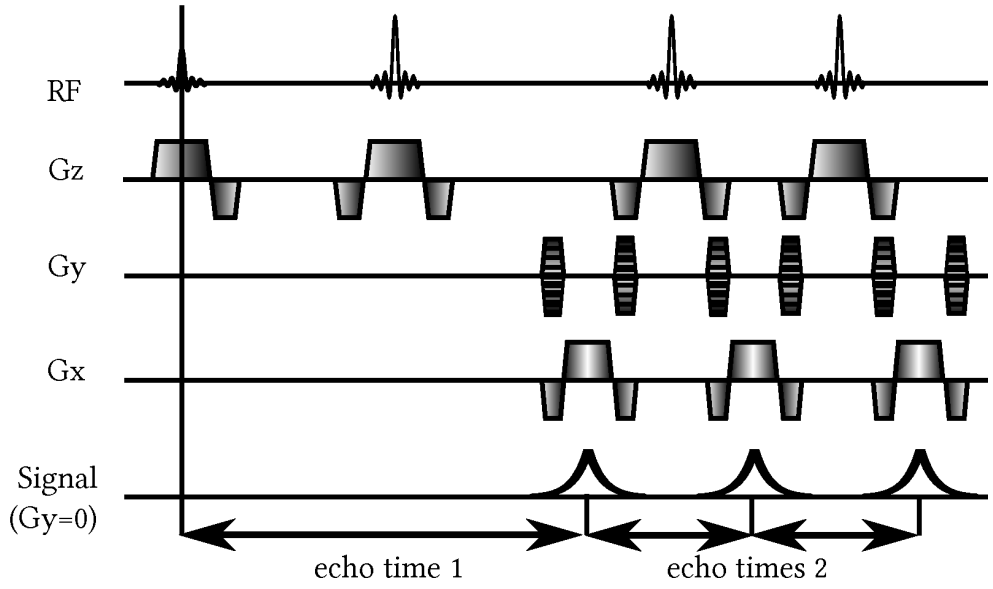

Figure 2.7: Pulse diagram for a deFSE sequence. Echo time 1 (TE_1) is used for the first echo and TE_2 for the timing of the echo train (details see Appendix 7.4 on page 101).

This upper limit is chosen because the human eye can not resolve more gray value steps. But when dealing with hyperpolarization the whole possible range of values has to be exploited for popper analysis.

The values retrieved from the scanner have to checked for popper receiver gain, otherwise signal can get clipped (then the signal intensities exceed the maximal number that can be recorded by the ADC) and then a comparison of signal is not possible anymore. The receiver gain at the clinical MRI was set to "low" in order to assure no clipping of the signal even when dealing with very high hyperpolarization.

Then a 2D Gaussian filter with a FWHM of half of the number of pixels in each direction was applied to the kSpace $\tilde{I}$. This assures low signal intensities for high values of k_x and k_y. Improving the image quality because no sharp rises of the signal occur at the borders of the kSpace.

Additionally the array size of the kSpace $\tilde{I}$ is doubled and filled with zeros, thus adding higher frequencies with zero amplitude to it ("zero filling of factor 2"). The resulting image - after the 2D Fourier transformation has been performed - has twice the resolution, presenting a smoother image I. This technique should not be used extensively (bigger filling factors) because otherwise a viewer can get false impression of the phantoms geometry and the image quality - especially when using simple phantom geometries.

The color bar of the resulting image I is presented in SNR (see 2.3.3 on page 16).

2.4.2 Extraction of signal intensities from images

A region of interest (ROI) is carefully selected in the images and the mean value of the signals (not the SNR) inside this ROI is calculated. The standard deviation serves as error. When dealing with thermally polarized signals all these values can be compared with in one experiment. In contrast, the hyperpolarization can have different initial signal strength: It originates from a chemical reaction that is manually driven by shaking. So before comparing these signals a correction factor must be calculated. Therefore a FID (see section 2.1.5 on page 7) with small flip angle is recorded prior to each imaging experiment (see 2.4.6 on page 24). The values extracted form the ROI is then divided by this correction factor.

2.4.3 Enhancement factors for hPHIP

In section 2.2.2 on page 12 the theoretical enhancement was calculated by comparing the density operators. In a real experiments several obstacles are present which hinder an optimal calculation of the experimental enhancement.

Shim The antiphase character of hPHIP signal can be concealed by bad shimming conditions. For example the antiphase signal from PASADENA experiments are typically separated by 7 to 14 Hz in a clinical scanner at $1.5\,\mathrm{T} \approx 63\,\mathrm{MHz}$ these signals can not be separated completely. This leads to partial cancellations of the signal.

Chemical reaction The precursor is never hydrogenated completely in one experiment. Hence, in order to regain the enhancement per proton the reaction rate has to be included in the calculation. However, this is difficult depending on the type of experiment performed.

Therefore, different measures of the enhancement are considered:

Signal gain

The "signal gain" (G) is the simplest number that can be calculated. It reflects how much more signal is added to the whole system by the hyperpolarization or hydrogenation. E.g. when a sample is completely hydrogenated the thermal reference will show a higher signal gain because of the additional protons. The measure H is a integral over the real part of a spectrum. The measure T is a integral over the real part too, but here a thermally polarized reference spectra prior to the experiment is used.

$$\mathrm{H} = \int \|\Re\left(\text{spectra}\right)\| \qquad \mathrm{T} = \int \|\Re\left(\text{th. ref.}\right)\| \tag{2.47}$$

$$\mathrm{G} = \frac{\mathrm{H}}{\mathrm{T}} = \begin{cases} = 1 & \text{no signal gain} \\ \approx \frac{\#\text{precursor protons}+2}{\#\text{precursor protons}} & \text{typically fully hydrogenated} \\ > \approx 1.25 & \text{signal gain due to hyperpolarization} \end{cases} \tag{2.48}$$

Since the reference T was acquired proir the experiments, the thermally polarized sampe after the experiments will show bigger signal gain due to the incorporated parahydrogen atoms.

Enhancement

The "enhancement" includes the amount of protons included in H and T. This if two different molecules have the same hyperpolarization performance but one has much more thermally polarized protons it's "signal gain" would be underestimated. Therefore E in-

cludes the number of participating protons.

$$\begin{aligned} \text{H'} &= \int_{\text{hp. area}} \|\Re\left(\text{spectra}\right)\| - \|\Re\left(\text{th. ref.}\right)\| \qquad \text{T'} = \int_{\text{th. area}} \|\Re\left(\text{th. ref.}\right)\| \\ \text{R} &= \frac{\text{\# thermal protons in th. area}}{2} \end{aligned} \tag{2.49}$$

$$\text{E} = \text{R} \cdot \frac{\text{H'}}{\text{T'}} = \begin{cases} = 0 & \text{Pure precursor} \\ 0 \leq E < 1 & \text{Little conversion, hyperpolarized or thermal} \\ = 1 & \text{Fully hydrogenated or hyperpolarized} \\ > 1 & \text{Enhancement due to hyperpolarization} \end{cases} \tag{2.50}$$

When two ”enhancements” are compared it will show, how much better the one or the other is. Additionally it is independent of the molecule involved. Nevertheless, it has the following drawbacks: When E is between 0 and 1 it dos not necessarily imply pure thermal polarization. The reaction can be so little that these value get generated. It is necessary to check for antiphase signal. Two different value of E can not be compared if the reaction conditions change during an experiment. This is especially true for hydrogenative PHIP and the hollow membrane fibers. The shaking experiments show almost the same reaction conditions per shake.

Enhancement per proton

The ”enhancement” assumes that 2 protons per molecule contribute to the hyperpolarization. This is equivalent to a full hydrogenation which was never seen in experiments. So the conversion rate has to be included.

$$\text{EpP} = \frac{\text{E}}{\text{conversion rate}} = \text{”Enhancement per proton”} \tag{2.51}$$

When two ”enhancements per proton” are compared it will show, how much better the one or the other is. This measure is independent of the molecule involved and it is independent of the rate of reaction. But the conversion rate has to be determined.

Closing remarks

Three measures (G, E, EpP) are introduced and they are not directly comparable among each other. There are some additional points that have to be considered for the calculation

of these numbers:

- The antiphase character of the signal can conceal polarization. This effect appears when the spectral shape of two antiphase peaks overlap. Theoretically it is possible to calculate the original peaks and to get the signal intensities separately. However, the loss due to the overlap of these antiphase signals is permanent and can not be exploited to get more signal.

- The thermal reference is typically small in signal and noisy compared to the hyperpolarized signal. This leads to a large error in enhancement factors but the error in the hyperpolarized signal can be very low. The second source of error is the division by the conversion rate this can lead to large errors too.

$$E = \frac{H'}{T'} \pm \left\| \frac{H'}{T'^2} \cdot \Delta T' \right\| \tag{2.52}$$

$$EpP = \frac{H'}{R \cdot T' \cdot \text{conversion rate}} \tag{2.53}$$

$$\pm \sqrt{\left(\frac{H'}{R \cdot c \cdot T'^2} \cdot \Delta T' \right)^2 + \left(\frac{H'}{R \cdot c^2 \cdot T'} \cdot \Delta c \right)^2} \tag{2.54}$$

- For the calculation of H' the subtraction can be neglected when the thermal spectra is small compared to the hyperpolarized signal and should be omitted when no thermal signal are in this area. The integration range can cover more that the two parahydrogen atoms. E.g when the polarization is transfered to another proton. Furthermore the spectra's should be phased correctly.

2.4.4 Enhancement factors for SABRE

The enhancement factors for SABRE are easier to calculat, because the thermal reference exists prior to the experiments. The enhancement can be calculated as the "enhancement per proton" with the conversion rate being equal to one. Additionally, antiphase signals due to J coupling are arising here, so that an integration can easily be performed. These integral values are then divided to retrieve the enhancement factors.

2.4.5 Enhancement, enhancement per proton and SNR of MR-images

In this thesis "enhancement" and "enhancement per proton" are given for spectroscopy data. The images are presented in signal to noise units (SNR) and if a thermally polarized image is compared to a hyperpolarized image a "SNR-enhancement" can be calculated.

These two numbers can almost never be compared directly! The main reason is that

images here are acquired such that all spectral peaks are mapped into one voxel.[1] In a complex spectra the single peaks are separated and the contribution of each peak can be measured and summed up. In the image, however, the data are acquired in time domain and no separation of the peaks due to theirs chemical shift or J coupling is realized.

2.4.6 Correction factors

Correction factors are necessary, when data from different shaking cycles are compared. Each time a different degree of hyperpolarization will be achieved and this must be corrected for. In images containing both thermal polarization and hyperpolarization this correction can not be applied, but in a separate plot showing the SNR from the two regions this effect can be corrected for.

$$\text{Correction factor} = \frac{\text{enhancement of this experiment}}{\text{average enhancement in all experiments}} \tag{2.55}$$

This scales the SNR values in the images as if in all experiments the same averaged hyperpolarization had been available.

[1] The other possibility is to spatially separate all peaks clearly. However, this results in long acquisition times (small bandwidth per pixel) and is not feasible when only small frequency differences are present and if T_2^* relaxation is not too fast.

Chapter 3

Imaging of Antiphase Hyperpolarization

Contents

In this chapter imaging strategies have been developed, which exploit the antiphase hyperpolarization - generated by hydrogenative PHIP - as a powerful contrast agent. The characteristic initial state evidenced as antiphase magnetization is not the ”usual” NMR initial state. This difference allows to exploit not only the high polarization level but additionally the antiphase character to deploy a color-coded contrast between thermally polarized protons and the hyperpolarized proton molecules. The basic ideas of this work have been published and are presented here in more detail.[34]

In the first part of this chapter, theoretical considerations regarding the special features of the antiphase hyperpolarization are presented. The way how to generate the hyperpolarization in a batch process and the used chemicals are presented in the following experimental methods. Subsequently, images, acquired with a gradient echo sequence, are shown for two different kind of model compounds. This part is followed by the presentation of the images acquired with a spin echo imaging sequence. Thereafter, a method is proposed to exploit the antiphase hyperpolarization as a contrast agent, e.g. for

biomedical imaging, where a clear separation from the thermally polarized background can be achieved. Finally both imaging sequences are compared.

3.1 Theoretical considerations

Before MRI experiments are performed the features of antiphase hyperpolarization and the differences to a thermally polarized sample should be studied theoretically.

First a thermally polarized sample is considered. The initial state arises from the thermal Boltzman polarization (equation 3.1). After rotating the magnetization into the transversal plane by a radio frequency pulse, popertied of the molecule due to chemical shifts (Ω_i) and J couplings (J_{ij}) will be revealed by the oscillating signal ($S^{\text{th}}_{\text{GE}}$, equation 3.2). Besides the oscillations, the different inter- and intra-molecular interactions will cause the signal to relax with the characteristic time T_2^*. During this time an imaging experiment can be performed with a gradient echo sequence (see chapter 2.3.4 on page 17). One step further, the signal available for a gradient echo, can be refocused by a $180°$ pulse and a spin echo is formed ($S^{\text{th}}_{\text{SE}}$, equation 3.3). This signal shows no longer the evolution due to chemical shift and the decay is subjected to T_2 relaxation.

$$\rho^{\text{th}}_{\text{initial}} = \sum \mathbf{I}_{iz} \tag{3.1}$$

$$S^{\text{th}}_{\text{GE}}(\text{TE}) \approx \sum \cos(\pi J_{ij} \cdot \text{TE}) \cdot e^{-i\Delta\omega_{ij}\cdot\text{TE}} \cdot e^{-\text{TE}/T_2^*} \tag{3.2}$$

$$S^{\text{th}}_{\text{SE}}(\text{TE}) \approx \sum \cos(\pi J_{ij} \cdot \text{TE}) \cdot e^{-\text{TE}/T_2} \tag{3.3}$$

$$\text{TE}^{\text{th}}_{\text{optimal}} = \text{TE}_{\text{min}} =: \text{TE}_{\text{short}} \tag{3.4}$$

Even though both signal behaviors are dominated by an exponential decay, the first $150\,\text{ms}$ will typically show an additional signal decrease due to the J couplings cosinusodial dependency. As a result of this, the echo time of a sequence should be chosen as short as possible (for the thermally polarized samples see figure 3.1(a) on the next page). Longer echo times will typically lead to smaller signal intensities in the image, because less signal is available (equation 3.4).

Distinct from that a PASADENA hPHIP signal will show a different time behavior. Only the chemical shift evolution and J coupling of *two* protons is visible, because mainly two protons are hyperpolarized. Due to the different starting operator (equation 3.5) an antiphase character manifests clearly in the signal as a sinusoidal shape in both the sequence types gradient echo (equation 3.7) and spin echo (equation 3.7):

$$\rho^{\text{hy}}_{\text{initial}} = \mathbf{I}_{1z}\mathbf{I}_{2z} \tag{3.5}$$

$$S^{\text{hy}}_{\text{GE}}(\text{TE}) = \sin(\pi J_{12} \cdot \text{TE}) \cdot e^{-i\Delta\omega_{12}\cdot\text{TE}} \cdot e^{-t/T_2^*} \tag{3.6}$$

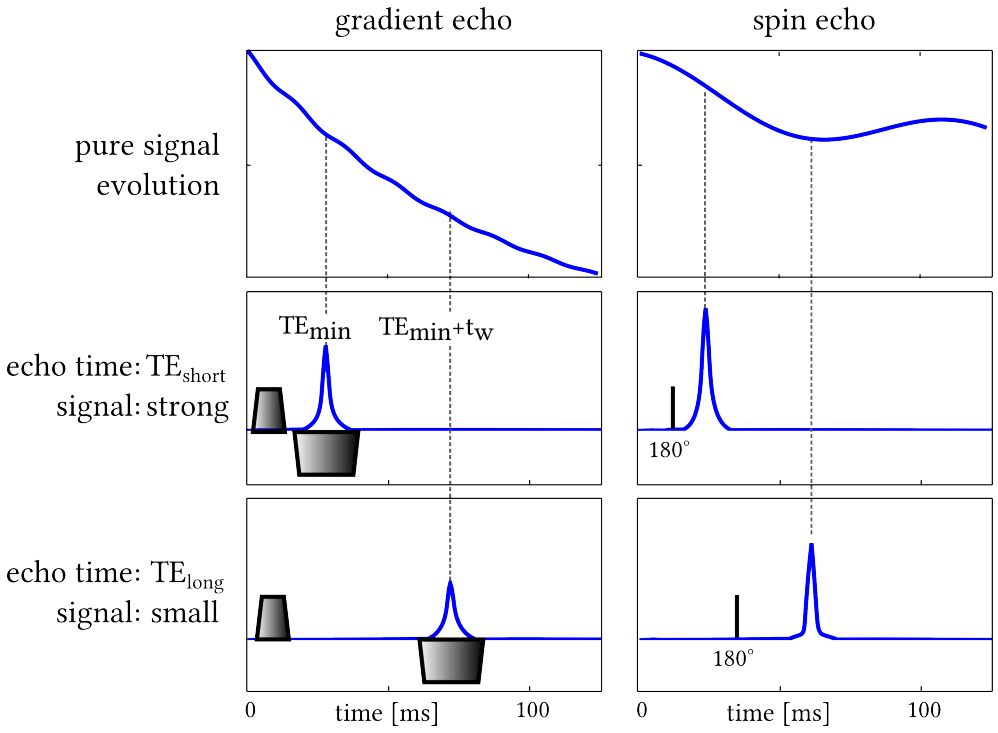

(a) Thermally polarized sample: for both sequences the *shortest* echo time leads to maximal signal.

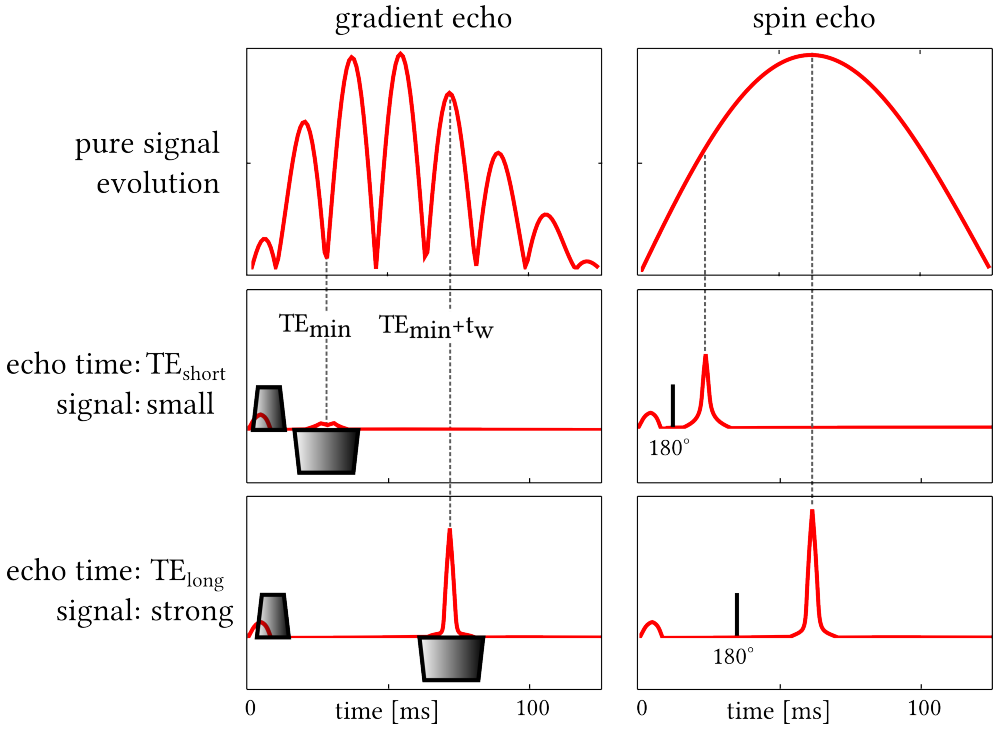

(b) Antiphase hyperpolarized sample: for both sequences the *longer* echo time leads to maximal signal.

Figure 3.1: Signal evolution for gradient echo (left column, including readout gradient) and spin echo sequence (right column, including the recofussing pulse) for a) the thermally polarized sample and b) the antiphase hyperpolarized sample. ($\omega = 50\,\mathrm{Hz}$; $J = 7\,\mathrm{Hz}$; $T_2^*/T_2 = 0.1\,\mathrm{s}/1\,\mathrm{s}$)

$$S_{\mathrm{SE}}^{\mathrm{hy}}(\mathrm{TE}) = \sin(\pi J_{12} \cdot \mathrm{TE}) \cdot e^{-\mathrm{TE}/T_2} \tag{3.7}$$

$$\mathrm{TE}_{\mathrm{optimal}}^{\mathrm{hy}} = \mathrm{TE}_{\mathrm{min}} + \mathrm{t_w} =: \mathrm{TE}_{\mathrm{long}} \tag{3.8}$$

Now the echo time selection is more complex, because a short echo time does not guarantee a maximal signal anymore (see figure 3.1(b)). This can be seen most clearly in the spin echo sequence. The gradient echo sequence the oscillations due to chemical shift introduce additional minima. The optimal echo time is now depending on concurrent processes: The exponential decay due to relaxation and the oscillations due to signal rephasing.

Typically the molecule hyperpolarized by PASADENA hPHIP is not an isolated AX spin system any more. Additional J couplings can lead to polarization transfer to nuclei in the molecule changing additionally the shape of the signal. However, the simple model presented here will still hold and experiments will be performed to demonstrate this.

3.1.1 Contrast mechanism

From the previous section it is clear that the two kinds of sigmals evolve very differently due to their different initial states. As shown, regarding the thermal signal there is not much one can do to improve the signals apart from choosing the shortest possible echo time. In the case of PHIP, however, more options are available. From figure 3.1 it can be seen that the selection of the echo times play a very important role in experiments where both samples are mixed. For example, if the chosen echo time is $\mathrm{t_{short}}$ the signal arising from the PHIP molecules will be almost negligible, while if $\mathrm{t_{long}}$ is chosen, the PHIP molecules will contribute with the maximal available signal. In those cases where the enhanced PHIP signal is high enough to eclipse the thermally polarized signals, the mere selection of the optimal echo time provides an excellent contrast method.

In the following sections this optimization is studied thoroughly. In the case of the gradient echo sequence two different molecules and varying T_2^* conditions were tested (results presented in section 3.3 on page 35). The spin echo sequence is also verified experimentally in section 3.4 on page 44.

However, in possible applications the concentration of hyperpolarized molecules will be very small compared to the thermally polarized background. Thus, the hyperpolarization might not be able to outweigh the thermal polarization. In such a realistic case a different method is necessary to deploy a contrast method.

The basic idea is to exploit the different echo time behaviors due to the antiphase character as explained above. Two spin echo or gradient echo images (I) acquired at

different echo times are subtracted from each other:

$$\Delta I = I(\mathrm{TE_{long}}) - I(\mathrm{TE_{short}}) \tag{3.9}$$

$$\Delta I(x,y) = \begin{cases} > 0 & \text{pixel with specific target molecule} \\ < 0 & \text{pixel with thermally polarized background} \end{cases} \tag{3.10}$$

While the hyperpolarization increases from image $I(\mathrm{TE_{short}})$ to image $I(\mathrm{TE_{long}})$ due to the antiphase character, the thermal polarization decreases.

This concept can be applied directly to the spin echo sequence, but requires some additional fine tuning when using the gradient echo sequence (the technical details are explained in the following sections). In the gradient echo sequence additional oscillations due to the chemical shift show up. These introduce additional minima in the hyperpolarized antiphase signal. For the subtraction image it is beneficial to increase the minimal echo time until such a minimum is reached. Also the relaxation due to T_2^* plays a big role in rendering the contrast. The subtraction method performs best, if the T_2^* for the target molecule is long, and the thermal polarization decays fast. This, however, resembles a typical case in *in vivo* imaging where only a small amount of target molecules is located in a big thermally polarized background.

The concept of this second subtraction contrast method is explored in section 3.5.

3.2 Experimental Methods

3.2.1 Precursor and catalyst

Hydrogenative PHIP requires a suitable combination of precursor and catalyst. Previous work has shown that hydrogenation of 1-Hexyne provides a stable hyperpolarization and experiments can be easily performed.[35] However, this system is not water soluble and therefore it is used only to investigate general features of the hyperpolarization. For *in vivo* applications the water soluble 2-hydroxyethylpropionate is used. Interesting results using this molecule have been introduced earlier.[22] The hyperpolarization generated in this molecule is lower than the hyperpolarization generated by 1-Hexyne but allows experiments in water (see figures 3.2 on the following page). The sample composition (see table 7.1 on page 98) was optimized to provide maximal signal enhancement when shaking several times.

1-Hexyne

The hydrogenation of 1-Hexyne (with para-hydrogen) produces hyperpolarized 1-Hexene (see figure 3.2(a) on the following page). Strictly speaking, the two protons of para-

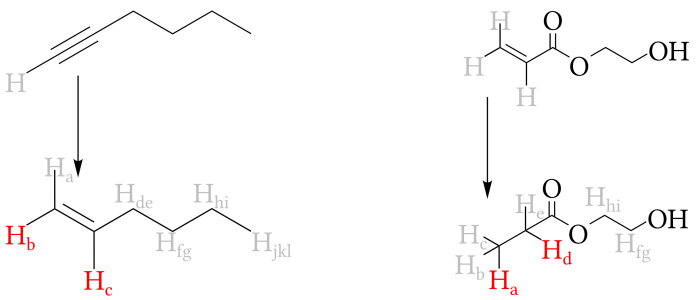

(a) Triple bonded 1-Hexyne and the hyperpolarized 1-Hexene with the two hyperpolarized protons in red after hydrogenation.

(b) Water solvable substrate 2-hydroxyethylacrylate and the resulting hyperpolarized 2-hydroxyethylpropionate

Figure 3.2: Substrates 1-Hexyne and 2-hydroxyethylacrylate used for hydrogenative PHIP. Catalysts are displayed in figure 7.1 on page 99.

hydrogen are added pairwise to 1-hexyne during the reaction, and labeled as H_b and H_c, cannot be considered as an AX spin system in the product molecule (see table 3.1(a)). The proton labeled as H_a is strongly coupled to one of the added protons, generating a strongly coupled three spin system. Thus, a fraction of the hyperpolarization is transferred to H_a. Additionally the protons labeled as H_d and H_e are also coupled to one of the former para-hydrogen protons and, depending on the reaction conditions, can also experience hyperpolarization transfer.

2-hydroxyethylpropionate

Hyperpolarized 2-hydroxyethylpropionate is simpler in terms of spin coupling (see table 3.1(b)). The parahydrogen spins are spatially separated from the other protons and consequently form an AX spin system. This makes simulations easier, along with the comparison to the experimental results.

Table 3.1: J [Hz] couplings of the hPHIP model compounds.

(a) Couplings of 1-Hexene. H_b and H_c are the protons from parahydrogen. H_a is strongly coupled to H_b at 1.5 Tesla (Δppm $= 0.8$).

	H_a	H_b	H_c	H_{de}	H_{fg}	H_{hi}	H_{jkl}
H_a		2.2	10.2	1.2	1.6		
H_b	2.2		17.1				
H_c	10.2	17.1		6.7			
H_{de}	1.2	1.6	6.7		7.1		
H_{fg}				7.1		7.1	
H_{hi}					7.1		7.0
H_{jkl}						7.0	

(b) Couplings of 2-hydroxyethylpropionate. The groups H_{abc} and H_{de} contain the two pH_2 protons.

	H_{abc}	H_{de}	H_{fg}	H_{hi}
H_{abc}		7.6		
H_{de}	7.6			
H_{fg}				4.6
H_{hi}			4.6	

3.2.2 Generation of parahydrogen

Parahydrogen has a highly ordered spin state and is therefore the source of the hyperpolarization (see theory section 2.2.1 on page 8). To prepare an enrichment in the para state of hydrogen, the latter was cooled down to 30 K in the presence of active charchoal. Under these conditions the transition from ortho- to parahydrogen is possible (For further information see theory section 2.2.1 on page 8). Two different apparatus were used.

1. Home build parahydrogen generator operating in batch mode. A cool down below 30 K is possible but care needs to be taken: Due to a freezing of hydrogen, blockages can occur that can lead to pressures well above the safety limits (figure 3.3(a)).

2. Commercial machine from Bruker™ for continuous generation of parahydrogen (figure 3.3(b)). A continuous generation of parahydrogen is possible with a flow rate of 200 $^{ml}/_{min}$. For filling the aluminum bottles a batch delivery mode is also possible.

The parahydrogen can be stored in aluminum bottles over days. So parahydrogen can be transported over long distances to generate hyperpolarization at a different location. For example the parahydrogen was generated in the ”Max Planck-Institut fr Polymerforschung” in Mainz and (most) experiments were performed at the ”Universitätsmedizin der Johannes Gutenberg-Universität” in Mainz.

(a) Custom built parahydrogen generator for batch mode generation. Image of the cryostat expander (left) and complete setup (right). The helium compressor (bottom left) and expander unit (on the table).

(b) Parahydrogen generator from Bruker™ and aluminum storage bottles for parahydrogen (on top).

Figure 3.3: Two different parahydrogen generators used for these experiments.

3.2.3 Generation of hyperpolarization via shaking

Once the bottles are filled with enriched parahydrogen a syringe was used to introduce it in a NMR tube sealed with a septum cap. For optimal reaction conditions the sample

tube was heated up to 70° C. The shaking and therefore generation of hyperpolarization is performed inside the homogeneous region of the magnetic field at 1.5 T and this leads to PASADENA conditions (see figure 3.4).

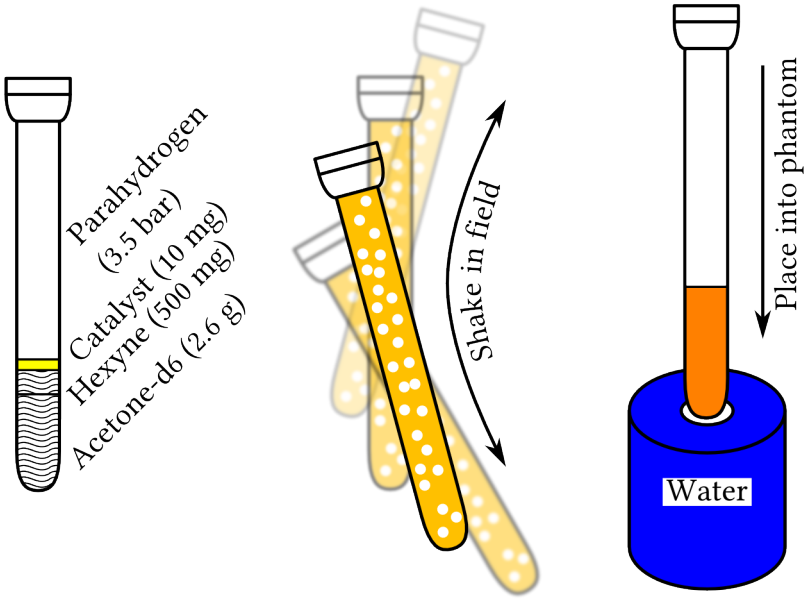

Figure 3.4: The prepared sample tube is pressurized with 3.5 bar of parahydrogen. By shaking, the chemical reaction is started thus generating the hyperpolarization. After quickly placing the tube in the magnet a measurement is started.

The resulting NMR spectra of both model compounds 1-Hexyne and 2-hydroxyethylacrylate (see figure 3.5) show the antiphase pattern theoretically predicted for PASADENA conditions (see section 2.2.2 on page 9). Large B_0 inhomogeneities lead to insufficient shim conditions and do not allow a separation of all involved J coupling splittings.

Reproducibility for the shaking method was achieved by following the protocol shown in figure 3.7 on page 34. Since the chemical reaction consumes the substrate the hyperpolarization will decrease over time. However, at the beginning of the reaction not all the catalyst is activated in the reaction. Typically, shakes 2 to 6 result in very high and rather stable hyperpolarization and afterwards the hyperpolarization decreases (see figure 3.6 on page 34).

The resulting enhancement per proton from the two model compounds can be seen in figure 3.6 on page 34. The highest enhancement can be achieved by 1-Hexyne and 2-hydroxyethylpropionate presents smaller enhancement per proton.

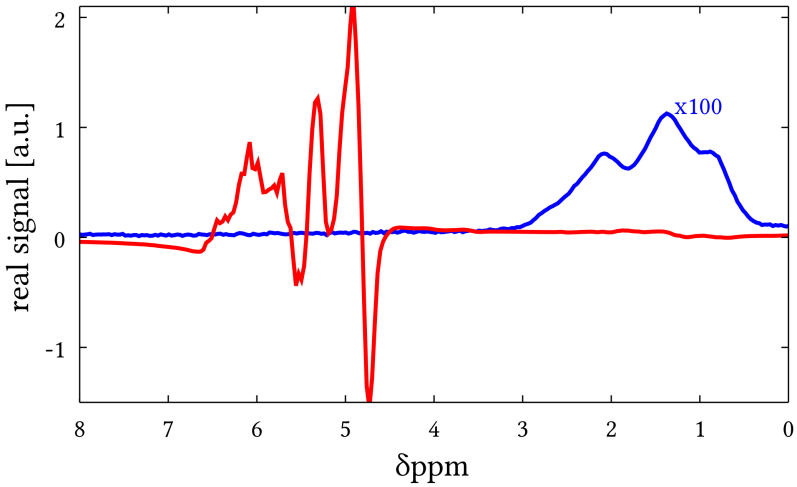

(a) Hyperpolarized 1-Hexene (red) and thermally polarized 1-Hexyne (blue, scaled up by a factor 100).

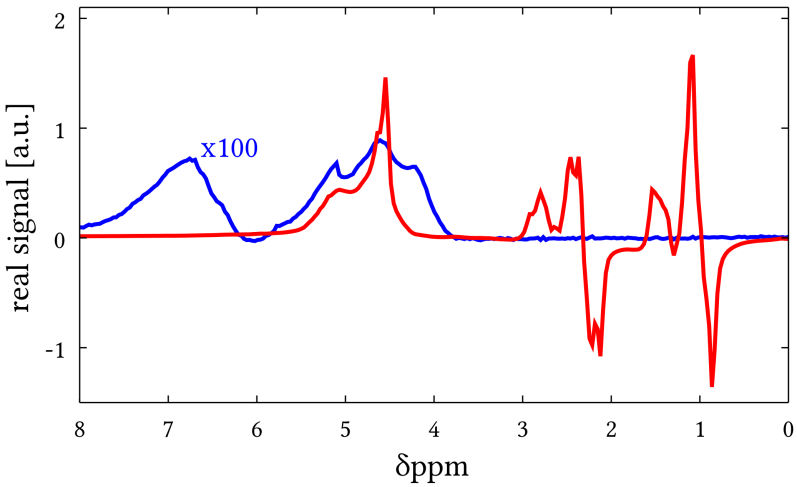

(b) Hyperpolarized 2-hydroxyethylpropionate (red) and thermally polarized 2-hydroxyethylacrylate (blue, scaled with a factor 100). The hyperpolarized peaks of 2-hydroxyethylpropionate are only located below 3 ppm where as the peaks between 4-5 ppm originate from hyperpolarized protons of the catalyst.

Figure 3.5: Spectra of hyperpolarized 1-Hexene and 2-hydroxyethylpropionate. The reader should keep in mind that the number of protons contributing to the thermal signal (blue) is bigger than for the hyperpolarized signal that is originated only from the two former para-hydrogen atoms. Basically only these two protons give rise to the hyperpolarized signal. (Thermal high resolution spectra available in Appendix 7.2 and 7.3).

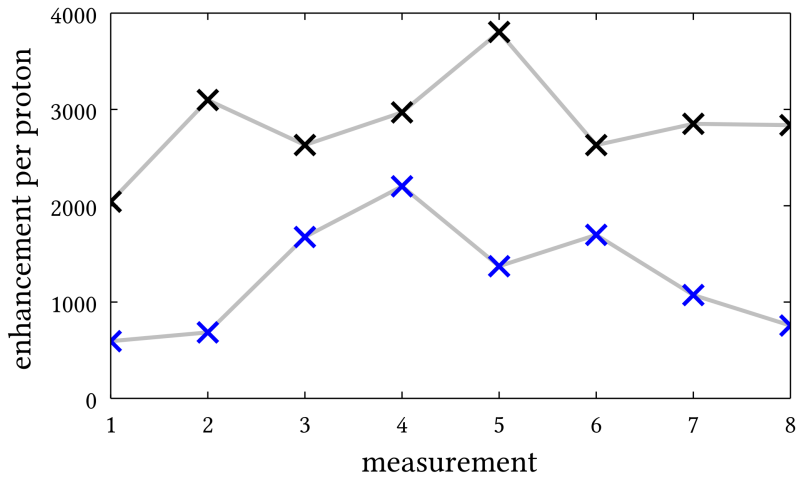

Figure 3.6: Enhancement factors per proton of hyperpolarized 1-Hexene (black) and hyperpolarized 2-hydroxyethylpropionate (blue) as a function of the shake number. During each shake a different amount of hyperpolarization is produced. When comparing MRI results with different enhancement factors a correction must be applied.

3.2.4 Experimental Setup

The samples were prepared in an argon atmosphere and filled in a 10 mm NMR tubes sealed by septum caps. A 1.5 Tesla MRI Scanner (Magnetom Sonata, Siemens Medical, Germany) was used. Experiments with gradient echo sequence were performed using a commercial (receiver) finger coil and the body coil for the radio frequency pulses (Magnetom Sonata, Siemens Medical, Germany). In order to apply the 180° pulses for the spin echo sequence a home build receive and transmitt coil was needed. The outer region of the phantom can be filled with water. The protocol described in figure 3.8 was followed in the experiments. This assures the automatic adjustment of the transmitter voltage and calibration of the receiver and no further calibration of the experiments is needed.

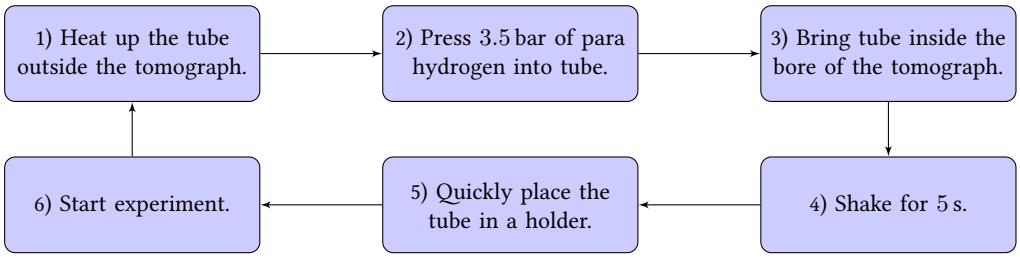

Figure 3.7: Measurement protocol for hyperpolarization experiments.

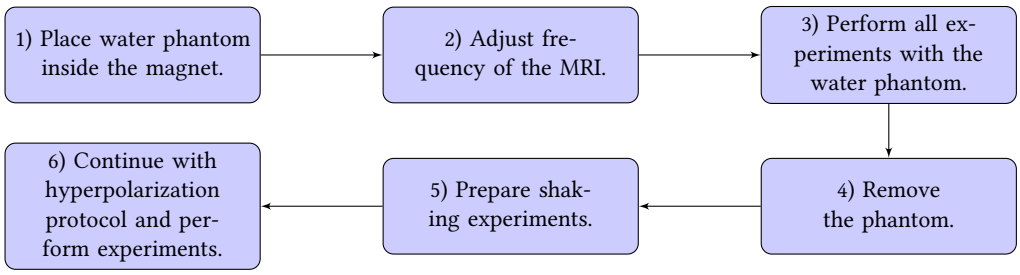

Figure 3.8: Measurement Protocol for PHIP samples in an clinical MRI-scanner.

3.3 Gradient Echo Sequence

The theoretical considerations from the beginning of this chapter on page 26 must be adapted for the gradient echo sequence. Most importantly the flip angle must be kept small, in order to acquire each line of the k-space with nearly the same amount of hyperpolarization. If the flip angle is too high the hyperpolarization will be exploited too fast and artifacts as described in the basic theory chapter 2.3.2 on page 15 will occur, reducing the image quality drastically.

The contrast between the thermal polarized bulk and the antiphase hyperpolarization was calculated:

$$S_{\mathrm{GE}}^{\mathrm{th}}(\mathrm{TE}) \approx \sum \cos(\pi J_{ij} \cdot \mathrm{TE}) \cdot e^{-i\Delta\omega_{ij}\cdot\mathrm{TE}} \cdot e^{-\mathrm{TE}/T_2^{*\mathrm{th}}} \tag{3.11}$$

$$S_{\mathrm{GE}}^{\mathrm{hy}}(\mathrm{TE}) = \quad \sin(\pi J_{12} \cdot \mathrm{TE}) \cdot e^{-i\Delta\omega_{12}\cdot\mathrm{TE}} \cdot e^{-t/T_2^{*\mathrm{hy}}} \tag{3.12}$$

Therefore two cases are considered: First, if the thermally bulk magnetization is subjected to stronger T_2^* relaxation as the antiphase hyperpolarization (see section 3.3.1). Secondly, the case where both are mixed in the same place and therefore having the same T_2^* relaxation times (see section 3.3.2 on page 41).

3.3.1 Imaging of pure hyperpolarized compound and thermal background

The first case, where the T_2^* of the thermally polarized region is smaller that in the hyperpolarized area, is realized by the phantom's geometry: The pure hyperpolarized compound surrounded by a thermal water reference. The intention is to test weather the signal evolution of the hyperpolarized compound can be exploited for generating a contrast against the thermally polarized signal of the background.

The used phantom (see figure 3.9 on the following page) consists of two concentric glass tubes, with the hyperpolarized molecules placed in the center and surrounded by a large volume of water. It was chosen such that a clear spatial distinction exists between the hyperpolarized and the thermal area. This allows for easier evaluation of both signals

separately. It is important to realize that the shim conditions are better in the inner area where the hyperpolarized compound is located. Consequently, the case $T_2^{*\mathrm{th}} < T_2^{*\mathrm{hy}}$ is studied.

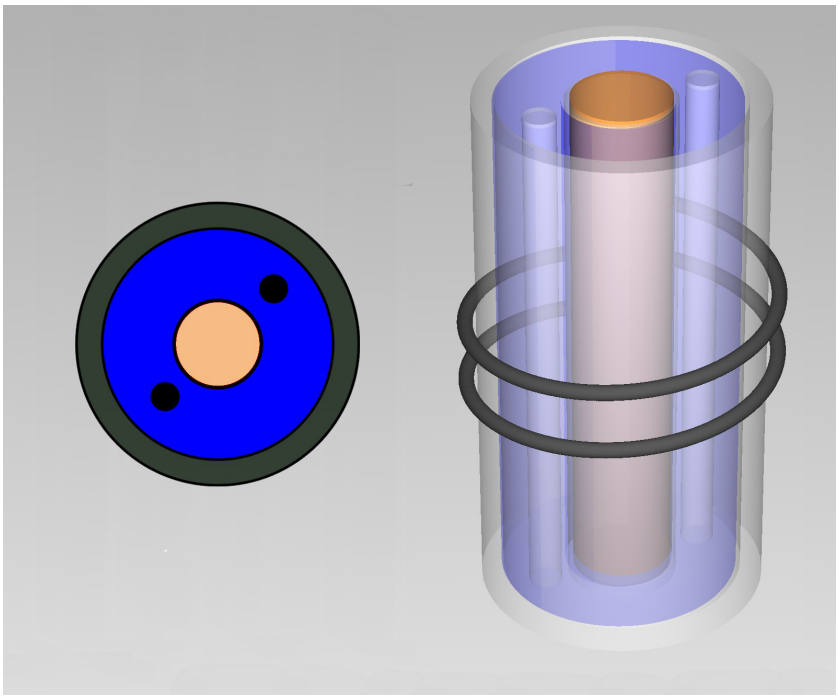

Figure 3.9: Geometry of the phantom. A cylinder filled with water (blue) surrounds the NMR-sample tube (orange). Solid bars are located in the water ares (black) to give the phantom more structure. The position of the MRI coil is indicated in the hollow 3D view on the right.

1-Hexyne

In figure 3.10 on the next page, the thermal (water) and the PASADENA hPHIP signal (1-Hexyne) are shown for the first 45 ms of the acquisition time. Since this is a strongly coupled system the distinction between oscillations due to chemical shift and J coupling is difficult. However a signal increase till 42 ms due to J coupling can be observed. Notice that due to the fast T_2^* relaxation in the thermally polarized area, the thermal signal (blue line) has almost completely decayed when the hyperpolarized signal (red line) reaches the first maximum due to the J-coupling (factor 5 difference in T_2^*).[1] These two effects work together in rendering the contrast between the two regions.

[1] The effect of the two different T_2^* is bigger in the FID than in the images because the images are acquired slice selective!

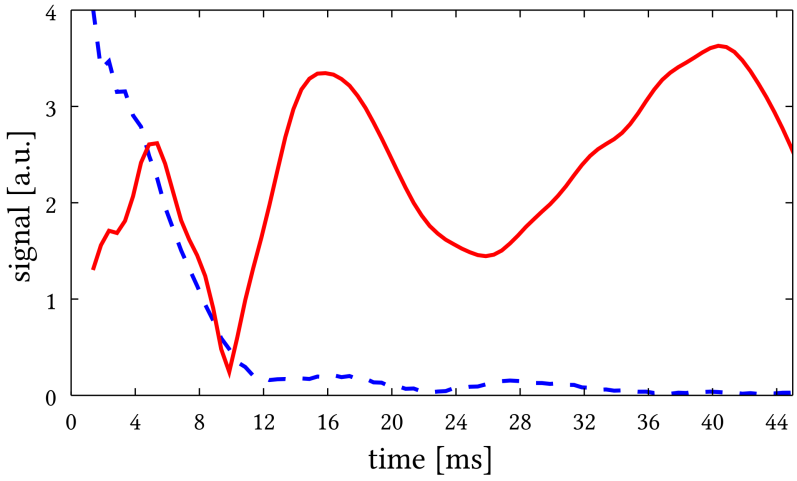

Figure 3.10: Time domain signal of hyperpolarized 1-Hexene (red) acquired prior to each imaging experiment (for spectra see figure 3.5 on page 33). Thermally polarized reference in blue. Measurement was performed by using a FID sequence with 10° flip angle, bandwidth: 1000 Hz, vector size: 2048.

The images, presented in figure 3.11, clearly show the phantom's geometry and that the signal intensities in the respective areas evolve differently. While the signal intensity of the water area decays the signal rising from the center with the hyperpolarized molecules oscillates and shows local maxima at echo times 15.8 ms and 42.0 ms, as expected from the FID signal amplitude displayed in Figure 3.10. In these images a very high contrast between thermally polarized and hyperpolarized areas is observed.

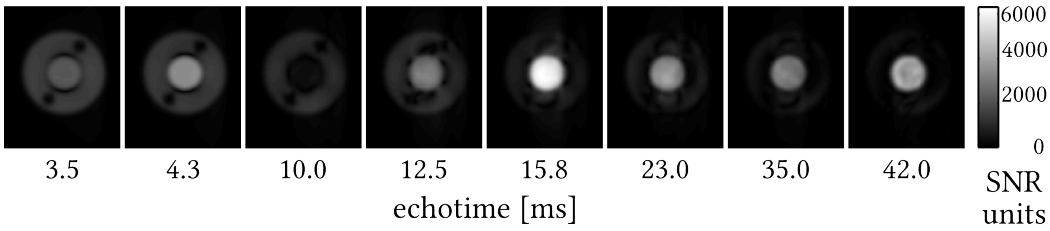

Figure 3.11: MR-images of hyperpolarized PHIP substance (1-Hexene) surrounded by thermally polarized water acquired at different echo times (TE_{min} + tw = 3.5 ms + tw) by individual experiments. The typical signal decay within the thermally polarized area can be observed. The intensity evolution of the hyperpolarized area, however, is generated by the hyperpolarized protons. Imaging was performed by using a slice selective gradient echo sequence with centric reordering, flip angle: 10°, repetition time: 45 ms, bandwidth: 600 Hz, FOV: 60 mm^2, acquisition matrix: 88 × 88, resolution: 0.7 $^{mm}/_{pixel}$ and slice thickness 10 mm.

A more quantitative analysis for the thermal and hyperpolarized image areas was performed by selecting regions of interest (ROI) inside the two areas and calculating the

mean signal for the different echo times (see figure 3.12). Due to different initial polarizations of the subsequent PHIP reactions the signal of the hyperpolarized area was normalized by a correction factor calculated from an FID acquired prior to each image (see 2.4.6 on page 24). The water region (outer area) of the phantom shows a signal of 0.58 a.u. for the shortest echo time followed by a decay down to a signal of 0.09 a.u. for the longest echo time. The signal in the hyperpolarized area, however, is dominated by the time evolution under J-coupling and chemical shift of the hyperpolarized protons. Starting from a signal of 1.16 a.u. for the shortest echo time the signal follows the shape of the FID (see figure 3.10 on the preceding page) down to 0.14 a.u. at 10.0 ms echo time. The rise at echo time 15.8 ms leads to a signal of 2.16 a.u. (a signal of 2.90 a.u. is achieved without correction due to different hyperpolarization levels) presenting outstanding contrast.

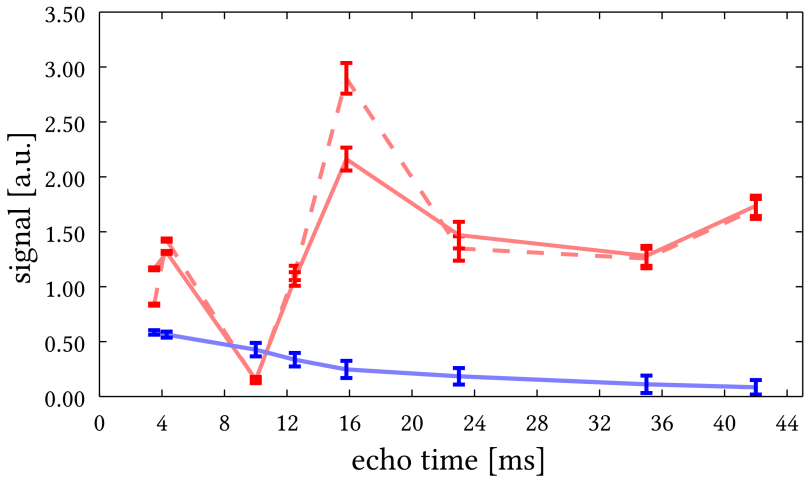

Figure 3.12: Signal of images at different echo times: Thermal water (blue line) and hyperpolarized area (dashed red line) and normalized to the amount of initial hyperpolarization (solid red line). Minima and maxima of the FID from figure 3.10 on the preceding page are resembled. The noise level of $(4.8 \pm 0.4) \cdot 10^{-4}$ a.u. is not visible in this scaling. The match is not exact since the T_2^* conditions differ.

2-hydroxyethylacrylate

To demonstrate the general applicability of the imaging approach the same MRI experiments for a different hyperpolarized molecule, namely the water soluble 2-hydroxyethylacrylate, were performed.

Figure 3.13 on the next page shows the thermal and the PHIP signals from within the phantom. The hyperpolarized signal shows strong oscillations due to the chemical shift and slower oscillations arising from the J coupling. Compared to hyperpolarized 1-Hexyne a faster oscillation can be observed, because of the smaller chemical shift of the hyperpolarized protons ($1 - 2$ ppm instead of $5 - 6$ ppm).

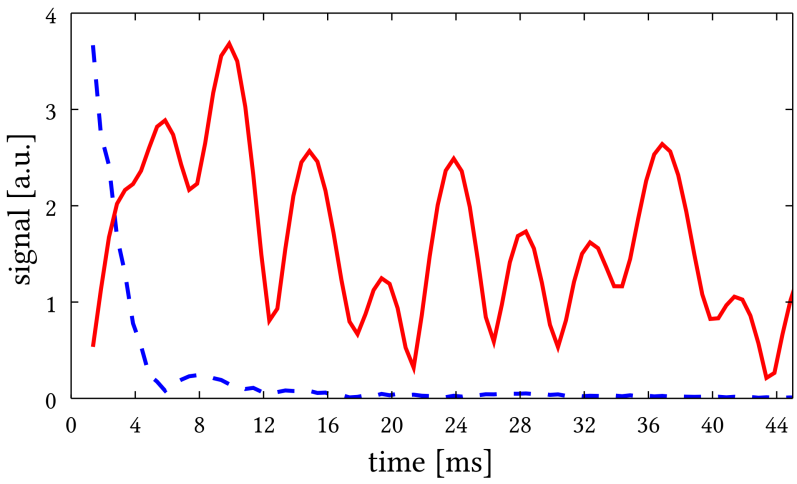

Figure 3.13: Time domain signal of hyperpolarized 2-hydroxyethylpropionate (red, for spectra's see figure 3.5 on page 33). Thermal reference is displayed as blue dashed line. Measurement was performed by using a FID sequence with 10° flip angle, bandwidth: 1000 Hz, vector size: 2048.

While the signal is close to zero directly at the beginning it rises to a maximum at approximately 10 ms. The large difference in T_2^* is present here as well since it depends on the geometry of the phantom.

The acquired MR-images (see figure 3.14) show the phantom's geometry clearly. As in the previous case, the signal in the thermal area decays with increasing echo time whereas the signal within the center shows maxima at 15.0 ms and 24.3 ms. This echo time dependency was expected from the FID in figure 3.13. A very high contrast between the two areas is observed, for example at TE= 15.0 ms.

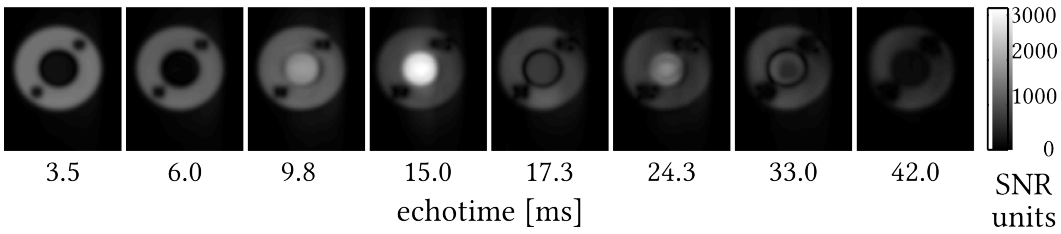

Figure 3.14: MR-images of hyperpolarized PHIP substance (2-hydroxyethylpropionate) surrounded by thermally polarized water acquired at different echo times by individual experiments. Notice the excellent contrast obtained for TE= 15.0 ms. Imaging was performed by using a slice selective gradient echo sequence with centric reordering, flip angle: 10°, repetition time: 45 ms, bandwidth: 600 Hz, FOV: 60 mm^2, acquisition matrix: 88×88, resolution: 0.7 $^{\text{mm}}/_{\text{pixel}}$ and slice thickness 10 mm.

The quantitative analysis of the signal intensities are presented in figure 3.15. The water region of the phantom shows a signal of 0.54 a.u. for the shortest echo time followed by a decay down to a signal of 0.18 a.u. for the longest echo time. The signal in the hyperpolarized area, however, is dominated by the time evolution under J coupling and chemical shift of the hyperpolarized protons.

Starting from a signal of 0.09 a.u. for the shortest echo time the signal rises to the maxima previously seen for the FID at 9.8 ms and 15 ms leading to a signal of 0.62 a.u. and 0.95 a.u.. A mininum is observed at 17.3 ms leading to a signal of 0.25 a.u.. Then another maxima is observed at 24.3 ms generating a signal of 0.50 a.u.. For higher echo times the signal falls down to 0.20 and 0.06 a.u..

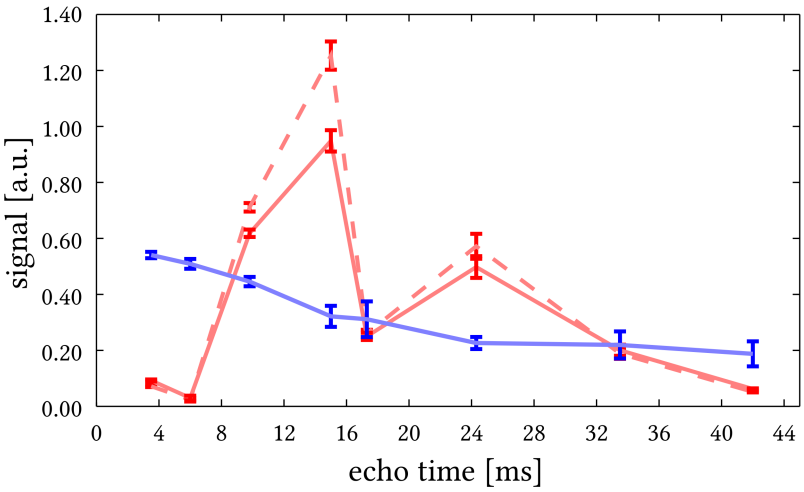

Figure 3.15: Signal of images at different echo times. Signal of thermally polarized water (solid blue line), hyperpolarized molecule (dashed red line) and corrected by the amount of initial hyperpolarization (solid red line). Minima and maxima of the FID from figure 3.10 on page 37 are reproduced. The noise level of $(3.7 \pm 0.2) \cdot 10^{-4}$ a.u. is not visible in this scaling. The match is not exact since only a single FID (out of eight) is presented and the T_2^* conditions differ.

Discussion

As shown, the intensity of the images acquired with different echo times follows the behavior of the respective FID. This allows a adjustments of the echo time in the sequence to obtain maximum MRI contrast. Of course the short T_2^* of the thermal background helps fostering the good MRI contrast. The data presented here demonstrate that a tiny amount of antiphase hyperpolarized protons can outweigh the signal of a large excess of thermal protons (see table 3.2 on the next page) at specific echo times for the beneficial case of the hyperpolarized area exhibiting a longer T_2^*. The concentration of the hyperpolarized compound necessary to generate this contrast is on the same order like those for in

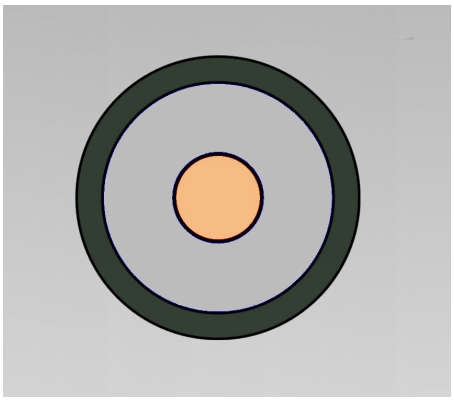

Figure 3.16: Geometry of the phantom: The NMR-sample tube is placed in the center surrounded by the finger coil.

vivo experiments described by Mansson et al.[6]. They demonstrated in vivo ^{13}C-MRI on large animals using a concentration of $0.3\,{}^{\text{mmol}}/_{\text{kg}}$ of ^{13}C enriched hyperpolarized 2-hydroxyethylpropionate (generated via PHIP starting from 2-Hydroxyethylacrylate and subsequent polarization transfer to the carbon nuclei). The experiments presented here represent a concentration of $1.5\,{}^{\text{mmol}}/_{\text{kg}}$, i.e. 5 times higher. However, the excellent contrast demonstrated here would easily allow for a reduction of the sample concentration.

Table 3.2: Proton density of the different samples calculated from table 4.1 on page 58 . The density of the PHIP ${}^{\text{protons}}/_{\text{cm}^3}$ is multiplied by the conversionrate of 5%. Basically only these protons give rise to the hyperpolarization.

Sample	${}^{\text{protons}}/_{\text{cm}^3}$	PHIP ${}^{\text{protons}}/_{\text{cm}^3}$
thermal H_2O	$6.69 \cdot 10^{22}$	
mix with 1-Hexyne	$1.08 \cdot 10^{22}$	$0.01 \cdot 10^{22}$
mix with 2-Hydorxyethylacrylate	$0.80 \cdot 10^{22}$	$0.01 \cdot 10^{22}$

3.3.2 Imaging of hyperpolarized compound mixed with thermal background

The presented images provide valuable proof-of-concept data for the contrast mechanism. The scenario of two spatially confined regions for the hyperpolarized substance and the thermal background might not completely resemble an *i*n vivo situation. In case of *in vivo* experiments the hyperpolarized substance would be distributed in the thermal environment and thus be present in the same MRI voxel.

In this situation the hyperpolarized substance and the thermal background exhibit very similar T_2^* times. For mimicking the in vivo situation a phantom consisting of a single tube containing the hyperpolarized compound and a protonated solvent was measured (see figure 3.16).

The same experiments as in the section before were performed. From figure 3.17 on

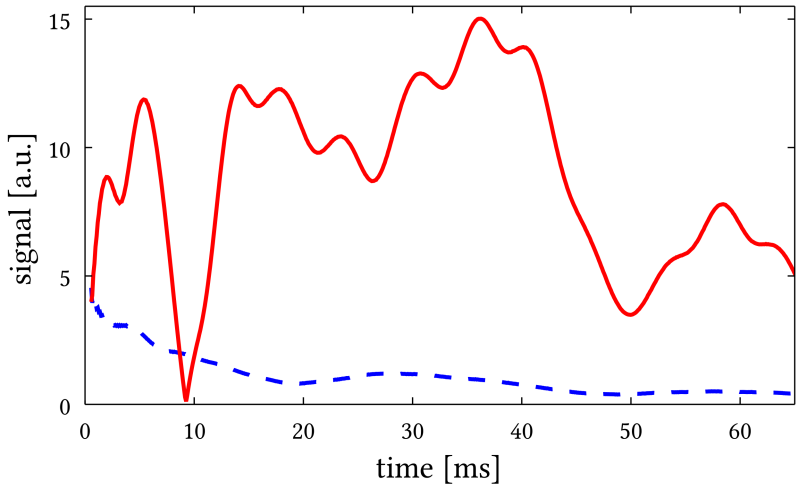

Figure 3.17: Time domain signal of hyperpolarized 1-Hexene with (protonated) acetone acquired prior to each imaging experiment. Measurement was performed by using a FID sequence with 10° flip angle, bandwidth: 1000 Hz, vector size: 2048.

the next page it can be seen that the T_2^* of all components times are now similar.

Images with different echo times were acquired under hyperpolarized and thermally polarized conditions (see figure 3.18 on the facing page) and the echo times where newly chosen to resemble interesting features of figure 3.17. The thermal image series (bottom) show the typical decay due to T_2^* relaxation and hardly any signal is obtained for echo times longer than 20 ms. In the hyperpolarized case (top) the features of the PHIP antiphase hyperpolarization and the J-coupling evolution are clearly visible. As before, a minimum of the signal intensity is found at approx. 11 ms and a maximum at 15 ms echo time resembling the shape of the FID of the hyperpolarized substance. Thus, also for this case of equal T_2^* times excellent contrast can be generated due to the different initial state of the hyperpolarized substance. The images show an artifact in phase encoding direction, due to the application of multiple RF pulses for the acquisition of subsequent k-space lines. This could be removed by the application of dedicated imaging methods for hyperpolarized substances such as the variable flip angle approach.[36]

Again, a more quantitative analysis was performed by selecting regions of interest (ROI) for the thermal and hyperpolarized image series and the mean signal for the different echo times was calculated (see figure 3.19 on the facing page). In the thermally polarized case the image shows a signal of 0.16 for the shortest echo time followed by a decay down to 0.01 for the longest echo time. The signal in the hyperpolarized area starts from 0.76 a.u. for the shortest echo time and the signal follows the shape of the FID (see figure 3.17) down to a signal of 0.35 at 11.2 ms echo time. The increase towards a maximum value at echo time 15.1 ms leads to a signal of 1.12.

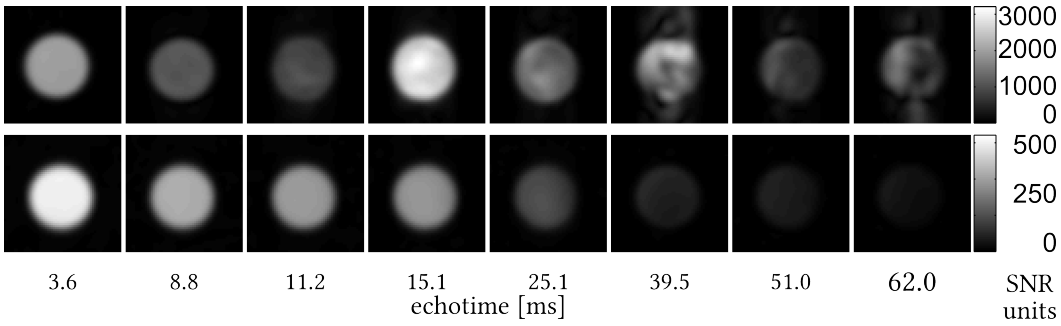

Figure 3.18: MR-images of hyperpolarized PHIP substance (1-Hexene) and thermally polarized acetone (non deuterated) mixed within a single tube acquired at different echo times in individual experiments. Images at the top were acquired under hyperpolarized conditions (and corrected by the different initial amounts of hyperpolarization); images at the bottom serve as thermal references. The signal oscillation in the hyperpolarized area due to the J-coupling and chemical shift of the hyperpolarized protons is observed. Imaging was performed by using a slice selective gradient echo sequence with centric reordering, flip angle: $10°$, repetition time: 45 ms, bandwidth: 600 Hz, FOV: $50\,\mathrm{mm}^2$, acquisition matrix: 88×88, resolution: $0.6\,{}^{\mathrm{mm}}/_{\mathrm{pixel}}$ and slice thickness $10\,\mathrm{mm}$.

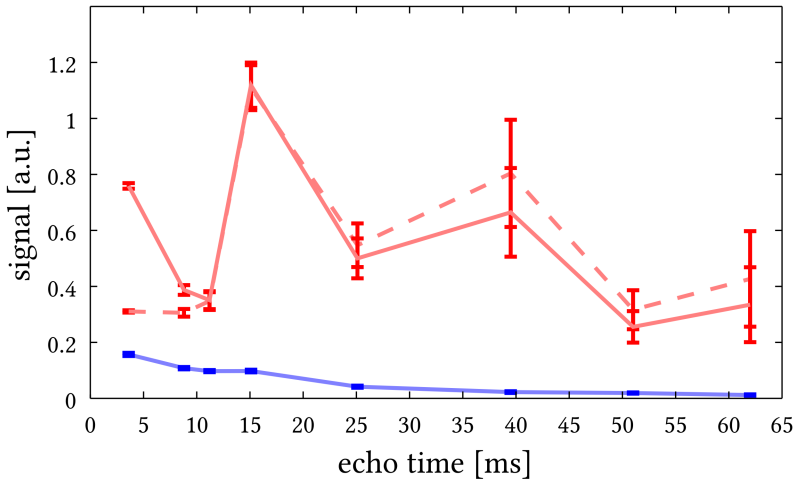

Figure 3.19: Signal of images at different echo times for equal T_2^* condition of thermally polarized and hyperpolarized compound. Signal for thermally polarized experiments (dashed blue line) and signal of the hyperpolarized area (dashed red line), corrected by the amount of initial hyperpolarization per image (solid red line). The noise level of $(3.5 \pm 0.3) \cdot 10^{-4}$ a.u. is not visible in this scaling. Minima and maxima of the FID from figure 3.17 on the preceding page are reproduced. The match is not exact since only a single FID (out of eight) is presented and the T_2^* conditions between imaging and FID experiment are not equal. Connecting lines are drawn to guide the eye.

Discussion

The presented results demonstrate that even if hyperpolarized signals exhibit the same T_2^* as the thermal background the antiphase character of the hyperpolarized protons makes it possible, that even a tiny amount of hyperpolarized sample ($0.01 \cdot 10^{22}\,/\mathrm{cm}^3$) outweight the signal of a large excess of thermal protons (for this phantom $4.92 \cdot 10^{22}\,/\mathrm{cm}^3$) at specific echo times. Moreover, the data establish a condition for the minimum amount of PHIP molecules with respect to the thermal molecules necessary to differentiate the signals. This minimum is obviously higher compared to the case of fast decaying thermal signal (see figures 3.10 and 3.14) and depends strongly on the generated hyperpolarization. For molecules which cannot be as effectively polarized as the ones presented in this work the concentration could be critical, deciding on the viability of the application to MRI.

3.3.3 Summary for gradient echo sequence

The experiments presented here demonstrate that simple variation of the echo time (TE = $\mathrm{TE}_{\mathrm{min}}$ + tw) is sufficient to generate outstanding contrast between a small amount of hyperpolarized and a large excess of thermally polarized molecules. The optimal waiting times can simply be found by recording an FID of the hyperpolarized substance prior to image acquisition. The achievable contrast, however, strongly depends on the transverse relaxation of the two types of coherences. Therefore, we considered different scenarios featuring different T_2^* times. The contrast is highest, when the T_2^* of the hyperpolarized molecules is longer than that of the background. However, excellent MRI contrast can be generated even under the less favorable situation of equal T_2^* times, as it would occur for in vivo MRI.

MRI data of two different molecules were presented to demonstrate the generality of the approach. The contrast generated here arises from the different kind of time evolution of the hyperpolarized proton signal. The contrast mechanism will be applicable for both PHIP conditions, i.e. PASADENA and ALTADENA[2].

3.4 Spin Echo Sequence

A spin echo ($\alpha_x - \frac{\mathrm{TE}_1}{2} - 180°_y - \frac{\mathrm{TE}_1}{2} -$ echo) sequence refocuses the effect of chemical shift evolution. According to the theoretical considerations (see chapter 3.1), the signal at echo time TE_1 will follow the pure J coupling evolution $\sin(\pi J \cdot \mathrm{TE}_1)$. Here an additional waiting time has to be introduced too to allow the system an evolution until a maximum is reached. Differently to the gradient echo sequence this maximum now depends only

[2]The initial density operator differs, however for a flip angle of $45°$ the findings can be transferred easily.

on the J coupling evolution. When acquiring MR-images, several different strategies are available to exploit the magnetization.

First, usage of a low flip angle and acquisition of each line of the kSpace with a new excitation pulse (requires perfect 180° pulses). Second, usage of a 45° flip angle to rotate maximal (single quantum) hyperpolarization into the transversal plane. Option 1 is not feasible because the required precision of 180° pulses could not be realized within the experimental setup. Option 2, however, requires a echo train (with echo time TE_2) in which all lines are acquired. Again several choices can be made:

- Use a gradient echo train for readout (e.g. EPI or spiral acquisition scheme). This is less complicated than a spin echo readout train but the image will be subjected to T_2^* relaxation, chemical shift and J coupling evolution.
- Use a spin echo readout train with $\mathrm{TE}_2 = \frac{1}{J}$. Thus each time the evolution due to J coupling reaches a maximum a k-space line is acquired. This leads to a strong T_2 weighted acquisition, since TE_2 typically lies around 40 to 100 ms.
- Decrease the TE_2 to acquire all lines in a very fast echo train.

The first two options are not feasible because of the possible T_2 or T_2^* weighing. The third option is possible if a very short echo time TE_2 can be realized:

It turns out that close to the fast pulse limit ($J_{AX}\mathrm{TE}_2 \wedge \Omega_i \mathrm{TE}_2 << 1$), theoretically, no further evolution due J coupling can be observed.[33] Here we take advantage of this effect, however, the gradient for encoding the spatial information needs time. This adds a lower limit to TE_2 depending on the desired resolution and field of view.

Stability of the echotrain

The use of an echo train questions, whether the magnetization is stable enough and artifact free images can be acquired. The MRI (Magnetom Sonata, Siemens, Erlangen) machine will be able to play out the fully balanced gradient scheme without major derivations. The most important remaining error source are imperfect refocusing pulses.

The density matrix after a spin echo scheme at optimal echo time shows its effect:

$$\rho_{\mathrm{TE}_1} = \cos(\beta)\left(\frac{I_{1,y}}{4} + \frac{I_{2,y}}{4}\right) + \frac{1}{2} I_{1,x} I_{2,x} + \tag{3.13}$$

$$\sin(\beta)\left(+\frac{I_{1,z}}{4\sqrt{2}} + \frac{I_{2,z}}{4\sqrt{2}} - \frac{I_{2,x} I_{1,y}}{2\sqrt{2}} - \frac{I_{1,x} I_{2,y}}{2\sqrt{2}}\right) \tag{3.14}$$

$$\left(\frac{1}{4} + \frac{\cos(2\beta)}{4}\right) I_{1,z} I_{2,z} \tag{3.15}$$

$$\rho_{\mathrm{TE}_1} \overset{\beta=\pi}{=} \frac{1}{4}\left(I_{1,y} + I_{2,y}\right) + \frac{1}{2} I_{1,z} I_{2,z} + \frac{1}{2} I_{1,x} I_{2,x} \tag{3.16}$$

The first line shows the two operators used for imaging $I_{1,y}$ and $I_{2,y}$. If the $180°$ degree pulse is not perfect a part of this magnetization will be transformed into different operators (see second and third line). For a two pulse experiment the imperfect refocusing pulse diminishes the observable signal. The imperfect pulses in the echo train will now cause additional rotations on this density matrix and the number of unwanted terms in the density matrix will grow fast. If only one echo time was used in the sequence a steady state will form after several pulses [37], but here the first echo times are different. The phase graph approach could reveal more details, but its not yet developed for a coupled multi spin system. The resulting images will show whether the system can establish a steady state or not.

Complete imaging sequence

According to these considerations the imaging sequence "dual echo time fast spin echo" (deFSE,see figure 3.20 on the facing page) was designed, consisting of two blocks:

- Get the maximum possible transversal magnetization by generating a single spin echo with echo time $\mathrm{TE}_1 = \frac{1}{2J}$ and $\alpha = 45°$.

- Acquire all lines under very stable conditions by generating a spin echo train with a very short echo time TE_2.

Besides the frequency, phase and slice encoding gradients (Gx, Gy, Gz), the sequence contains additional gradients left and right of the $180°$ pulses. These gradients are called crusher gradients and are required to remove FID components after imperfect $180°$ pulses. [26]

3.4.1 Variation of first echo time

Thermally polarized sample

First, the dependency of the first echo time TE_1 was investigated. Figure 3.21 on the next page shows the time evolution of thermally polarized 2-hydroxyethylacrylate. Each point stems from a new experiment with sufficient time ($5 \cdot T_1$) in between the experiments. The first echo shows the highest signal intensity of 3.2 since here very little time evolution took place. With increasing echo time TE_1 the signal falls down till 0.8 with additional small modulations. These stem from all the J couplings present in the thermally polarized molecule.

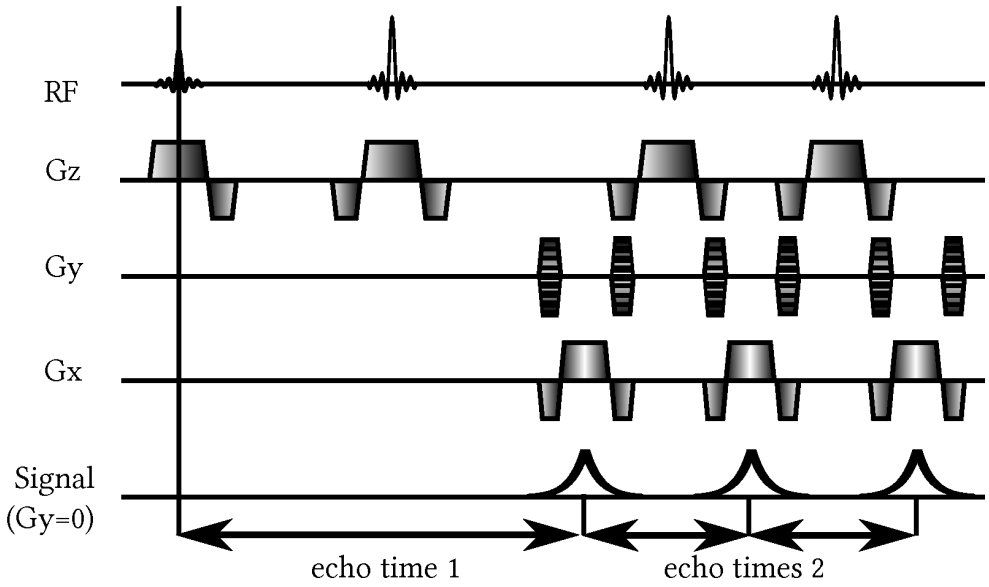

Figure 3.20: Pulse diagram for a deFSE sequence. After the slice selective excitation a first echo is generated at TE_1 where the central kspace line is recorded. This is followed by the acquisition of the remaining lines of the kspace in a echo train with echo time TE_2. Multiple images can be acquired by repeating the echo train for one image seamlessly (details see Appendix 7.4 on page 101).

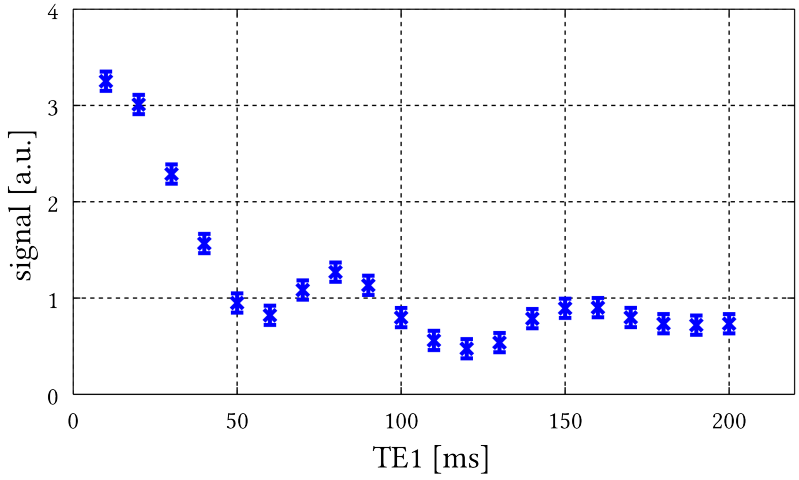

Figure 3.21: Signal of the first echo for different TE_1 at thermally polarized conditions. The signal shows a decay from 3.2 down to 0.8 with additional oscillations stemming from all present J couplings involved in 2-hydroxyethylacrylate. The noise level of $(3.2 \pm 0.1) \cdot 10^{-4}$ a.u. is not visible in this scaling. Data were acquired using a centric reordered deFSE sequence, flip angle: 45°, echo time 1: variable, presented data point correspond to the center of kspace.

Hyperpolarized sample

The hyperpolarized molecule 2-hydroxyethylpropionate shows a completely different behavior compared to the prior thermally polarized case (see figure 3.22). Minimal signal is recorded for the shortest echo time of $TE_1 = 3\,ms$. The signal rises until an echo time of $TE_1 = 20\,ms$. Besides a small dip the signal stays on this high level until an echo time of $TE_1 = 35\,ms$ and falls down towards the initial signal level until $TE_1 = 60\,ms$. The theoretical simulation were performed with SIMPSON[38] and include a flip angle distribution of 20%.

The experimental results match the simulations, even the small dip at 25 ms was reproduced within the errors. The results differ from a perfect sinusoidal shape because here five protons ($CH_3 - CH_2-$) are involved. This leads to a splitting of the peaks and one triplet and one quartet are formed, showing additional oscillations with 2J and 3J. The three evolutions overlap, forming the simulated time domain data.

In comparison to the highest thermal signal of 3.2, here a hyperpolarized signal up to 127.3 a.u. was achieved.

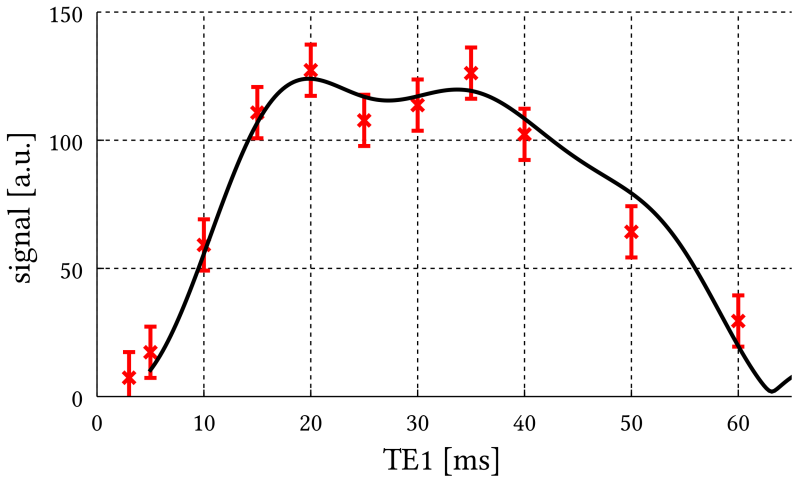

Figure 3.22: Signal of the first echo for different TE_1 at hyperpolarized conditions (red points). Theoretical time evolution (solid black line) for this spin system. The signal recorded here show much higher amplitude than the thermally polarized ones (see figure 3.21). The noise level of $(3.2 \pm 0.1) \cdot 10^{-4}$ a.u. is not visible in this scaling. Data were acquired using a centric reordered deFSE sequence, flip angle: 45°, echo time 1: variable, presented data point correspond to the center of k-space.

3.4.2 Imaging with deFSE sequence

The previous section demonstrated how to generate maximal transversal magnetization. This alone does not guarantee successful imaging, the amount of magnetization needs to be kept constant as well. The effect of a long echo train was investigated by acquiring six

images in one single echo train. In the following section the images acquired at different TE_1 are presented.

Images within the echo train

A single combination of $TE_1 = 20\,\text{ms}$ and $TE_2 = 3.5\,\text{ms}$ is presented generating six subsequently acquired images in one single echo train. While the first image shows the highest SNR of 40000 it also shows strong artifacts in phase encoding direction. The underlying signal in the echo train is not constant because of the inhomogeniety of the $180°$ pulse. Therefore additional magnetization is rotated from the z direction into the transversal plane. The second image already shows less artifacts but also significant less SNR. The last image acquired $668\,\text{ms}$ after the excitation pulse still shows 20000 SNR units.

Despite the high SNR the first image is not useful because of the strong artifact. The $180°$ pulses were not accurate enough, leading to a constant mixing between transversal and longitudinal magnetization within the echo train. After the first image was acquired (36 refocusing pulses were played out) the system has reached a state stable enough to provide images of very good quality. The last image was acquired more than half a second after the initial excitation pulse and still shows significant hyperpolarization (this last image is shown in figure 3.24 on the next page with adequate windowing). This demonstrates that this hyperpolarization can be preserved over a long time.

The fast pulse limit stated above is not strictly met here: $J \cdot \text{TE}_2 = 0.03 \wedge \Omega \cdot \text{TE}_2 = 0.3$. Especially the product of chemical shift difference and echo time is not very small compared to 1. However, it is sufficient to stop the evolution due to J coupling.

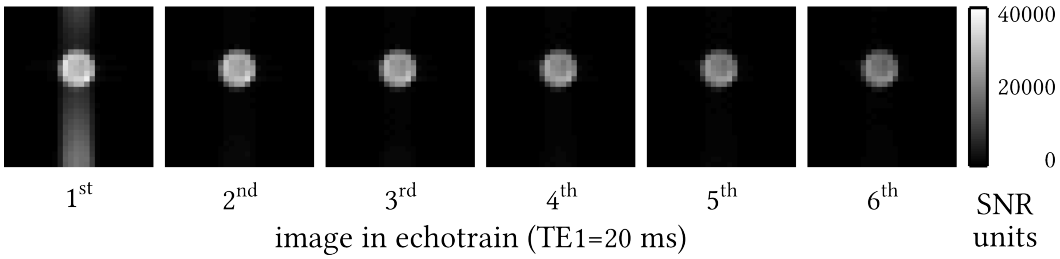

Figure 3.23: Images generated within a echo train with hyperpolarized 2-hydroxyethyl-propionate. A fixed set of $TE_1 = 20\,\text{ms}$ and $TE_2 = 3.5ms$ was used. The magnetization during the first image was not stable leading to artifacts, later images show almost no artifacts (see 3.24 on the next page for propper scaling). Imaging was performed using a centric reordered deFSE sequence, flip angle: $45°$, time per image: $126\,\text{ms}$, echo time 1: 20 ms, echo time 2: 3.5 ms, bandwidth: $1375\,{}^{\text{Hz}}/_{\text{pixel}}$, matrix size: 36×36 (presented: 30×20), phase encoding: up-down, resolution: $1.36\,{}^{\text{mm}}/_{\text{pixel}}$, crusher gradients: $40\pi\,/_{\text{voxel}}$ and slice thickness $10\,\text{mm}$.

Images at different TE_1

Now the images acquired with different TE_1 are presented (see figure 3.24). As a result of the previous section the last (6^{th}) image of the echo train are presented. The upper images show the hyperpolarized images ranging up to to 20000 SNR units. The signal shows an oscillation with a minimum starting from $TE_1 = 3$ ms, a maximum at $TE_1 = 20$ ms and minimum at 60 ms. The images are of good quality showing almost no artifacts in phase encoding direction. The images in the bottom are acquired under thermally polarized conditions but the first image of the train is presented, thus more artifacts are present in both directions.

The signals from the hyperpolarized sample follow the signal shape of figure 3.22 on page 48. Images of high quality and good SNR can be generated even with the 6^{th} image in the train.

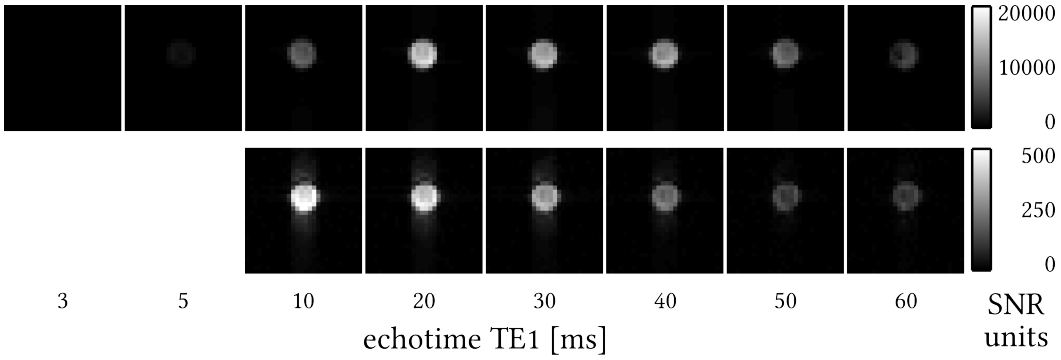

Figure 3.24: Signal intensity in dependency of TE_1 for hyperpolarized 2-hydroxyethyl-propionate (top) and thermally polarized reference (bottom). The hyperpolarized images follow the J coupling evolution. Imaging was performed using a centric reordered deFSE sequence, flip angle: $45°$, time per image: 126 ms, echo time 1: variable, echo time 2: 3.5 ms, bandwidth: $1375\,{}^{\text{Hz}}/_{\text{pixel}}$, matrix size: 36×36 (presented: 30×20), phase encoding: up-down, resolution: $1.36\,{}^{\text{mm}}/_{\text{pixel}}$, crusher gradients: $40\pi\,/_{\text{voxel}}$ and slice thickness 10 mm.

3.4.3 Discussion

These experiments demonstrate that the dual echo time fast spin echo sequence can be used to generate artifact free images with high SNR. Since several images can be acquired in the same echo train, averaging techniques can be used to generate even higher SNR values. A variation of the first echo time leads to massive signals. The dependency on TE_2 was not studied but a minimal time was chosen with respect to the field of view and resolution. However, the magnetization in the echo train is robust (even though

a flip angle inhomogeneity of 20% is predicted for the 180° pulses) and can be used to acquire at least six images, where only the first images shows severe disturbances. The optimal echo time can be determined by investigating the J evolution e g. hyperpolarized 2-hydroxyethylpropionate shows a wide maxima for $\mathrm{TE}_1 = \frac{1}{2 \cdot 2J}$.

3.5 Contrast against thermal background

In all experiments presented here the hyperpolarization could be identified by its strong signal. However, this method can fail if the amount of substance has to be reduced, or if the hyperpolarization process is less effective.

If the hyperpolarized compound and the thermal background have the same T_2^* or T_2 values and the amount of hyperpolarization is equal or even smaller than the initial thermal polarization, we encounter the most disadvantageous situation, and recording a single image is not sufficient to generate sufficient contrast.

A more universal method is needed to unambiguously identify regions containing hyperpolarized fluid. As is well-known in MRI, contrast can be improved by taking differences of images recorded under different conditions.[39,40] In our case it is sufficient to simply acquire two images with different echo times and the antiphase hyperpolarized character of the hyperpolarization is exploited: For both sequences two images with specific echo times can be chosen such that the hyperpolarization shows minimal signal and the thermal polarization shows maximal signal (TE_a) and vice versa (TE_b).

A subtraction image of both images ($I(\mathrm{TE}_b)$ - $I(\mathrm{TE}_a)$) will lead to negative values at the places of thermally polarized substance and positive signal values at places where hyperpolarization is located. Note that the procedure relies on the fact that while the PHIP signal increases due to the J-coupling evolution, the thermal signal decreases. This choice of echo times for the subtraction allows the signal originating from hyperpolarization to appear positive. Signals from the thermal background, however, will be always negative, as polarization decays over time with T_2^* or T_2[3]. This allows for unambiguous differentiation of both kind of spins.

3.5.1 Gradient Echo Sequence

The subtraction images of the gradient echo images with hyperpolarized 1-Hexene and 2-hydroxyethylpropionate are presented in figure 3.25 on the following page.

In both cases a clear separation of the two signals is achieved. Since for these images the phantom exhibiting a favorable T_2^* was used this clear separation was expected. The hyperpolarized areas are clearly positive (6000 and 3000 SNR units) and the thermally

[3] Again, the hyperpolarized signal is of course also subjected to these relaxation parameters.

polarized areas are -2000 and -1000 SNR units.

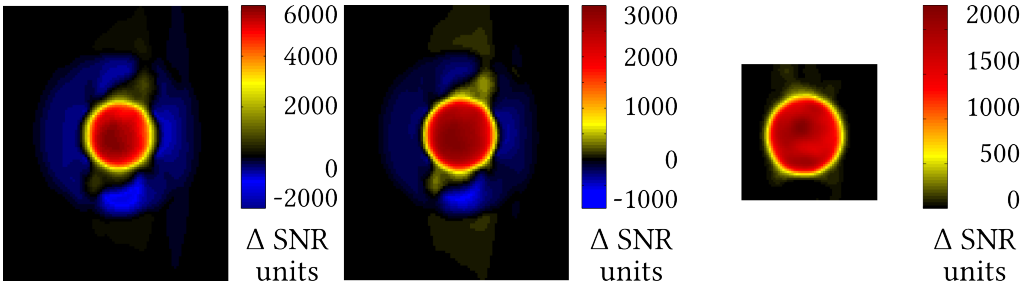

(a) Hyperpolarized 1-Hexene and thermally polarized water: Image at echo time 15 ms subtracted from image at echo time 10 ms (images at figure 3.11 on page 37).

(b) Hyperpolarized 2-hydroxyethylpropionate and thermally polarized water: Image at echo time 15 ms subtracted from image at echo time 6 ms (images at figure 3.14 on page 39).

(c) Hyperpolarized 2-hydroxyethylpropionate and thermally polarized solvent at the same location: Image at echo time 15.1 subtracted from image at echo time 11.5 (images at figure 3.18 on page 43)

Figure 3.25: Subtraction GRE-image of hyperpolarized PHIP compounds at favorable echo times. Separation of area with thermally polarized protons (blue) and area with hyperpolarized protons (red) can be achieved by considering the signal sign.

3.5.2 Spin Echo Sequence

The hyperpolarized and thermally polarized spin echo sequence images were acquired in different experiments, but under the same conditions therefore both are put in one image (see figure 3.26).

Signal values for the hyperpolarized area range up to 10000. The thermal areas show signal down to -500. A clear separation of the two areas can be realized with these deFSE subtraction images.

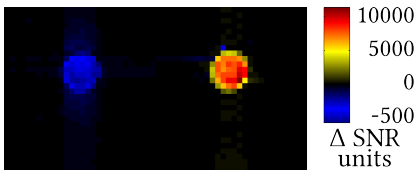

Figure 3.26: Subtraction deFSE-image: Hyperpolarized 2-hydroxyethylpropionate and thermally polarized water at $TE_{1b} = 20$ ms and $TE_{1a} = 10$ ms. Note that the color bar is not symmetric but ranges from -500 to 10000.

3.5.3 Discussion

The very high SNR of hyperpolarized substances is sufficient to generate an excellent contrast in the difference images (3.25(a) to 3.25(b) on this page and 3.26) even with the

drawback of the thermally polarized substance contributing small negative values to the same voxel (3.25(c) on the facing page) if both substances are mixed.

The high and stable amount of hyperpolarization achieved in the experiments shown here allow for a drastic reduction of the concentration of the hyperpolarized compound. The limit for this method is of course reached when the signal intensity in the hyperpolarized area is comparable to the noise of the images. For the case of the hyperpolarized and thermally polarized substances occupying the same volume a differentiation by sign is obviously not longer possible and the condition of the hyperpolarized signal being higher than the thermal signal must be fulfilled to generate e.g. a contrast to more distant parts of the body.

The acquisition of two images instead of one is of course a drawback for in vivo MRI because co-registration problems could occur. However, this is also true for MRI of ^{13}C hyperpolarized substances where co-registration with a proton image is needed to provide anatomical information. Moreover for the gradient echo sequence, this problem can be easily solved by applying a multi-echo sequence and subtracting two images with different echo times.

3.6 Comparison between Gradient and Spin Echo Sequences

Both imaging sequences presented, the gradient echo and the dual echo time fast spin echo sequence, are very suitable for imaging of antiphase hyperpolarization. There are distinct differences because both sequences function in different ways:

***In vivo* application** The *in vivo* application of the gradient echo sequence is expected to be possible without security concerns. The energy deposition of the rf pulses and the (neural) stimulation level of the gradients are within the safety limits. Additionally the timing is in a region where most parameters can be modified without exceeding these limits. Furthermore the product sequence of the vendor can be used for these experiments.

The deFSE sequence operates close to the safety limits, thus even small changes in any parameter can be problematic. Depending on the geometry the parameters have to be adjusted carefully. In the case of deFSE no certified product sequence exists, leaving the responsibility for the safety of this sequence in the hands of the programmer.

Optimal echo time The optimal echo time for the GRE depends on the chemical shift[4] and J coupling, where the optimal echo time for the deFSE is determined by J coupling only. This is an advantage for the deFSE because less minima occur with in the available

[4] and therefore also on the resonance frequency of the NMR/MRI system

transversal magnetization. However, if distinct minima are wanted the gradient echo sequence should be favored.

Flip angle The GRE requires low flip angles to save sufficient magnetization for all k-space lines. The deFSE can use a maximal flip angle because of the echo train. Here the deFSE sequence has an advantage because more signal can be used for imaging.

Weighting The images of the GRE are T_1 weighted, because each excitation uses the magnetization stored in longitudinal direction. Additionally the relaxation due to T_2^* is important depending on the chosen echo time. The signal in the deFSE is subjected to T_2 relaxation. Depending on the relaxation constants one or the other sequence may be advantageous.

Bandwidth per pixel The bandwidth per pixel has lower limits for both sequences. In case of the GRE it should be as high as possible because otherwise the oscillations will introduce unwanted k-space weightings. The deFSE sequence should always operate in the fast pulse limit and therefore the bandwidth per pixel can only be high anyway. However, a high bandwidth per pixel results in smaller SNR values in the resulting image.

Resolution and FOV The GRE has fewer limits for the resolution and FOV, because the optimal echo time will typically lies beyond $5\,\mathrm{ms}$. A modern MRI scanner will have enough time to play out the required gradients. Of course the flip angle has to be decreased with higher resolution in phase encoding direction.

The deFSE in contrast has a fixed time for the echo train of typically less than $4\,\mathrm{ms}$. Within this time a fully balanced gradient scheme has to played out together with additional crusher gradients. Here the limits of the system can be easily reached. Clearly the GRE sequence has an advantage here.

Signal to noise The signal to noise ration depends on all the points stated above, but it depends mainly on the available hyperpolarization. This is strongly connected to the flip angle and therefore the deFSE sequence leads to higher signal to noise ratios.[5]

Number of images When using a GRE sequence the available magnetization has to be used carefully. Thus, if multiple images (at the same echo time) are demanded the flip angle has to be reduced drastically. The deFSE sequence can acquire multiple images in a single echo train, which can be averaged to lead to even higher SNR values.

[5] It is not possible to conclude this from images presented here, because different coils were used!

Contrast to thermally polarized substance Since both contrast mechanisms relies on the antiphase character the subtraction method can be applied to both imaging sequences. The deFSE sequence might have an advantage here, because more hyperpolarization can be used for imaging. This can help if very little hyperpolarization is present. On the other hand, multiple echo times can easily be acquired with the gradient echo sequence and subtraction images are easier to generate. Also, with a gradient echo sequence a minimum for the subtraction image can be chosen because of the chemical shift.

PASADENA or ALTADENA All experiments presented for the two sequences were acquired under PASADENA conditions. When performing the hyperpolarization process under $45°$-ALTADENA (see section 2.2.2 on page 9) conditions no antiphase doublets are present but the two peaks (from the two protons) are $180°$ dephased. In such a system no J couplings of the hyperpolarized components is visible. But still the signal will show zero intensity for very short echo times.

The proposed work flow for gradient echo images does not change: First find the maxima inside the FID, then choose the optimal echo times.

The use of a spin echo sequence will lead to problems: The refocusing of the chemical shift leads to zero signal at any echo time. With the readout centered around this minimum severe imaging artifacts will arise. However, when the readout is positioned asymmetric in the echo artifact free images might be achieved.

3.7 Conclusion

In this chapter a successful method for exploiting the hydrogenative PHIP antiphase hyperpolarization as a contrast agent in MRI experiments is presented. A subtraction image is used and a separation by sign is achieved where the thermal polarization ranges down to -500 in the worst case and the hyperpolarization ranged up to 2000 in the worst case. Unless the relaxation times are extremely small ($< 20\,\mathrm{ms}$) this method can always be applied.

The signal of the molecules could be reduced by one order of magnitude and the area in the subtraction images could still be clearly identified. This reduction would allow a concentration of $0.15\,\mathrm{mmol/kg}$. Mansson et al.[6] used a concentration of $0.15\,\mathrm{mmol/kg}$ for $^{13}\mathrm{C}$ *in vivo* imaging. But here, in the case of proton imaging, no hetero nuclei coil is needed and still a unambiguous differentiation can be achieved.

Two different types of imaging sequences can be used to render the contrast: a gradient echo and a spin echo sequence. Gradient echo sequences are easier to handle because it has fewer limitations. Also, this sequence was expected to perform well for an antiphase hyperpolarization, because of the much simpler sequence design. The double

echo time fast spin echo is more complicated because it requires an echo train. However even with large flip angle inhomogeneities present, images from the second acquisition within the echo train were of good quality and high SNR.

The optimal echo time for both sequence is determined by the J coupling, and the chemical shift difference should also be included when using the gradient echo sequence. The optimal echo time can be obtained either by simulations or by simple experimental observation. The theoretical considerations were presented assuming an AX spin system, which is of course not applicable in most molecules, but the main results are still valid. Specifically J coupling optimized molecules could be designed to exploit maximum of contrast between thermal and hyperpolarized samples.

The spin echo sequence seems the most promising approach for future applications because multiple images can be acquired easily, which allows for a higher temporal resolution using the batch mode hyperpolarization. This can be especially interesting if using this hyperpolarization for perfusion measurements. Both presented sequences have different advantages and disadvantages as already discussed and - depending on the application - it is possible to choose the best.

Within this chapter a method was developed to exploit the character of the antiphase hyperpolarization of PHIP for imaging. A part of the question formulated in the introduction is answered:

> *Is it possible to perform proton MR-imaging experiments with PHIP hyperpolarized contrast agents, where a clear separation of background and contrast agent is possible* and the hyperpolarization is available continuously and ready for transport?

A small amount of molecules can now be differentiated from a large thermal background of the same nuclei, similar to hetero nuclei imaging which has some disadvantages such as necessary co-registration and additional hardware. The following chapters will deal with an optimization of the hyperpolarization process itself and will tackle the problem of delivery.

Chapter 4

Continuous Hyperpolarization with hydrogenative PHIP

Contents

The previous chapter addressed imaging of antiphase hyperpolarization on the proton channel and the contrast mechanism. Now the challenge remains to provide a method to overcome short T_1 relaxation times.

Hence, the basic idea presented here is to increase the surface for the liquid - gas interface, allowing for a very efficient self-driven delivery of parahydrogen into the liquid phase though diffusion. This is achieved by pumping the liquid through hollow fiber membranes. Now the liquid is not confined into a tube as in the chapter before, but can be transported rapidly into the MR magnet for experiments.

Due to this very fast delivery, shortly after generation of the hyperpolarization, only little relaxation can occur. Additionally averaging techniques are now available including the possibility to use very high flip angles.

In this chapter the experimental setup is presented in detail, together with the pitfalls that come with this special setup. Then spectroscopy experiments are performed with two sample compositions. One with higher catalyst concentration for large enhancements and one with low catalyst concentration for experiments with a prolonged

lifetime of the hyperpolarization. Additionally MRI images are presented for the signal enhanced experiments.

4.1 Theoretical considerations

In this chapter still hydrogenative PHIP is used in order to generate the hyperpolarization - just the way how exactly the hydrogenation is performed was changed. Therefore, the same considerations as found in the previous chapter are applicable here.

4.2 Experimental Methods

4.2.1 Precursor and catalyst

For this kind of experiments the water soluble precursor 2-hydroxyethylacrylate was used (see section 3.2.1 on page 29). The flow setup requires much more liquid, thus the sample composition was adjusted accordingly. The amounts of the required chemicals are now in the oder of gramm and not milligramms (see table 4.1).

Table 4.1: Composition of samples for hydrogenative PHIP experiments under continuous parahydrogen supply.

(a) for high signal (MRI Experiments)

Chemical	Amount
2-hydroxyethylacrylate	7.5 g
Rh(nor)(ppbs)BF_4	0.5 g
D_2O	180 ml

(b) for extended time (spectroscopy)

Chemical	Amount
2-hydroxyethylacrylate	31 + 8 g
Rh(nor)(ppbs)BF_4	0.3 g
D_2O	100 ml

4.2.2 Generation of parahydrogen

In this setup a continuous supply of parahydrogen is required. The same apparatus as in section 3.2.2 on page 31 was used but in a mode that allows a delivery of 200 $^{ml}/_{min}$ of 90% parahydrogen.

4.2.3 Generation of hyperpolarization via hollow membrane fibers

Here, a hollow fiber membrane module (Membrana, SC, USA) is used that allows the shaking process to be replaced by a diffusion driven process. These modules were originally designed to degas a liquid, but the reverse process of possible too. Roth et al.[22] used the hollow fibers to transport the parahydrogen, but in this chapter the outer area of the membrane module is filled with parahydrogen (see figure 4.1 on the next page), which can diffuse into the liquid by passing through the hollow fiber membrane. The liquid is

pumped through the hollow fiber membrane and contains subsequently parahydrogen for the PHIP reaction. After leaving the membrane module the fluid is hyperpolarized and flows towards the MR receive coils. In principle no outlet for the gas phase of the membrane module is required, because parahydrogen is simply consumed. However, the generator supplies parahydrogen with a minimal pressure of 6 bar and the experimental setup was only able to withstand a pressure of up to 4 bar over a long time. Therefore, the parahydrogen outlet valve was adjusted such that the pressure inside the module was kept below 4 bar.

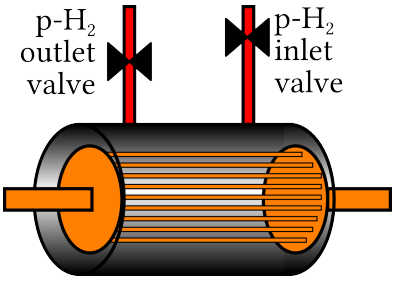

(a) Schematic drawing

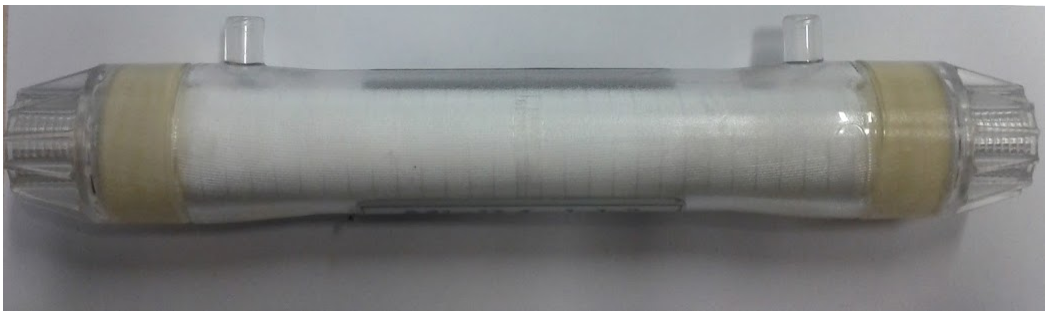

(b) Photo: The hollow fiber membranes are directed from left to right and are fixed with glue. The in- and outlet for the fluid can be equipped with Luer adapters.

Figure 4.1: Hollow fiber membrane module used for these experiments (Membrana, SC, USA). The liquid enters from the left and flows though the fibers. The parahydrogen is supplied from the top and fills the whole gas space (gray) of the module

4.2.4 Experimental Setup

The setup consists of a closed circular flow system equipped with a membrane pump, the hollow fiber membrane module, a detection chamber and a reservoir. The membrane module is placed in a water bath for heating to provide high reaction rates (see figure 4.2 on the following page). The parahydrogen outlet of the generator is directly connected with the module. The detection chamber was a Festo™ tube of 8 mm diameter. The tubing and connector of the system were typically 3 mm Festo™ tubes.

The module was placed in the stray field of the 4.7 Tesla MRI machine[1], thus the experiments were performed under ALTADENA conditions at 0.05 Tesla. The receiver gain was adjusted to make optimal use of the 16 bit register of the receiver (-32.768 till 32.767). Signal values of up to 15.000 were recorded and noise values up to 1000, allowing the display of the images in SNR representation. All components - including the pump - of this setup can be placed anywhere in the stray field since no magnetic parts have been used.

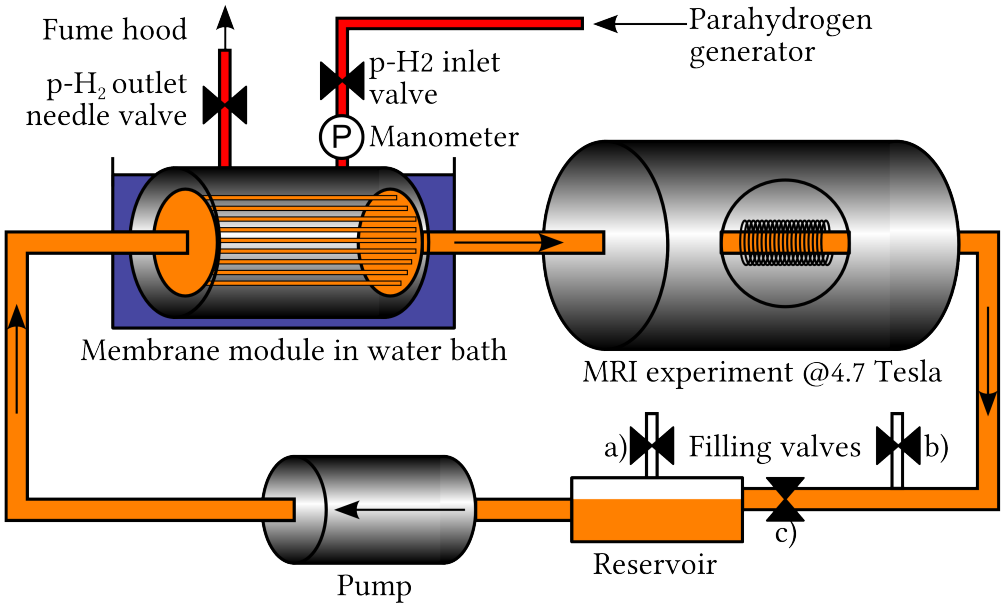

Figure 4.2: Circular flow setup for continuous supply of parahydrogen. The pump transports the fluid though the membrane module (@0.05 Tesla) in which the fluid is heated by the surrounding water bath. Parahydrogen is continuously supplied from the generator. The hyperpolarized fluid leaves the module and NMR experiments are performed inside the magnet. The reservoir helps avoiding bubbles inside the system.

Filling the setup with chemicals

Prior to any experiment the system was tested for pressure tightness by applying 7 bar of nitrogen gas. The system was considered tight when no pressure decay greater than 0.05 bar was detected within 2 minutes.

Afterwards the chemicals were filled into the system under exclusion of oxygen: After flushing the system for around 30 seconds with N_2 the pressure was reduced to 0.5 bar. In oder to fill the liquid into the system valve c was closed and the fluid was filled into the system through valve a. After each filling step pressure was released through valve b by a syringe. The filling was stopped when the reservoir was filled completely.

[1]Horizontal bore magnet and MARAN console, Oxford Instruments(UK)

Starting the experiment

The pump ($50\,{}^{\text{ml}}/_{\text{min}}$) was switched on until no gas bubbles entered the reservoir anymore. After opening the parahydrogen supply hyperpolarization can be available. However, before experiments can be performed the pressure inside the flow system has to be adjusted to 3.7 bar via the parahydrogen outlet needle valve.[2] The MRI/NMR experiments can be started at any time, but the system needs some time to reach a equilibrium of temperature and pressure. Also remaining N_2 gas will be flushed out over time.

Detection

The fluid leaves the membrane module in a hyperpolarized state. Until it reaches the detection chamber it is subjected to T_1 relaxation whereas the thermal polarization is typically following a T_1 build up. During the time $t_{\text{transport}}$ the fluid is transported though a magnetic field gradient from 0.05 Tesla to 4.7 Tesla. Thus, directly after the hyperpolarization at time $t = 0$ the magnetization of the protons M_H^i is subjected to a exponential decay with T_1 until thermal equilibrium M_T is reached. The relaxation T_1 is again depending on the actual magnetic field strength that changes with time:

$$\text{Signal} \propto \sum_i^{\text{all protons}} \int_{t=0}^{t_{\text{transport}}} M_T^i - (M_T^i + M_H^i) \cdot \exp\left(-\frac{t}{T_1^i(B(t))}\right) \cdot dt \tag{4.1}$$

$$\overset{M_H >> M_T}{\approx} \sum_i^{\text{all protons}} \int_{t=0}^{t_{\text{transport}}} M_H^i \cdot \exp\left(-\frac{t}{T_1^i(B(t))}\right) \cdot dt \tag{4.2}$$

$$= \text{Signal}(t_{\text{transport}})$$

However, the position of the connection tube between module and MR coil was changed and no signal change was observed. Therefore - within this setup - the signal was independent of the exact path through the magnetic field. The position of the module matters, because of the small velocity of the fluid in it. Within the here presented field strengths, no T_1 build-up or decrease can be observed.

Therefore, when seeing signal changes by moving the membrane module, it is not due to changed relaxation constants or changed pathways.

Safety concerns about this setup

Compared to the shaking experiments in the previous chapter, these experiments are more complicated.

[2] This pressure was chosen, because is is half of the tightness testing pressure. This assures that no bursting of tubes can occur.

- Parahydrogen was supplied to the experiment with a rate of $200\,^{\mathrm{ml}}/_{\mathrm{min}}$. No leakage should occur because none of the electric components (gradient system, coils, control units, amplifier etc.) was explosion protected.
- The chemicals should not have contact with ambient air. First to protect the health of the experimentators and second to protect the integrity of the catalyst.
- The 2-hydroxyethylacrylate shows the tendency to polymerize when not treated very carefully.
- The connections from the membrane modules to the tubes showed the tendency to leak - especially when heated.

A careful checking and testing of the system must be performed prior to any experiment. Additionally to the necessary caution required here the experiment is time-limited. As soon as all precursor is consumed the experiment must be finished. This adds an extra difficulty to the experiments.

4.3 Spectroscopy

The hyperpolarized signals from this setup differ from the ones in the previous shaking experiments not because of the membranes used but mainly because of the different field strengthens (see figure 4.3 on the next page). The reaction takes place permanently at 0.05 Tesla and detection occurs at 4.7 Tesla. An ALTADENA signal pattern is observed where the two hyperpolarized protons have an antiphase signal. This shows in the real part of the spectra as one positive peak and a negative and in the FID of this pattern shows as oscillation starting in a local minimum at time zero.

Discussion

The exemplary spectrum presented here shows that the membrane technology allows for high hyperpolarization with an ALTADENA peak pattern. The position of the membrane module can be changed easily to shorten the delivery time or change to PASADENA conditions. However, the heating bath did not fit inside the small bore of the 4.7 Tesla magnet and without heating the conversion rate is to low.

This method of generating hyperpolarization was exploited for imaging and spectroscopy experiments, which will be presented in the following section.

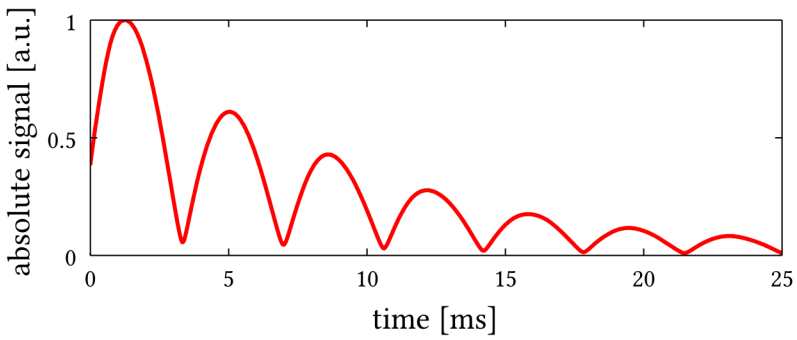

(a) FID of hyperpolarized 2-hydroxyethylpropionate

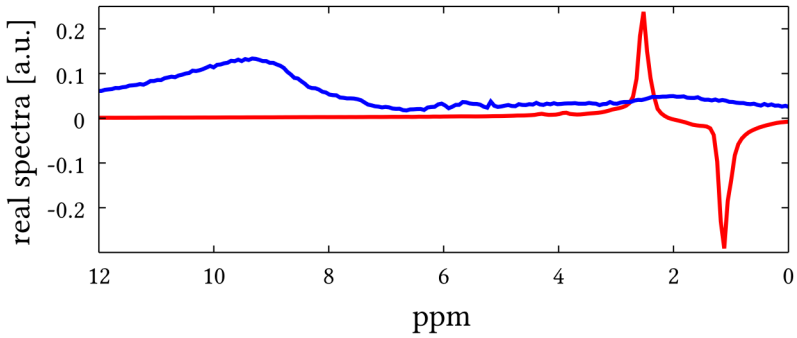

(b) Spectra of hyperpolarized 2-hydroxyethylpropionate and the and thermally polarized reference.

Figure 4.3: Signal of 2-hydroxyethylpropionate hyperpolarized by the membrane method. The module is placed in the stray field, leading to a ALTADENA PHIP reaction with two peaks in antiphase orientation (red). The signal from the thermally polarized fluid is scaled by a factor of 100 (blue).

4.4 Signal enhanced experiments and imaging

In these experiments the parameters where chosen such that a high reaction rate was achieved (as can be seen from the spectroscopic data in the previous section). The temperature of the water bath was set to $95\,^{\circ}$ that allows for a high conversion rate of the chemicals (see table 4.1(a) on page 58).

The enhancement[3] shows an increase as soon as parahydrogen is supplied to the system (see figure 4.4 on the following page). Due to the fast reaction conditions the hyperpolarization lasted only for approximately 2 minutes and MRI experiments were performed within this time. Figure 4.5 on the next page shows the acquired images of hyperpolarized 2-hydroxyethylpropionate. The thermal reference shows a maximal signal to noise of 8. The images under hyperpolarized conditions show SNR ratios starting from $20,000$ down till $2,500$. The optimal echo time of 4.9 ms was chosen to be constant

[3] not to be mistaken as "enhancement per proton". See section 2.4.3 on page 20 for further explanation.

for all images.

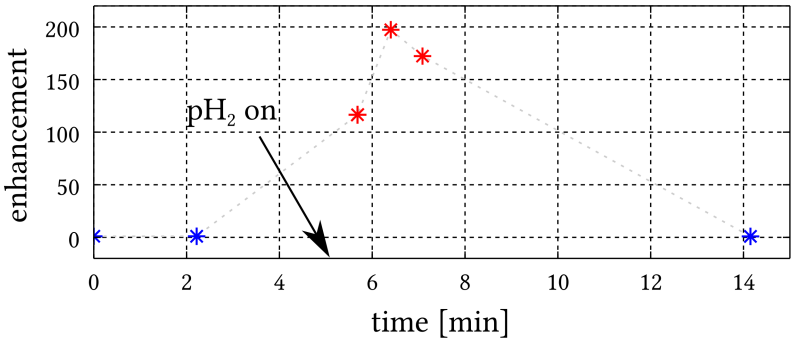

Figure 4.4: The enhancement over time shows significant enhancements but only over a short time period. When parahydrogen is supplied to the setup a instant rise of the enhancement is visible. After approximately 4 minutes all substrate was consumed by the reaction and only thermal signals can be observed.

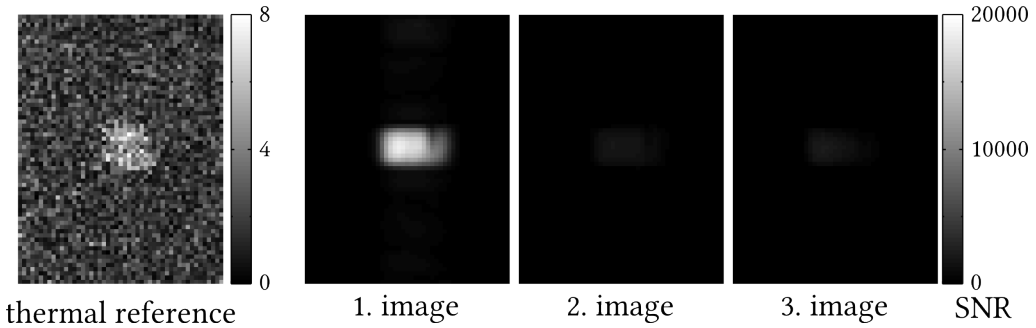

Figure 4.5: MRI Images acquired with hyperpolarized 2-hydroxyethylpropionate directly after the spectroscopic experiments in figure 4.4. A longitudinal slice orientation is presented showing the detection chamber from the side. The first image (left) is acquired without supply of parahydrogen thus showing the thermal reference. The first hyperpolarized image shows a very high SNR ratio. The signal decay arises because the substrate is hydrogenated and less 2-hydroxyethylpropionate is available for hyperpolarization. Imaging was performed using a linear ordered gradient echo sequence, flip angle: 45°, repetition time: 50 ms, echo time: 4.9 ms, bandwidth: 625 $^{\text{Hz}}/_{\text{pixel}}$, matrix size: 128×64 (presented: 32×64), phase encoding: up-down, resolution: 0.9 $^{\text{mm}}/_{\text{pixel}}$ and no slice selection.

Discussion

These experiments demonstrate that continuous imaging of an hyperpolarized fluid is possible. The membrane module offers the possibility to perform gradient echo imaging with high flip angles because new hyperpolarization is always supplied. The fact that the reaction ended very quickly is an indicator for a fast reaction and therefore a high

conversion rate.

The reaction rate was not determined but can be estimated to $5 - 7\%$[4]. This results in enhancement per proton of $\approx 2800 - 4000$ for these experiments.

Hydrogenative PHIP with high performance can best be realized in a linear flow system, where a big reservoir of substrate is available. In such a system molecules once hyperpolarized (and hydrogenated) would not be send though the membrane module again. In the following chapter the reaction conditions were changed to allow for longer observation of the hyperpolarization.

4.5 Measurements with extended experiment time

Here, a longer observation time of the generated hyperpolarization was intended, thus the temperature of the water bath was set to $80\,^{\circ}$ and a different mix of chemicals was chosen (see table 4.1(b)), where much more substrate and less catalyst were used.

The enhancement over time (see figure 4.6 on the following page) shows the result of these changes: The duration of the experiment increases significantly to cover several hours. After the acquisition of several thermal references (see first image of figure 4.7) the parahydrogen is supplied to the system. For the sake of clarity two figures are presented, one only containing the enhancement over the time and one containing representative spectra showing clearly whether a antiphase hyperpolarization was available. In both figure the color red indicates a antiphase hyperpolarization and blue the thermally polarization. So, a signal increase can be observed until 160 minutes (see image 2-4 in 4.7). The signal within the first 40 minutes has to be considered an initial phase. At the first drop of the enhancement the remaining nitrogen in the reservoir was vented. After this the pressure in the system was slowly building up and the enhancement increases slowly until a maximal enhancement is reached at 160 minutes. From 160 minutes till 210 minutes the signal decreases drastically and finished at an enhancement of 1. All precursor molecules are hydrogenated and only thermally polarized subtrate is present - therefore no hyperpolarization can be generated (see image 5 in 4.7).

The proof that neither a damaged catalyst nor a failure in the parahydrogen supply is the reason for this signal drop, is a new signal rise at 290 minutes when fresh precursor was injected into the system. A quick rise in signal intensity can be seen (see image 6 in 4.7). Unfortunately the membrane module started failing short after, thus the experiment was stopped and a last thermal reference was acquired (see image 6 in 4.7).

[4]The reaction rate in shaking experiments at 70 °C is always lower than 5%. Here, we will have at least this conversion rate: A heating bath of 95 °C was used, but at lower pressures.

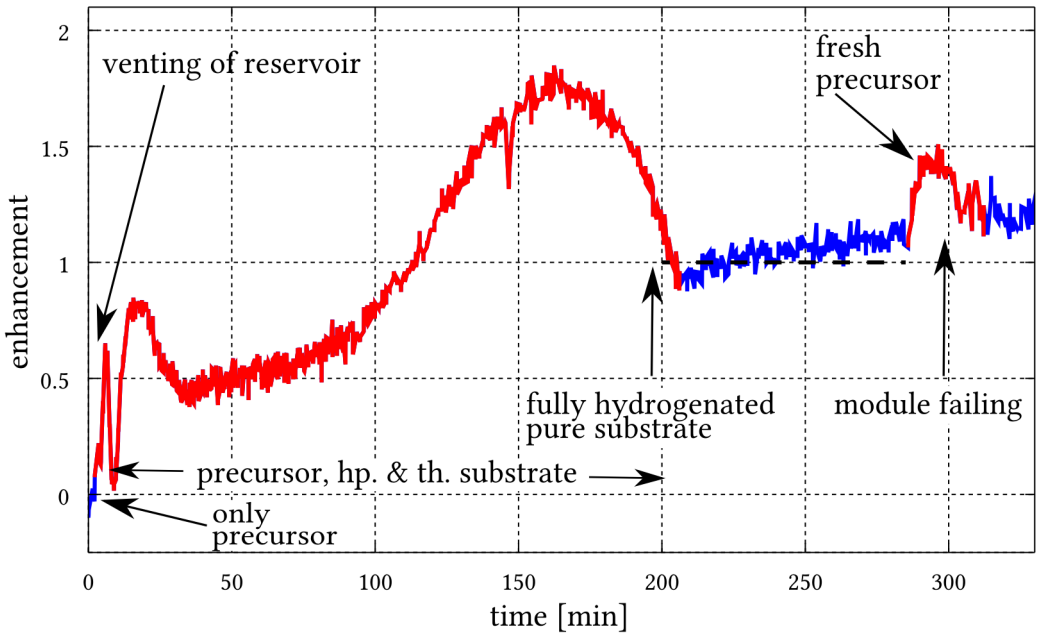

Figure 4.6: The enhancement over time calculated for all acquired spectra's (each 5 seconds one spectra). After an initial phase where nitrogen gets flushed out and a steady state of parahydrogen settles, the enhancement rises until a maximal enhancement of 1.75. After 200 min all substrate is hydrogenated and the enhancement level reaches 1. After a second injection of non-hydrogenated substrate the enhancement factor rises again, but due to a failing of the membrane module the experiment had to be stopped. From this figure alone it can not be concluded if a hyperpolarization was present, but it can be seen from the spectroscopy data itself (see figure 4.7 on the facing page).

Discussion

Clearly the duration of the experimental time was prolonged until hours. As a trade off the level of hyperpolarization was significantly lower. However, these experiments show that hyperpolarization with hydrogenative PHIP can be maintained with this specific setup over hours if the reaction conditions are set accordingly.

4.6 Conclusion

The use of membrane modules allows for a continuous generation of hyperpolarization. Depending on the reaction conditions such as temperature and pressure, a distinct conversion rate can be chosen and therefore an exact amount of hyperpolarization can be obtained.[5]

Here, two extreme cases were considered. One with very high conversion rate where high hyperpolarization was available only for a short time of 2 minutes. Another case

[5]The determination of the exact dependency was beyond the scope of this thesis.

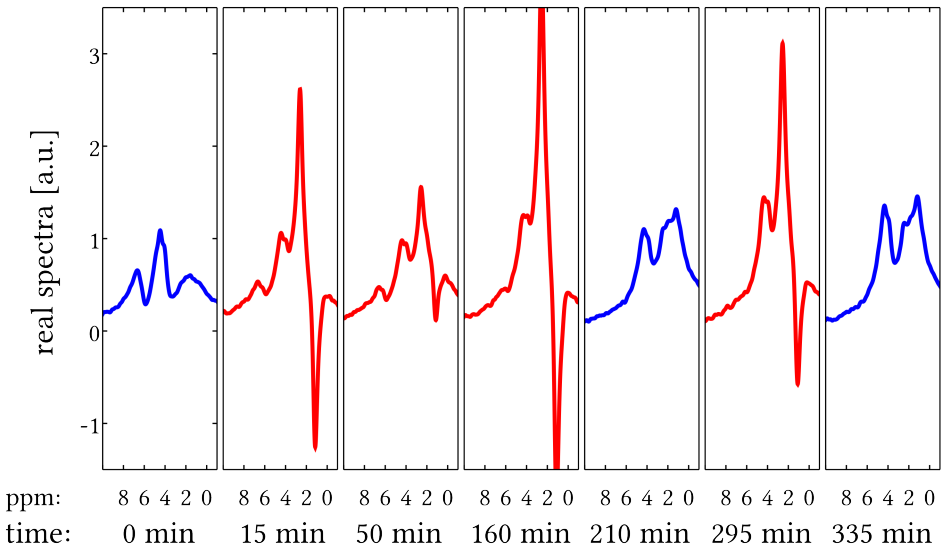

Figure 4.7: Spectra from different time points from figure 4.6 on the facing page. The first spectra is thermally polarized (blue) and only the precursor of the substrate is present. This results in a enhancement factor of zero. The second spectrum shows a clear antiphase signal and is therefore displayed in red as a sign for hyperpolarization. The contribution from the thermally polarized protons is still visible due to the small enhancement. After full hydrogenation the enhancement level reaches 1 since only thermally polarized substrate is present. The peak prior seen on the left ($6-7$ ppm) has vanished and a new peak on the right side has formed ($1-3$ ppm). A injection of precursor (290 min) leads to a instant rise of enhancement, clearly visible due to the antiphase character.

with different reaction conditions showing very low conversion rates exhibiting a hyperpolarized antiphase signal in the same order as the thermal peaks in the molecule but over a very long time. Depending on the desired application both methods can be feasible.

This approach increases the application of hydrogenative PHIP significantly: It is not necessary to work in a batch mode any more and large amounts of hyperpolarization are available. Experiments from Roth et al.[22] used the membrane modules, but the hyperpolarized fluid was confined within an NMR tube. Here, the hyperpolarized fluid could be taken directly from the outlet of the module and could be applied.

The technical requirements for this setup are very small compared to other hyperpolarization methods. The continuous supply of parahydrogen requires a custom setup or it can be bought commercially. The membrane module is commercially available too and in combination with plastic tubes the setup is extremely mobile and flexible. The parahydrogen can be supplied over a long tube (here 7 m) and the remaining parts of the setup are non magnetic, thus all of the components can be placed even inside the magnet. This setup will not allow such extreme reaction conditions as presented by Hovener et al.[41] where up to 10 bar parahydrogen can be used but their setup is also less mobile.

Within this chapter a method was developed to generate an antiphase hyperpolarization by continuous supply of parahydrogen. For a real continuous mode the precursor has to be supplied constantly. Also a transport of the hyperpolarized molecule from the place of generation into the place of detection was realized. The second part of the initial question has been tackled.

> Is it possible to perform proton MR-imaging experiments with PHIP hyperpolarized contrast agents, where a clear separation of background and contrast agent is possible *and the hyperpolarization is available continuously and ready for transport?*

The advantages of the hollow fiber membranes will also be exploited in the following chapter, by applying it to non-hydrogenative PHIP, allowing for real continuous experiments. Thus, a more detailed conclusion will be available there. This chapter shows only a limited amount of experiments, but proved that this simple setup works for hydrogenative PHIP and that it can withstand high temperatures and pressure over a long time.

Chapter 5

Continuous Hyperpolarization with SABRE

Contents

With the PHIP hyperpolarization method SABRE ("Signal Amplification By Reversible Exchange")[21,42] the full potential of the hollow fiber membrane technique will be available. The SABRE process allows for a transfer of the spin order of parahydrogen onto a substrate by contact on a catalyst. This leaves the chemical structure of the substrate unchanged allowing for very efficient hyperpolarization of the substrate. This process critically relies on the exchange rates of hydrogen and substrate. Both components have to reside long enough at the catalyst for the transfer to occur, but should not stay there until relaxation processes have reduced the polarization to a thermal level.

A experimental setup with membrane modules is very advantageous here because parahydrogen can be delivered efficiently and continuous hyperpolarization can be maintained. Furthermore the membrane module offer a efficient removal of the resulting orthohydrogen.

In this chapter the new method "Continuous hyperpolarization with SABRE" was explored and analyzed. The experimental setup, however, is basically the same as for the continuous hydrogenative PHIP experiments.

The following aspects are investigated: An example spectrum of hyperpolarized pyridine will introduce the characteristics of the SABRE hyperpolarization (see chapter 5.3 on page 72). Depending on the field strength where the spin order transfer takes place, different enhancement factors can be observed. First, this dependency is verified by results from literature (chapter 5.4.1 on page 74). Then sample composition is changed to match *in vivo* conditions and the efficiency and field dependency is checked again (chapter 5.4.2 on page 76). Afterwards, MRI experiments are performed at the optimal field strength (chapter 5.5 on page 77). Finally - starting on page 79 - the most important aspect of continuous hyperpolarization is presented: the enhancement over long times.

5.1 Theoretical considerations

In this chapter a different method for generating the hyperpolarization is used. Signal Amplification by Reversible Exchange (SABRE) transfers the spin order of parahydrogen onto a molecule without changing its chemical structure.[21,43] Only the nuclear spin states of the atoms inside the molecule are changed and therefore the molecule can be hyperpolarized again after the polarization relaxed to the thermal level. The remaining limiting factor for this kind of experiments is the supply of parahydrogen. With the help of hollow fiber membranes and a continuous parahydrogen generator SABRE can be performed continuously and efficiently. Experiments on a hyperpolarized fluid can be performed over hours depending on the robustness of the hollow fiber membranes.

When a SABRE experiment with pyridine at 70 Gauss is performed, its three peaks show a high negative enhancement (see figure 5.2 on page 73). The transversal magnetization will evolve with oscillations due to the different chemical shifts (Ω) involved. In contrast to the hydrogenative PHIP the magnetization will be maximal at time zero because all magnetization is in phase.

$$\rho = a \cdot I_x^{\text{para}} + b \cdot I_x^{\text{meta}} + c \cdot I_x^{\text{ortho}} \qquad a, b, c < 0 \tag{5.1}$$

$$\mathcal{H} = \Omega^{\text{para}} I_z^{\text{para}} + \Omega^{\text{ortho}} I_z^{\text{ortho}} + \Omega^{\text{meta}} I_z^{\text{meta}} \tag{5.2}$$

In this case MRI experiments can be performed as usual when spins with large chemicals shifts are involved: A short echo time will lead to high SNR in the images. Depending on the bandwidth per pixel the different peaks appear in the same voxel or they are spatially separated.

If an additional thermal polarization $+I_x^{\text{thermal}}$ with the same level of signal is in-

volved, the signal will be zero at the beginning of the FID. However, when the images are acquired with a low bandwidth per pixel the peaks will be separated spatially and a minimal echo time can be chosen. If it is desired that all spectral peaks are mapped at the same location a high bandwidth per pixel has to be used. This results in a short acquisition window and here the echo time is important for the signal intensity. The optimal echo time is where the transversal magnetization is maximal.

The SABRE hyperpolarization can have different features if the transfer of the spin order of parahydrogen occurs at a field different than 70 Gauss (here a optimal transfer of the spin order of parahydrogen onto the pyridine occurs due to chemical shift and J coupling evolution) or if a different catalyst and substrate is used. The spectroscopy and imaging results of this chapter are therefore limited to pyridine. But the results regarding the use of membrane modules are more general. Therefore the performance of the hyperpolarization with membrane modules was tested.

5.2 Experimental Methods

5.2.1 Substrate and catalyst

The SABRE process needs a substrate and a suitable catalyst to transfer the spin order of parahydrogen onto the molecule (see theory section 2.2.3 on page 13). In these experiments an Iridium-based catalyst together with pyridine was used (see figure 5.1).

The catalyst was activated prior to the experiments by bubbling hydrogen through the solution before the addition of deuterated water (see table 5.1 on the next page). After the color changed from yellow to transparent - indicating the activation of the catalyst - deuterated water was added and the filling of the flow setup commenced.

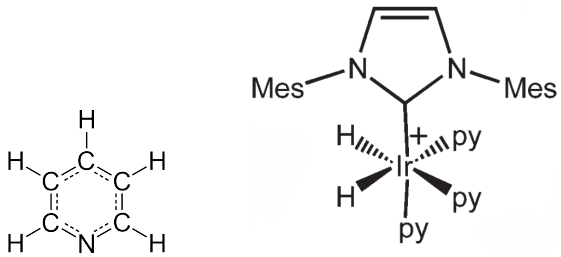

(a) Pyridine (b) Iridium catalyst

Figure 5.1: Chemicals for SABRE experiments.

Table 5.1: Composition of samples for SABRE experiments.

(a) SABRE with methanol

Chemical	Amount
Pyridine	0.1 ml
Ir(IMes)(cod)Cl	40 mg
Methanol (*d*6)	24 ml
D_2O	120 ml

(b) SABRE in pure water

Chemical	Amount
Pyridine	0.1 ml
Ir(IMes)(cod)Cl	40 mg
D_2O	120 ml

5.2.2 Generation of parahydrogen

The same commercial parahydrogen generator as for experiments in section 3.2.2 on page 31 was used.

5.2.3 Generation of hyperpolarization via hollow fiber membranes

SABRE converts parahydrogen to orthohydrogen to generate hyperpolarization. The membrane module is now needed for two tasks (see figure 4.1 on page 59). First to supply parahydrogen to the fluid and second to remove orthohydrogen from the fluid. If orthohydrogen can not be removed efficiently experiments will show poor enhancements because the fraction of parahydrogen in the solution will be reduced.

With the parahydrogen generator an 8-fold exchange per minute of the gas inside the membrane module can be realized. Orthohydrogen that diffuses from the liquid into the gas space will be removed quickly by the stream of parahydrogen. This allows for a high parahydrogen concentration in the whole system and excellent conditions for the SABRE process.

5.2.4 Experimental Setup

The experimental setup and filling procedure remained unchanged from that presented in chapter 4.2.4 on page 59 - except the heating water bath was not used. Now the membrane module could be moved freely within the stray field of the 4.7 Tesla magnet. Also, the hydrogen outlet is now mandatory for the experiments (see section 5.2.3).

5.3 Spectroscopy

First a single scan of the continuously hyperpolarized pyridine is presented to introduce the spectrum of the hyperpolarized molecule (see figure 5.2 on the facing page). The hyperpolarized pyridine peaks emerge between 7 to 9 ppm. They are inverted relative to the thermal peak of water and orthohydrogen between 4.5 and 5 ppm. The peak from the orthohydrogen at 4.7 ppm emerges from orthohydrogen dissolved in the solution.

In this experiment an enhancement of -300 ± 20 for the ortho peak of pyridine was achieved. The two other peaks show a smaller enhancement of -160 ± 20 (para) and -100 ± 20 (meta). The height of the peaks of pyridine will be investigated in section 5.4 on the next page and imaging with this underlying spectrum will be presented in section 5.5 on page 77.

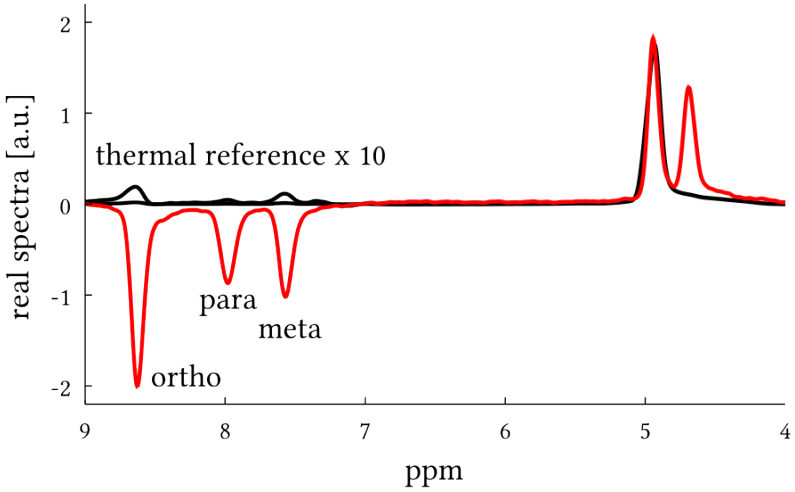

Figure 5.2: Spectrum of hyperpolarized pyridine (red) and corresponding thermal reference (black). Pyridine peaks are located between 7 to 9 ppm, residual water of the solvent (D_20) at 4.9 ppm, and orthohydrogen at 4.7 ppm. The hyperpolarization was generated at a field of 70 Gauss outside the spectrometer and detected inside at 4.7 Tesla.

Methanol was required for activation of the catalyst, so experiments with separate activation of the catalyst was performed to increase bio compatibility. Additionally shaking experiments with the same same compositions were performed: The enhancement factors achieved here were significantly lower than the enhancement factors generated by the hollow membrane fiber experiment.

Table 5.2: Best enhancement factors of pyridine at 70 G.

Enhancements	via shaking	via membranes
pyridine, catalyst, D_2O, methanol	-136 ± 19	-300 ± 20
pyridine, catalyst, D_2O,	-7 ± 2	-150 ± 10

Discussion

By using the SABRE method and hollow fiber membranes, pyridine can be efficiently hyperpolarized and large negative enhancements are achieved for the spin order transfer at 70 Gauss. The shaking method is not capable of generating comparable performance.

Most importantly it was shown that methanol is not necessary to produce an hyper-

polarization via SABRE and the catalyst can be activated prior to the experiments. However, the signal intensity is much lower compared to the experiments with methanol indicating only partial activation, but still high enhancement factors can be achieved. Here the membrane module can clearly show its advantages: Instead of a enhancement of -7 ± 2 obtained in a shaking experiment, an enhancement of -150 ± 10 is generated by the membrane setup.

Therefore it is feasible to relinquish from methanol in the composition of the sample. This step comes with several advantages for this experimental setup, because methanol dissolves the hollow membrane fibers and the tubing.

The absence of methanol and the use of pure water as solvent brings the SABRE method a big step closer to *in vivo* applications since methanol is not bio compatible.

5.4 Field dependency

The activation of the catalyst can be done either during the experiment by adding sufficient methanol to the solution. For better bio compatibility a activation prior to the experiments is necessary.

5.4.1 With methanol in the solution

The magnetic field at the place of the reaction has a crucial influence on the amplitude of the hyperpolarization.[42] The signal behavior of all three pyridine peaks was investigated by placing the membrane module at different locations in the stray field of the magnet. Each field value was observed over a time period of 10 minutes resulting in 60 acquired spectra. Figure 5.3 on the next page shows the normalized signal behavior of the ortho peak from experiments presented here as well as from literature (Cowley et al.[42], 100% methanol). The normalization of the best enhancement of the ortho peak to -1 allows to compare the two different sets of experiments.

The curves for the different peaks show the same behavior: A maximal (negative) signal is observed at 70 Gauss. For other field strengths the signal is smaller. The data acquired here are in good agreement with the data reported in literature.[42] There is one minor disagreement for the ortho peak at 60 Gauss and one major disagreement for the meta peak from 100 Gauss to 140 Gauss.

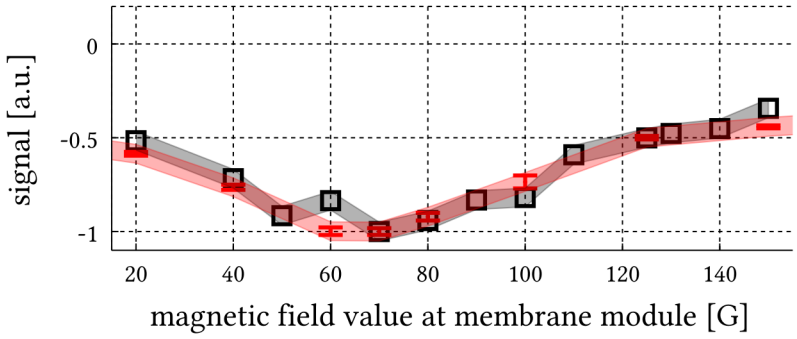

(a) ortho

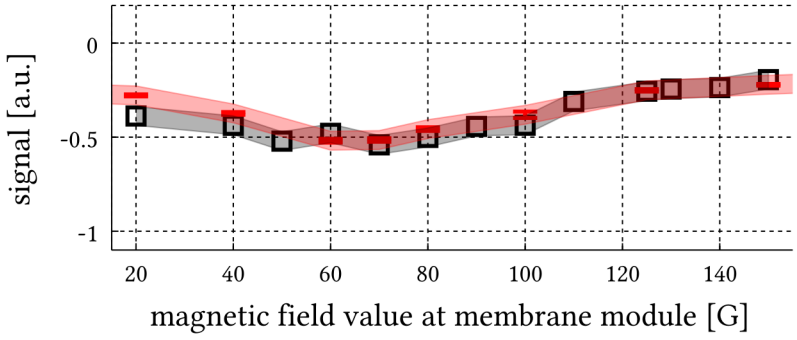

(b) para

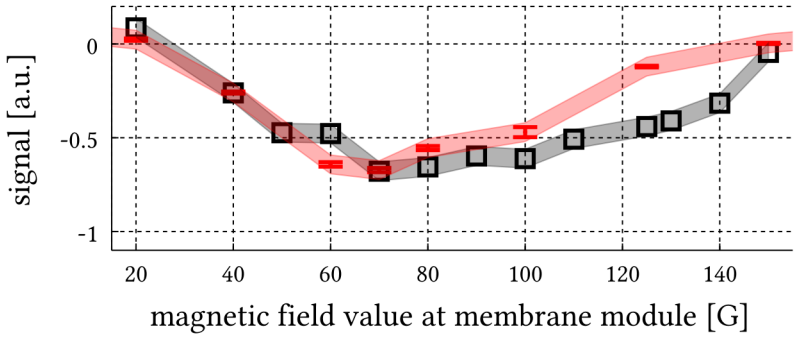

(c) meta

Figure 5.3: Field dependency of the SABRE hyperpolarization (red) compared to the literature (black, box). The data were normalized such that the ortho peak reaches a signal of -1 at 70 Gauss.

The error of the recorded spectra is small, but when comparing the different experiments, several other sources of errors have to be considered. The center of the module is placed at the indicated field strength, but the outer ends of the module can see significant gradients within the stray field (± 5 Gauss). The experiments in literature were performed with 100% methanol and in a more homogeneous field.

Discussion

The field dependency of SABRE hyperpolarization is in good agreement with the literature, although the experiments had different premises. The literature data were acquired in 100% methanol in a much more homogen field. A comparism with 100% methanol is not possible with the membrame technique because the the hollow fiber membranes can not withstand the solvent methanol. Since the methanol is only required for the activation of the catalyst these experiments can be compared.

It was shown that the best enhancement factors for all peaks of pyridine can be achieved at a field strength of 70 Gauss. Any other field strength in the range from 20 Gauss to 150 Gauss leads to smaller enhancements. The meta peak of hyperpolarized pyridine even changes its phase orientation leading to a positive signal at 20 Gauss. The method SABRE is therefore not restricted to the production of negative (antiphase) signal intensities. Under certain conditions positive hyperpolarization (in phase with thermal polarization) can be produced.

5.4.2 Field dependency with pure water

As already introduced before it is possible to generate SABRE hyperpolarization without additional methanol. The field dependency of the enhancement was investigated (see figure 5.4 on the facing page). While the best enhancement is still achieved at 70 Gauss the different positions in pyridine are now hyperpolarized with different efficiencies.

The meta peak of pyridine reaches the highest enhancement factor of -150 ± 10, while the ortho peak only reaches -127 ± 10 and the para peak -131 ± 10. This is reverse to the experiments with methanol included.

Discussion

Pyridine in pure water can be hyperpolarized best at a field strength of 70 Gauss. Even though no methanol was added the enhancement factors still reach up to -150 ± 10 for the meta peak. Omitting of methanol does not change the shape of the field dependency drastically in comparison to experiments with 20% or even 100% methanol.

It is advantageous that the optimal field strength lies at 70 Gauss because such a field strength can be realized by an electro magnet or in the stray of field of most MRI machines. For later applications no complicated devices must be build in order to realize this field strength.

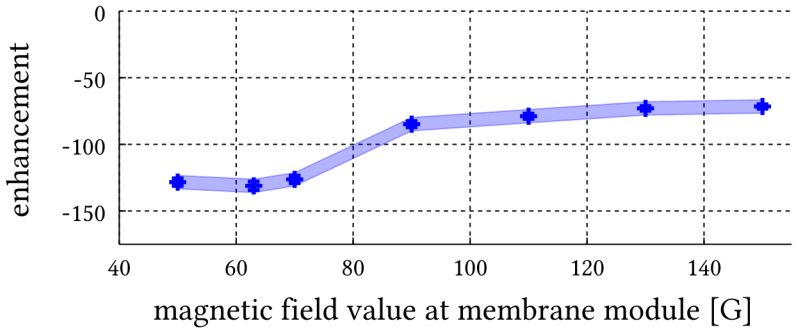

(a) ortho

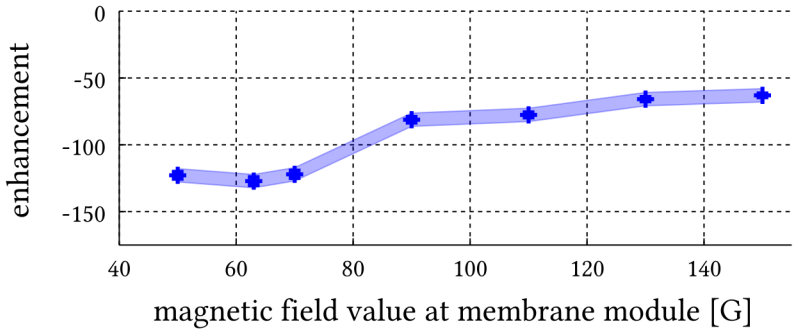

(b) para

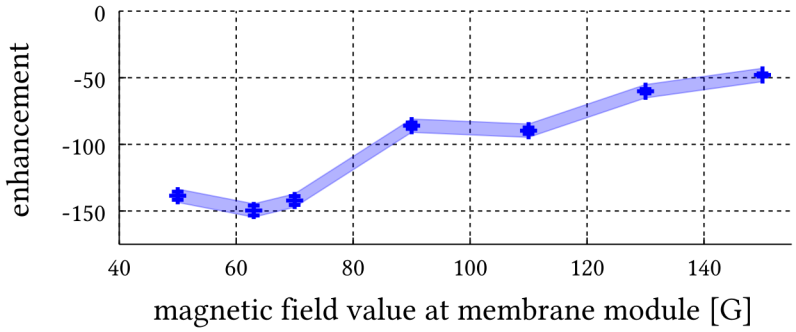

(c) meta

Figure 5.4: Field dependency of the enhancement factor when no methanol is present in the experiment.

5.5 Imaging Expriments

This flow setup allows for MRI experiments with high flip angles because fresh hyperpolarized fluid is always transported into the detection chamber. Therefore a gradient echo sequence with a flip angle of 90° and a repetition time of TR = 1 s was chosen. The chosen TR results in 60 acquisition per minute instead of 6 as for the prior spectroscopy experiments. Experiments showed that this does not lead to a loss in signal, because the

exchange of the fluid in the detection chamber is still fast enough.

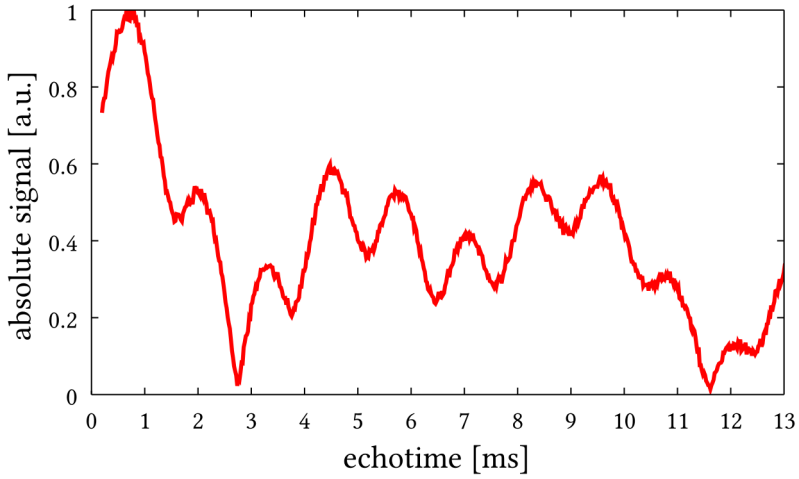

Figure 5.5: Presented MRI experiments were performed with a different sample composition, containing less water than the other experiments. The hyperpolarized pyridine is in antiphase to the hydrogen peak and there fore the signal shows a rise directly at the beginning. Due to the different chemical shifts involved large oscillations can be observed in the absolute transversal magnetization.

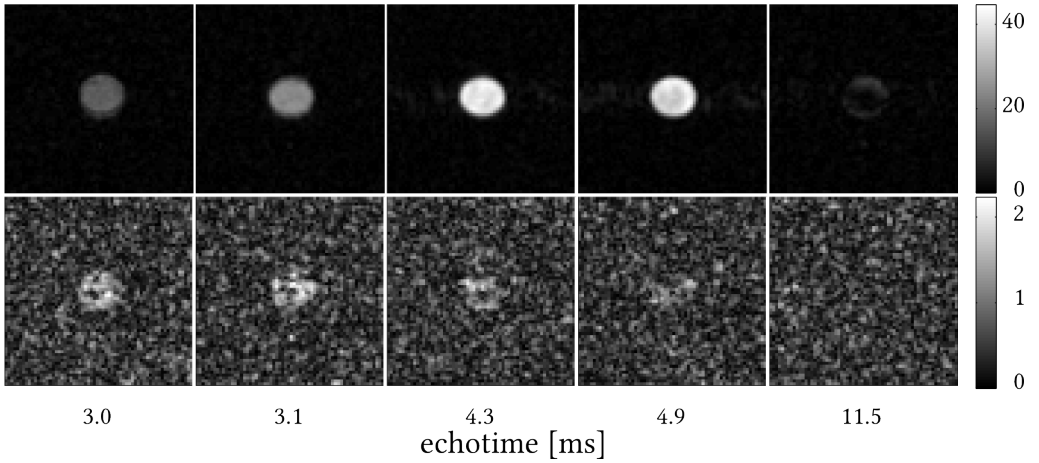

Figure 5.6: MR Images of hyperpolarized pyridine and hydrogen (see 5.5 for spectral information). A transversal projection is presented showing the round detection chamber with the fluid flowing though the plane. Imaging was performed using a gradient echo sequence, flip angle: 90°, repetition time: 1 s, echo time: variable, bandwidth: 1040 $^{\text{Hz}}/_{\text{pixel}}$, matrix size: 128×64 (presented: 64×64), phase encoding: left-right, resolution: 0.67 $^{\text{mm}}/_{\text{pixel}}$.

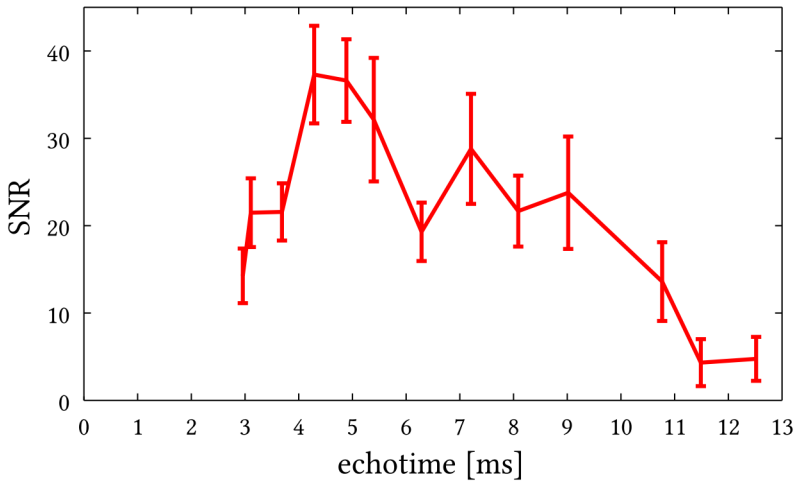

Figure 5.7: SNR of images at echo times from 2.9 till 12.5 ms and transversal magnetization of the FID.

The minimal echo time of 3.0 ms resulted in an image with 14 ± 3 SNR (see figures 5.6 to 5.7 on pages 78–79). The SNR follow the shape of the FID up to 21 ± 3 SNR for echo times of 3.2 and 3.7 ms and reaches a maximal SNR values of 37 ± 5 SNR at a echo time of 4.3 ms. With further increasing echo time the SNR does not follow the FID exactly any more and the error increases. The last image acquired shows an SNR of 5 ± 4 at a echo time of 11.5 ms.

Discussion

It is possible to acquire hyperpolarized images of pyridine with satisfactory SNR, even when only 10 $^{\text{mmol}}/_{\text{l}}$ of pyridine is present. Additionally a flip angle of 90° can be used to acquire the hyperpolarized signal. The shape of the FID is reproduced for the first five images, later the large errors prohibit an exact evaluation. However, the SNR falls down till the expected minimum at 11.5 ms.

The images how small distortions in phase encoding direction that arise due to the pulsative pulse generated by the membrane pump in combination with the decreased TR. This leads to small fluctionations in the available hyperpolarization within the detection chamber.

5.6 Reproducibility over time

All data presented before were acquired in one single long term experimental setup (see figure 5.8 on the next page). In this plot all spectroscopy experiments are shown in chronological order. Six spectra per minute were acquired.

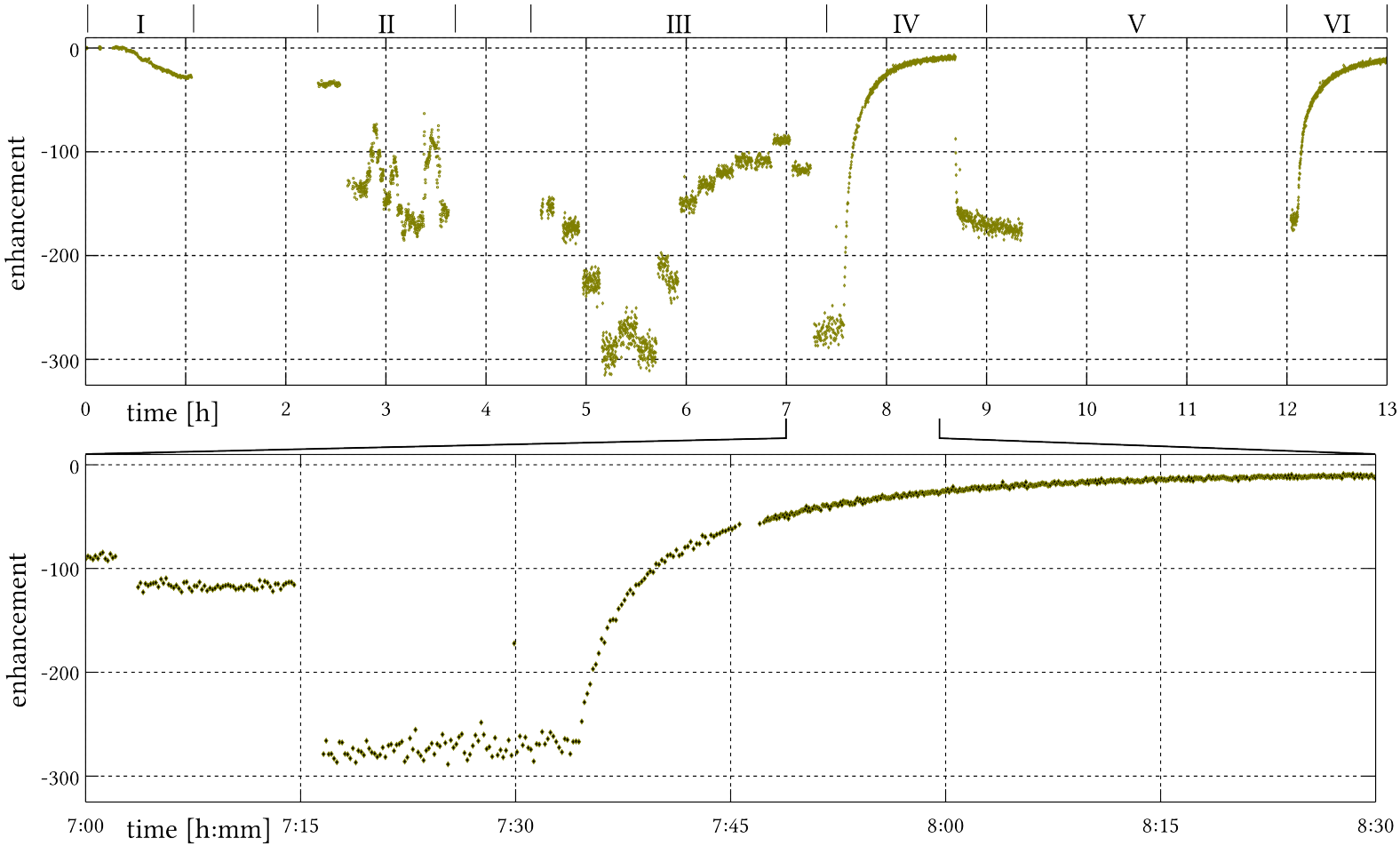

Figure 5.8: Enhancement per proton for the ortho peak of SABRE hyperpolarized pyridine (figure). The hyperpolarization was present over 12 hours (see text for explanation of different experiments in the sectors I-VI). Experiments in sector IV are shown in more detail below.

Starting from the initial switch on of parahydrogen the plot shows the enhancement during preparation of the experiment (sector I + II). This included a readjustment of the receiver gain and some optimization of vector size and bandwidth of the spectroscopy sequence. Enhancement factors in these areas (and only there) do not corresponding to the real enhancement factors because the thermal reference was acquired later with different parameters.

In sector III the module was placed at different magnetic fields and the corresponding enhancement factors can be seen here as a plot over time (3 hours). These results were presented before with the corresponding field strength (see figure 5.3 on page 75).

After these experiments the parahydrogen supply was turned off (sector IV) leading to a decay of enhancement until all parahydrogen inside the system (including parahydrogen in the reservoir) was converted.

After restoring the parahydrogen supply (sector V) the enhancement does not reach 300 again although the module was placed at the optimal field strength of 70 Gauss. The reason was a leakage of pyridine through the membrane fibers, that occurred during the experiments in sector IV. Due to the decreased pressure in the gas phase the liquid was pressed out in the gas phase. The MRI experiments were also performed in sector V. After theses experiments the performance of the hyperpolarization was checked again in sector VI, showing the same enhancement factors as in the beginning of sector V.

Discussion

In the first 4 hours (section I and II) different initial experiments were performed such as changing the pumping speed, receiver gain, fixing connections tubes, checking for pressure tightness. Additionally the connections were moved within the stray field to ensure that the spin order transfer occurs only in the membrane module. This resulted in an optimized experimental setup that remained unchanged until the end of the experiment.

The experiments in section III show the time domain results of figure 5.3 on page 75. However, there were more field strengths tested than shown in in the plot 5.3. Magnetic fields over 150 Gauss were not presented, because the stray field of the magnet was too inhomogeneous.

Shutdown of the parahydrogen supply does not end of the hyperpolarization immediately (sector IV). There is still parahydrogen left in the fluid, the gas space of the membrane module and most importantly for this slow decay: the remaining parahydrogen inside the reservoir. Parahydrogen inside the fluid is converted to orthohydrogen very quickly. The parahydrogen in the gas space of the membrane module can diffuse through the high surface of the hollow membrane fibers quickly. In contrast to that the parahydrogen in the big reservoir has only a one small gas/liquid interface and therefore diffusion is very slow leading to a long lasting decay of hyperpolarization. As soon as

the supply with parahydrogen is restored the signal rises very quickly again. However, the hyperpolarization does not recover to the previous enhancement factors. This effect could be traced back to a loss of pyridine while the the parahydrogen supply was turned off. During this time the pressure in the gas space of the module was lower than the pressure inside the liquid system. This lead to a leakage of pyridine into the fume hood and less pyridine was available for the hyperpolarization.

The MRI experiments were performed in sector V. The achieved enhancements were the same at the beginning as in the end, thus the MRI experiments were performed with constant enhancement factors. During the $2\frac{1}{2}$ hours of the experiments 15 minutes were used to acquire proton images. The remaining time was used to attempt ^{13}C MRI and spectroscopy by placing the module inside a mu-metal shield. This turned out to be unsuccessful even though transfer of the polarization onto the hetero nuclei has been reported[44]. The low natural abundance of ^{13}C as well as decreased signal intensity due to flow were most likely responsible for this failure.

5.7 Summary

In this chapter the efficiency and performance of the SABRE method using membrane modules was investigated. The sample composed of pyridine, methanol, catalyst and deuterated water showed higher enhancement factors than the sample without methanol. The optimal reaction field strength is 70 Gauss for both sample compositions as also reported in the literature.[42] Imaging experiments can be performed and result in good quality images of the detection chamber.

The most important feature of the section is the achieved continuous hyperpolarization. The experiment was stopped after 12 hours of experiments with hyperpolarized fluid.

5.8 Conclusion

The use of membrane modules can improve the SABRE method to supply a continuous stream of hyperpolarized fluid over at least 12 hours. This experimental setup can provide a hyperpolarization as long as enough parahydrogen is supplied and no leakage though the hollow fiber membranes was detected. Additionally a higher enhancement that in shaking experiments was achieved.

This almost instantaneously available hyperpolarization can be exploited in many ways. For instance, high flip angles such as 90° are possible and the signal will stay constant. Typically when dealing with a hyperpolarized sample, one has to use small flip angles to preserve longitudinal magnetization for later experiments, but here freshly

hyperpolarized fluid is constantly delivered. This allows for MRI imaging or 2D spectroscopy with high SNR and resolution.

Furthermore, hyperpolarized pyridine can be generated without using methanol. The process loses efficiency, but the gain compared to the thermal polarization is still huge. Therefore using SABRE for *in vivo* application becomes more feasible.

Another advantage of the instant available hyperpolarization is that relaxation due to T_1 is less critical. Of course the fluid has still to be transported to the place of detection, and this should happen as fast as possible. But in the setup used here the substrate is held in a hyperpolarized state as long as it is in the module and relaxation becomes only relevant when the fluid leaves the module. If small connection tubes are used the transportation time is negligible and the hyperpolarization is only decreased by a very small amount during the transport.

Especially for the SABRE method the use of the hollow fiber membranes shows significant advantages over other hyperpolarization methods that work in a batch mode. For example with DNP allows for a continuous generation of hyperpolarization, but the necessity of a small microwave cavity reduces the available amount of hyperpolarized substance[45].

SABRE also offers the possibility to hyperpolarize a new class of molecules. Possibly molecules relevant for medical or biological processes can be hyperpolarized with SABRE and with the results in this chapter efficient ways of exploiting this hyperpolarization are presented.

The use of the membrane module is not restricted to a closed circular system. A linear system with a reservoir and a membrane module could also be realized. At the outlet of the membrane module the hyperpolarized molecules could be siphoned off. With hydrogenative PHIP such a system is possible too, but it can not be kept easily in a stand-by mode. With SABRE the outlet can be closed without loosing substrate where as hydrogenative PHIP will consume its substrate.

This linear system mode allows for investigations where the hyperpolarized fluid ca not be retained. An example for such an application are perfusion experiments. Again all advantages apply: The decay due to T_1 is the simple transportation time but high flip angles can be used.

Chapter 6

Discussion

To put this thesis in a more general framework, it is worth to compare the achievements of other hyperpolarization techniques. DNP, hyperpolarized gases and hetero nuclei PHIP methods have contributed very interesting concepts to MRI. For instance, DNP and hetero nuclei PHIP methods allow for molecular imaging of specific hyperpolarized molecules. Hyperpolarized gases are more used to image the gas space in e.g. the lung and offer them self no specific targeting on biomolecules.[46]

The hyperpolarization enhanced measurement of nuclei (DNP and PHIP) has been preferred for a variety of different applications like *in vivo* ph mapping[7] or real-time metabolic imaging[10]. These methods achieve the best contrast because they use different nucleus for imaging (see figure 1.2 on page 3). In this thesis a method was presented which achieves comparable imaging contrast on the basis of proton measurements by using the different time evolution of thermally polarized molecules compared to hyperpolarized background. The exact imaging parameters for the contrast mechanism have to be calculated for each molecule individually. Since the basic idea relies on the ^{1}H - J coupling of a double or single bond, most molecules can be used, but this has to be checked individually.

The proton has the largest gyromagnetic ratio γ is highest compared to all other nuclei, and therefore offers optimal signal detection, that is proportional to $\gamma^{\frac{3}{2}}$ for hyperpolarized nuclei. Also, lower magnetic field gradients are required due to the high gyromagnetic ration of the proton. In the case of ^{13}C a four times stronger gradient field has to be used for the same resolution. Only if this is possible regarding the limits of the gradient system, the same resolution can be achieved with ^{13}C measurements.

Another important influence on the signal is the natural abundance of NMR-active nuclei. E.g. the amount of NMR-active ^{13}C is only 1.1% of all carbon isotopes. In order to overcome this, expensive and complicated labelling techniqeus can be used for the target molecule. On the other hand, the thermally polarized background signal gets suppressed,

allowing for very good contrast on the hetero nuclei. Whereas the large thermally polarized background of protons contributes sigificantly to the signal of the proposed method.

Proton magnetic resonance imaging is the standard application of clinical MRI machines. If a different nucleus is of interest, special coils that can observe both types of nuclei have to be purchased or built. Especially in medical imaging large coils are needed and they are difficult to design. With the proton hyperpolarization presented in this thesis the whole variety of vendor proton coils are available. Also, this reduces the initial costs for performing such experiments.

Parahydrogen Induced Polarization (PHIP) is based on a chemical reaction, where the spin order of parahydrogen is exploited directly thus allowing for high enhancement factors. Large amounts of hyperpolarized molecules can be produced within a short time, depending only on the amount of catalyst and dissolved molecule in the solvent - the hyperpolarization can be generated inside the hollow fiber membranes. In DNP for comparison, a small amount of sample can be hyperpolarized in a microwave resonator.[13,45] However, this can be compensated by flow systems, where a continuous stream of hyperpolarized molecules is supplied, but still the amounts are more restricted as for PHIP ($1.8\,\mathrm{ml/min}$[47] vs. $50\,\mathrm{ml/min}$).

The hyperpolarization is available instantaneously after the chemical reaction. The limit is basically only the speed of the reaction, which can be controlled by the temperature and pressure. Hovener et al.[41] have implemented up to $10\,\mathrm{bar}$ at a temperature of $150°$ Celcius and achieved for very good hydrogenation. The setup that is presented in this thesis is not able to provide such conditions, but has the advantage of fewer technical requirements. In contrast, DNP require a build up time of the hyperpolarization typically on a timescale of $5 \cdot \mathrm{T}_1$.[13]

High enhancement factors can be reached, because the spin order of parahydrogen is exploited directly. The theoretical limit of hydrogenative PHIP ranges up to 10^5[17], whereas the theoretical enhancement limit of liquid state DNP is given by the fraction of the electron and the target nucleus gyromagnetic ratio, e.g. $\frac{\gamma_e}{\gamma_H} \approx 660$.[13] Solid state DNP, however, offers much higher enhancements of up to 10^5 and is not restricted to protons, but is more demanding on the technical side.[13]

Limits of the method

The limited lifetime of the hyperpolarized stage is a general problem of hyperpolarization techniques, and the proton shows typically rapid relaxation rates. In this thesis a flow setup was designed that allows for high flow rates and a short delivery time of about $40\,\mathrm{ms}$. For DNP, where similar problems arise due to the limited lifetime, sophisticated shuttle systems[48] and flow setups[45,47] have been developed. Compared to the T_1 relax-

ation time, the transport time of 115 ms[48] is small too - but the target nuclei is usually ^{13}C. In this case, the ratio of lost hyperpolarization is smaller due to the longer relaxation times on this nucleus.

One way to overcome the short relaxation times of the proton was proposed by Carravetta and Levitt[24],where a singlet state can be formed originating from the spin order of parahydrogen. Due to external interaction the hyperpolarization is accessible and the lifetime can be increased to minutes rather than seconds.[25] However, this requires a restriction onto a symmetric molecule and has therefore a smaller field of application.

Nevertheless, the inherent short T_1 of protons might still be too short for *in vivo* application. This time limit will set upper boundaries for resolution and signal. Even though the proposed circular flow setup can provide large amounts of hyperpolarized molecule, the deliverable amount of molecule is limited for *in vivo* experiments. The advantage of the continuous delivery might not be exploitable and under these conditions the ^{1}H hyperpolarization will remain concealed within the thermally polarized background. In contrast, a image acquired with hyperpolarization on a hetero nuclei such as ^{13}C or ^{15}N does not have the problem of background separation. The necessary image for co-registration is acquired on the proton channel.

The draw back of limited choice for molecules is the most important hindrance for future applications of the findings within this thesis:

In this thesis three kinds of molecules were hyperpolarized: 1-hexene and the water solvable 2-hydroxyethylpropionate as sample compounds for the hPHIP and pyridine as sample compound for the SABRE method. All these molecules can not be used for *in vivo* applications because of their toxicity, but they served here as a proof of principle for the development of new PHIP hyperpolarization imaging strategies.

However, there are already interesting molecules for *in vivo* applications such as barbituric acid derivatives[49] but many more molecules are needed for specific applications. In contrast, DNP can hyperpolarize a wider variety of molecules. Additionally, radicals can be used universally for the hyperpolarization of different molecules.

Furthermore, for *in vivo* application of PHIP the catalyst has to be removed because of their toxicity and for safety reasons. Again, this problem can only be solved from the chemical side and similar problems arise for DNP. It is possible to attach the catalyst (or radicals) onto a matrix but when they are attached the performance of the processes reduce.[47]

The concentrations needed in this thesis to generate a contrast ($1.5\,^{\mathrm{mmol}}/_{\mathrm{kg}}$) are within the same range as e.g. for PHIP-13C imaging of Mansson et al.[6] ($0.3\,^{\mathrm{mmol}}/_{\mathrm{kg}}$). An additional reduction of the concentration presented in this work is possible, the resulting lower contrast and can be compensated by the subtraction image method.

Applications

In the current form, the application of proton hyperpolarization under continuous conditions can be used for basic investigation of the features of the hyperpolarization. In this thesis, for example, it was used to reproduce the magnetic field dependency of the SABRE process first reported by Cowley et al.[42].

The intend of the work was to investigate if proton PHIP hyperpolarization can be exploited in medical imaging. A first step was taken within this thesis and imaging strategies were presented using model molecules. When thinking towards application, the remaining hydrogen can be removed by the use of another hollow fiber membrane for degassing of the fluid. This degassing module can also act as a temperature control, in case a hydrogenation reaction was performed at high temperatures. After these steps a *in vivo* tests should be performed to assess the effect of T_1 relaxation.

This - more physical work - has to be completed in the future by the work of chemists: The final delivery of the hyperpolarized and non-toxic molecule should only contain water as solvent and not the catalyst.

Assuming that this can be realized, then this method has to prove it self compared to most recent applications of the more mature low temperature DNP. Here the applications have already reached a level where *in vivo* application in animals is done regularly[50–52] and large amounts of molecule can be hyperpolarized for the use in big animals such as pigs[53]. Even apparatus that can reliably remove the radical have been developed.[54] The DNP community is stronly pushing forward for *in vivo* application in humans.

Especially in the light of the short T_1 proton hyperpolarization will have a difficulties to monitor metabolic processes. After a injection the hyperpolarized will be transported in the blood stream and can reach a desired destination - including transportation processes into cells - after seconds.

Yet, proton hyperpolarization can take grip for application because it can offer higher resolution and the existing standard equipment of a clinical MRI scanner can be used. Further, DNP offers best enhancement when freezing the molecule down to several Kelvin, where hydrogenative PHIP performs best when heating the molecule ($50° - 100°$ Celsius). This difference can allow for hyperpolarization of different molecules. The SABRE process was performed at room temperature, that would allow even for experiments with temperature sensitive molecules. Additionally this hyperpolarization is available immediately and no build up time is required.

In summary, the PHIP technique for MRI with medical purpose is a promising technique with some advantages and disadvantages when compared to more mature techniques as DNP or hyperpolarized gases. The results presented in this thesis intend to prove it as a strong candidate in these areas.

Chapter 7

Summary and Outlook

Along this thesis, the question

> ”Is it possible to perform proton MR-imaging experiments with PHIP hyperpolarized contrast agents, where a clear separation of ^{1}H background and ^{1}H contrast agent is possible and the hyperpolarization is available continuously and ready for application?”

was tackled and encouraging results were obtained.

Several aspects were investigated, their detailed discussion can be found in the chapters ”Imaging of Antiphase Hyperpolarization” (chapter 3 on page 25), ”Continuous Hyperpolarization with hPHIP” (chapter 4 on page 57) and ”Continuous Hyperpolarization with SABRE” (chapter 5 on page 69).

Briefly, in chapter 3 molecules are hyperpolarized by a hydration reaction and can be used as a contrast agent. High contrast was achieved even though the ^{1}H background signal is enormous. The second finding serves to overcome one of the major problems when working with hyperpolarized signals, the short T_1 relaxation times. In this thesis the possibility to achieve continuous hyperpolarization was shown for the hyperpolarization mechanisms hPHIP (chapter 4) and SABRE (chapter 5).

Two basic MR-imaging sequences that are commonly used in MRI, namely the gradient echo and the spin echo sequence, can be used for rendering a contrast between a proton hyperpolarized molecule and a thermally polarized background by a simple variation of the echo time. A contrast can be established by either pure signal strength, or, more reliably, by a subtraction image. In order to find optimal echo times, several factors, such as the J coupling, the chemical shift and relaxation times, have to be considered.

Continuous generation of hyperpolarization and fast delivery is a very important step towards the application, because of the short proton relaxation times. This problem was tackled by the use of hollow fiber membranes that allow a very efficient delivery of

parahydrogen - the driver for the hyperpolarization. This method can be used for both PHIP methods: hydrogenative PHIP and SABRE.

The enhancement per proton could be significantly increased for SABRE experiments: With shaking experiments a maximal enhancement of 136 could be achieved, whereas enhancement factors as large as 300 were achieved by using hollow fiber membranes. The hydrogenative PHIP experiments allowed for a enhancement up to 4000.

Outlook

The work presented here was focused on the methodology of PHIP-MRI, because only very few substrate/catalyst combinations would be suitable for *in vivo* experiments. Therefore, these achievements shall draw attention to the advantages of this method. In this light, the remaining weakness of lacking biological compatibility can hopefully be overcome.

When thinking of an application for *in vivo* experiments, the security question has to be dealt with in more detail. Especially, the flow setup relies on an skilled experimentator in order to allow for safe experiments.

The hollow membrane fiber experiment was designed to be a circular flow setup. For later applications this setup should be changed to a linear setup where substrate or precursor get pumped from a reservoir through the hollow membrane fiber directly into an animal, for example. For the application of hydrogenative PHIP the fluid has to be cooled prior to administration and, in all cases, hydrogen has to be removed from the liquid phase. This can be achieved by the use of another membrane module for degassing. Depending on the scope of the experiment, the toxic catalyst has to be removed, too.

Bibliography

[1] The Universal Label: Even thyme is just hydrogen and time. http://xkcd.com/1123/, 2012.

[2] The Nobel Prize in Physiology or Medicine 2003 was awarded jointly to Paul C. Lauterbur and Sir Peter Mansfield for their discoveries concerning magnetic resonance imaging. http://www.nobelprize.org/nobel_prizes/medicine/laureates/2003/, 2009.

[3] Web Source. Mrt einer hirnmetatase eines bronchialkarzinoms (t1 nach kontrastmittelgabe). http://en.wikipedia.org/wiki/File:Hirnmetastase_MRT-T1_KM.jpg, 2008.

[4] Web Source. http://www.mr-ct-frankfurt.de/images/gelenkekniecols2.jpg, 2011.

[5] Web Source. http://www.ordination-gruenberger.at/images/metastasen_zyste_mrt.jpg, 2011.

[6] S. Mansson, E. Johansson, P. Magnusson, C. M. Chai, G. Hansson, J. S. Petersson, F. Stahlberg, and K. Golman. C-13 imaging - a new diagnostic platform. *European Radiology*, 16(1):57–67, 2006. DOI 10.1007/s00330-005-2806-x.

[7] F. A. Gallagher, M. I. Kettunen, S. E. Day, D. E. Hu, J. H. Ardenkjaer-Larsen, R. in't Zandt, P. R. Jensen, M. Karlsson, K. Golman, M. H. Lerche, and K. M. Brindle. Magnetic resonance imaging of ph in vivo using hyperpolarized c-13-labelled bicarbonate. *Nature*, 453(7197):940–943, 2008. DOI 10.1038/Nature07017.

[8] U. Bommerich, T. Trantzschel, S. Mulla-Osman, G. Buntkowsky, J. Bargon, and J. Bernarding. Hyperpolarized 19f-mri: parahydrogen-induced polarization and field variation enable 19f-mri at low spin density. *Physical Chemistry Chemical Physics*, 12(35):10309–10312, 2010.

[9] C. Cudalbu, F. Kurdzesau, R.B. van Heeswijk, K. Uffmann, S. Jannin, V. Denisov, D. Kirik, and R. Gruetter. Feasibility of in vivo15n mrs detection of hyperpolarized 15n labeled choline in rats. *Physical Chemistry Chemical Physics*, 12(22):5818–5823, 2010.

[10] K. Golman, R. in't Zandt, and M. Thaning. Real-time metabolic imaging. *Proceedings of the National Academy of Sciences of the United States of America*, 103(30):11270–11275, 2006. DOI DOI 10.1073/pnas.0601319103.

[11] E. Y. Chekmenev, J. Hovener, V. A. Norton, K. Harris, L. S. Batchelder, P. Bhattacharya, B. D. Ross, and D. P. Weitekamp. Pasadena hyperpolarization of succinic acid for mri and nmr spectroscopy. *Journal of the American Chemical Society*, 130 (13):4212, 2008. DOI Doi 10.1021/Ja7101218.

[12] D. M. Wilson, K. R. Keshari, P. E. Z. Larson, A. P. Chen, S. Hu, M. Van Criekinge, R. Bok, S. J. Nelson, J. M. Macdonald, D. B. Vigneron, and J. Kurhanewicz. Multi-compound polarization by dnp allows simultaneous assessment of multiple enzymatic activities in vivo. *Journal of Magnetic Resonance*, 205(1):141–147, 2010. DOI DOI 10.1016/j.jmr.2010.04.012.

[13] A. Abragam and M. Goldman. Principles of dynamic nuclear-polarization. *Reports on Progress in Physics*, 41(3):395–467, 1978.

[14] J. H. Ardenkjaer-Larsen, B. Fridlund, A. Gram, G. Hansson, L. Hansson, M. H. Lerche, R. Servin, M. Thaning, and K. Golman. Increase in signal-to-noise ratio of > 10,000 times in liquid-state nmr. *Proceedings of the National Academy of Sciences of the United States of America*, 100(18):10158–63, 2003. DOI 10.1073/pnas.1733835100.

[15] C. R. Bowers and D. P. Weitekamp. Para-hydrogen and synthesis allow dramatically enhanced nuclear alignment. *Journal of the American Chemical Society*, 109(18): 5541–5542, 1987.

[16] M. G. Pravica and D. P. Weitekamp. Net nmr alignment by adiabatic transport of para-hydrogen addition-products to high magnetic-field. *Chemical Physics Letters*, 145(4):255–258, 1988.

[17] J. Natterer and J. Bargon. Parahydrogen induced polarization. *Progress in Nuclear Magnetic Resonance Spectroscopy*, 31:293–315, 1997. DOI 10.1016/S0079-6565(97)00007-1.

[18] K. Münnemann and H.W. Spiess. Nuclear magnetic resonance: The art of signal enhancement. *Nature Physics*, 7(7):522–523, 2011. DOI 10.1038/nphys2004.

[19] L. S. Bouchard, K. V. Kovtunov, S. R. Burt, M. S. Anwar, I. V. Koptyug, R. Z. Sagdeev, and A. Pines. Para-hydrogen-enhanced hyperpolarized gas-phase magnetic resonance imaging. *Angewandte Chemie. International Ed. In English*, 46(22):4064–8, 2007. DOI 10.1002/anie.200700830.

[20] L. S. Bouchard, S. R. Burt, M. S. Anwar, K. V. Kovtunov, I. V. Koptyug, and A. Pines. Nmr imaging of catalytic hydrogenation in microreactors with the use of para-hydrogen. *Science*, 319(5862):442–445, 2008. DOI 10.1126/science.1151787.

[21] R. W. Adams, J. A. Aguilar, K. D. Atkinson, M. J. Cowley, P. I. P. Elliott, S. B. Duckett, G. G. R. Green, I. G. Khazal, J. Lopez-Serrano, and D. C. Williamson. Reversible interactions with para-hydrogen enhance nmr sensitivity by polarization transfer. *Science*, 323(5922):1708–1711, 2009. DOI 10.1126/science.1168877.

[22] Meike Roth, Petra Kindervater, Hans-Peter Raich, Joachim Bargon, Hans W. Spiess, and Kerstin Münnemann. Continuous 1h and 13c signal enhancement in nmr spectroscopy and mri using parahydrogen and hollow-fiber membranes. *Angewandte Chemie*, 122(45):8536–8540, 2010. DOI 10.1002/ange.201002725.

[23] K. Golman, R. i Zandt, M. Lerche, R. Pehrson, and J. H. Ardenkjaer-Larsen. Metabolic imaging by hyperpolarized 13c magnetic resonance imaging for in vivo tumor diagnosis. *Cancer Research*, 66(22):10855–10860, 2006. DOI 10.1158/0008-5472.can-06-2564.

[24] M. Carravetta and M. H. Levitt. Theory of long-lived nuclear spin states in solution nuclear magnetic resonance. i. singlet states in low magnetic field. *Journal of Chemical Physics*, 122(21):214505–14, 2005. DOI 10.1063/1.1893983.

[25] María Belén Franzoni, Lisandro Buljubasich, Hans W. Spiess, and Kerstin Münnemann. Long-lived 1h singlet spin states originating from para-hydrogen in cs-symmetric molecules stored for minutes in high magnetic fields. *Journal of the American Chemical Society*, 134(25):10393–10396, 2012. DOI 10.1021/ja304285s.

[26] M.A. Bernstein, K.F. King, and X.J. Zhou. *Handbook of MRI pulse sequences*. Elsevier Academic Press, 2005. ISBN 9780120928613.

[27] E.M. Haacke. *Magnetic resonance imaging: physical principles and sequence design*. J. Wiley and Sons, 1999. ISBN 9780471351283.

[28] Z.P. Liang and P.C. Lauterbur. *Principles of magnetic resonance imaging: a signal processing perspective*. IEEE Engineering in Medicine Biology, 2000. ISBN 9780780347236.

[29] M.T. Vlaardingerbroek and J.A. Boer. *Magnetic resonance imaging: theory and practice*. Springer, 2003. ISBN 9783540436812.

[30] P.T. Callaghan. *Principles of nuclear magnetic resonance microscopy*. Oxford University Press, 1993. ISBN 9780198539971.

[31] J.F. Dechent. *Magnetresonanztomographie mit hyperpolarisierten antiphasischen Protonensignalen*. PhD thesis, 2009.

[32] R. W. Adams, S. B. Duckett, R. A. Green, D. C. Williamson, and G. G. R. Green. A theoretical basis for spontaneous polarization transfer in non-hydrogenative parahydrogen-induced polarization. *Journal of Chemical Physics*, 131(19):–, 2009. DOI 10.1063/1.3254386.

[33] L. A. Stables, R. P. Kennan, A. W. Anderson, R. T. Constable, and J. C. Gore. Analysis of j coupling-induced fat suppression in diet imaging. *Journal of Magnetic Resonance*, 136(2):143–151, 1999. DOI 10.1006/jmre.1998.1628.

[34] Jan F. Dechent, Lisandro Buljubasich, Laura M. Schreiber, Hans W. Spiess, and Kerstin Munnemann. Proton magnetic resonance imaging with para-hydrogen induced polarization. *Physical Chemistry Chemical Physics*, 2012. DOI 10.1039/C2CP22822J.

[35] M. Roth. *Sensitivity enhancement in NMR by using Parahydrogen Induced Polarization.* PhD thesis, 2010.

[36] L. Zhao, R. Mulkern, C.H. Tseng, D. Williamson, S. Patz, R. Kraft, R.L. Walsworth, F.A. Jolesz, and M.S. Albert. Gradient-echo imaging considerations for hyperpolarized 129xe mr. *Journal of Magnetic Resonance-Series B*, 113(2):179–183, 1996. DOI 10.1006/jmrb.1996.0173.

[37] Klaus Scheffler. A pictorial description of steady-states in rapid magnetic resonance imaging. *Concepts in Magnetic Resonance*, 11(5):291–304, 1999. DOI 10.1002/(sici)1099-0534(1999)11:5<291::aid-cmr2>3.0.co;2-j.

[38] Mads Bak, Jimmy T. Rasmussen, and Niels Chr Nielsen. Simpson: A general simulation program for solid-state nmr spectroscopy. *Journal of Magnetic Resonance*, 147 (2):296–330, 2000. DOI 10.1006/jmre.2000.2179.

[39] Hale Ersoy and Frank J. Rybicki. Mr angiography of the lower extremities. *American Journal of Roentgenology*, 190(6):1675–1684, 2008. DOI 10.2214/ajr.07.2223.

[40] A. Newatia, G. Khatri, B. Friedman, and J. Hines. Subtraction imaging: applications for nonvascular abdominal mri. *American Journal of Roentgenology*, 188(4):1018, 2007. DOI 10.2214/AJR.05.2182.

[41] J. B. Hovener, E. Y. Chekmenev, K. C. Harris, W. H. Perman, L. W. Robertson, B. D. Ross, and P. Bhattacharya. Pasadena hyperpolarization of c-13 biomolecules: equipment design and installation. *Magnetic Resonance Materials in Physics Biology and Medicine*, 22(2):111–121, 2009. DOI 10.1007/s10334-008-0155-x.

[42] Michael J. Cowley, Ralph W. Adams, Kevin D. Atkinson, Martin C. R. Cockett, Simon B. Duckett, Gary G. R. Green, Joost A. B. Lohman, Rainer Kerssebaum, David Kilgour, and Ryan E. Mewis. Iridium n-heterocyclic carbene complexes as efficient catalysts for magnetization transfer frompara-hydrogen. *Journal of the American Chemical Society*, 133(16):6134–6137, 2011. DOI 10.1021/ja200299u.

[43] K.D. Atkinson, M.J. Cowley, P.I.P. Elliott, S.B. Duckett, G.G.R. Green, J. Lopez-Serrano, and A.C. Whitwood. Spontaneous transfer of parahydrogen derived spin order to pyridine at low magnetic field. *Journal of the American Chemical Society*, 131(37):13362–13368, 2009. DOI 10.1021/Ja903601p.

[44] Lyrelle S. Lloyd, Ralph W. Adams, Michael Bernstein, Steven Coombes, Simon B. Duckett, Gary G. R. Green, Richard J. Lewis, Ryan E. Mewis, and Christopher J. Sleigh. Utilization of sabre-derived hyperpolarization to detect low-concentration analytes via 1d and 2d nmr methods. *Journal of the American Chemical Society*, 2012. DOI 10.1021/ja3051052.

[45] Jan G. Krummenacker, Vasyl P. Denysenkov, Maxim Terekhov, Laura M. Schreiber, and Thomas F. Prisner. Dnp in mri: An in-bore approach at 1.5t. *Journal of Magnetic Resonance*, 215(0):94–99, 2012. DOI 10.1016/j.jmr.2011.12.015.

[46] J. M. Wild, J. Schmiedeskamp, M. N. J. Paley, F. Filbir, S. Fichele, L. Kasuboski, F. Knitz, N. Woodhouse, A. Swift, W. Heil, G. H. Mills, M. Wolf, P. D. Griffiths, E. Otten, and E. J. R. van Beek. Mr imaging of the lungs with hyperpolarized helium-3 gas transported by air. *Physics in Medicine and Biology*, 47(13):N185, 2002.

[47] S. Ebert, A. Amar, C. Bauer, M. Kolzer, P. Blumler, H. W. Spiess, D. Hinderberger, and K. Munnemann. A mobile dnp polarizer for continuous flow applications. *Applied Magnetic Resonance*, 43(1-2):195–206, 2012. DOI 10.1007/s00723-012-0344-7.

[48] M. Reese, D. Lennartz, T. Marquardsen, P. Höfer, A. Tavernier, P. Carl, T. Schippmann, M. Bennati, T. Carlomagno, F. Engelke, and C. Griesinger. Construction of a liquid-state nmr dnp shuttle spectrometer: First experimental results and evaluation of optimal performance characteristics. *Applied Magnetic Resonance*, 34(3-4): 301–311, 2008. DOI 10.1007/s00723-008-0131-7.

[49] Meike Roth, Joachim Bargon, Hans Wolfgang Spiess, and Achim Koch. Parahydrogen induced polarization of barbituric acid derivatives: 1h hyperpolarization studies. *Magnetic Resonance in Chemistry*, 46(8):713–717, 2008. DOI 10.1002/mrc.2234.

[50] S. J. Kohler, Y. Yen, J. Wolber, A. P. Chen, M. J. Albers, R. Bok, V. Zhang, J. Tropp, S. Nelson, D. B. Vigneron, J. Kurhanewicz, and R. E. Hurd. In vivo13carbon metabolic imaging at 3t with hyperpolarized13c-1-pyruvate. *Magnetic Resonance in Medicine*, 58(1):65–69, 2007. DOI 10.1002/mrm.21253.

[51] Albert P. Chen, John Kurhanewicz, Robert Bok, Duan Xu, David Joun, Vickie Zhang, Sarah J. Nelson, Ralph E. Hurd, and Daniel B. Vigneron. Feasibility of using hyperpolarized [1-13c]lactate as a substrate for in vivo metabolic 13c mrsi studies. *Magnetic Resonance Imaging*, 26(6):721–726, 2008. DOI 10.1016/j.mri.2008.01.002.

[52] S. J. Nelson, D. Vigneron, J. Kurhanewicz, A. Chen, R. Bok, and R. Hurd. Dnp-hyperpolarized c magnetic resonance metabolic imaging for cancer applications. *Appl Magn Reson*, 34(3-4):533–544, 2008. DOI 10.1007/s00723-008-0136-2.

[53] A. Flori, F. Frijia, V. Lionetti, J. H. Ardenkjaer-Larsen, V. Positano, G. Giovannetti, R. F. Schulte, F. Wiesinger, F. A. Recchia, L. Landini, M. F. Santarelli, M. Lombardi, and L. Menichetti. Dnp methods for cardiac metabolic imaging with hyperpolarized 1-c-13 pyruvate large dose injection in pigs. *Applied Magnetic Resonance*, 43(1-2): 299–310, 2012. DOI 10.1007/s00723-012-0350-9.

[54] J. H. Ardenkjaer-Larsen, A. M. Leach, N. Clarke, J. Urbahn, D. Anderson, and T. W. Skloss. Dynamic nuclear polarization polarizer for sterile use intent. *NMR in Biomedicine*, 24(8):927–932, 2011. DOI 10.1002/nbm.1682.

Appendix

7.1 Acknowledgments

Vielen, herzlichen Dank an alle Menschen, die durch Ihre Unterstützung einen Teil zu dieser Arbeit beigetragen haben! Insbesondere möchte ich mich bedanken bei:

7.2 Supplenentary Information

7.2.1 Preparation and Properties of Chemicals

Table 7.1: Composition of samples for hydrogenative PHIP. Chemicals are filled in a 10 mm NMR tube and sealed with a septum cap.

(a) 1-Hexyne

Chemical	Amount
1-Hexyne	500 mg
Rh(COD)(dppb)BF_4	10 mg
Acetone ($d6$)	2600 mg

(b) 2-hydroxyethylacrylate

Chemical	Amount
2-hydroxyethylacrylate	500 mg
Rh(nor)(ppbs)BF_4	10 mg
D_2O	2600 mg

Catalyst for 1-Hexyne

CAS: 79255-71-3, structure see figure 7.1 on the facing page.

Catalyst for 2-hydroxyethylacrylate

Structure see figure 7.1 on the next page.

1. Ligand: 3,3'-(1,4ButaneDiylbis(PhenylPhospineidene)Bis-Propane) Sulfonic Disodium Salt
2. Catalyst: Bis(norbornadiene)rhodium(I)tetrafluoroborate (CAS:36620-11-8)
3. Take 117 mg of Ligand and dissolve in 20 ml D_2O
4. Dissolve 50 mg Cat and dissolve in 10 mg d_6-acetone. Add via syringe.
5. Stir for 10 min .
6. Remove acetone with "Lösungsmittelrotationsverdampfer" then freeze drying.
7. Storage in glovebox (at least when filling the sample tube, or perform degassig).

Images of Catalysts

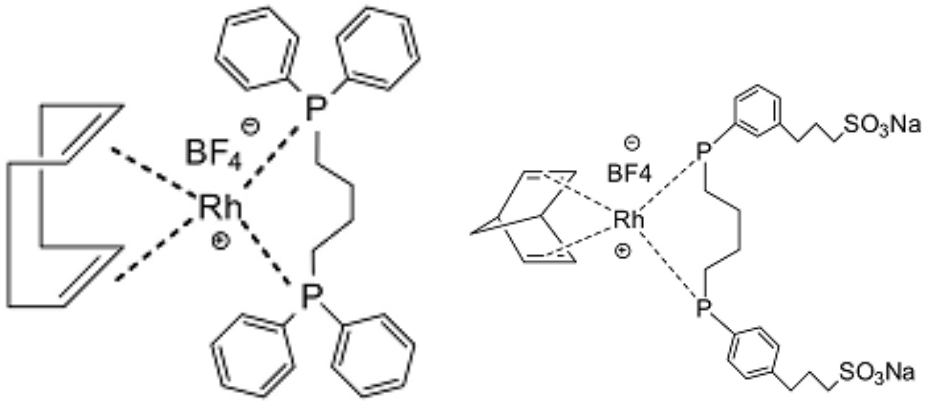

(a) $Rh(COD)(dppb)BF_4$ for hydrogenation of 1-Hexyne

(b) $Rh(nor)(ppbs)BF_4$ for hydrogenation of 2-hydroxyethylacrylate

Figure 7.1: Catalysts for substrates (see figure 3.2 on page 30).

7.2.2 High resolution spectras

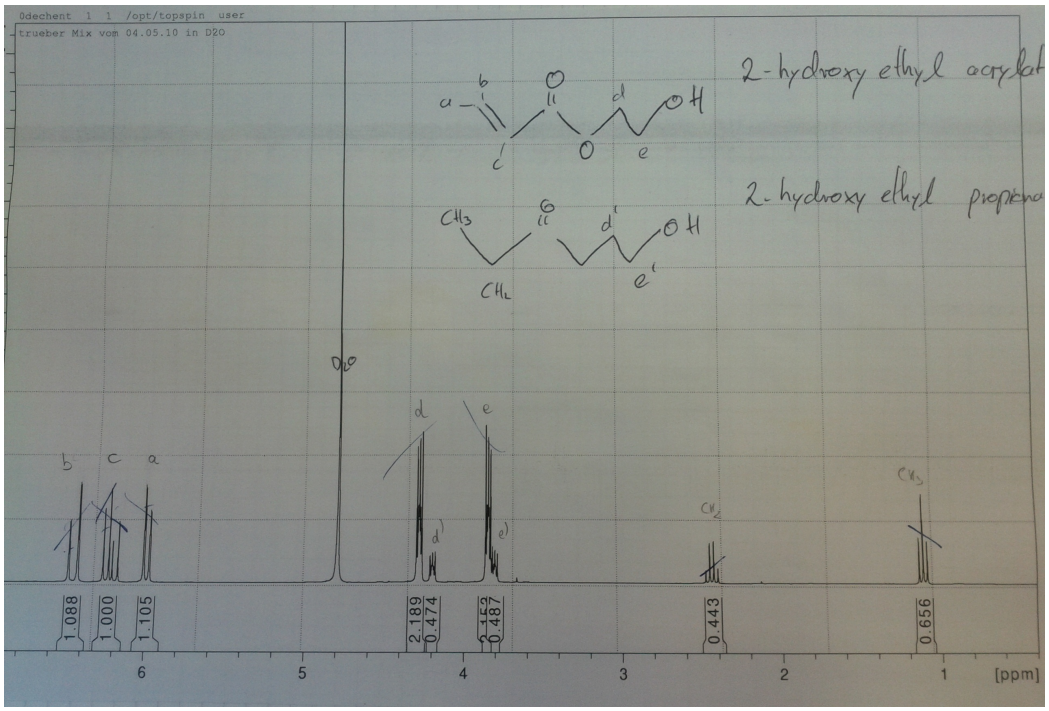

Figure 7.2: High resolution spectra of 2-hydroxyethylacrylate and 2-hydroxyethyl-propionate at 7 Tesla (for structure of molecule see 3.2 on page 30).

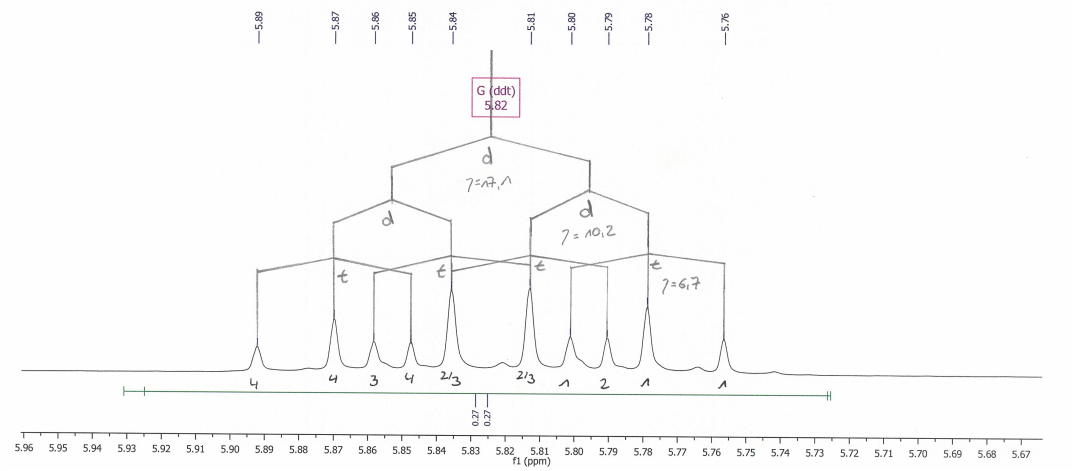

(a) PHIP proton H_c

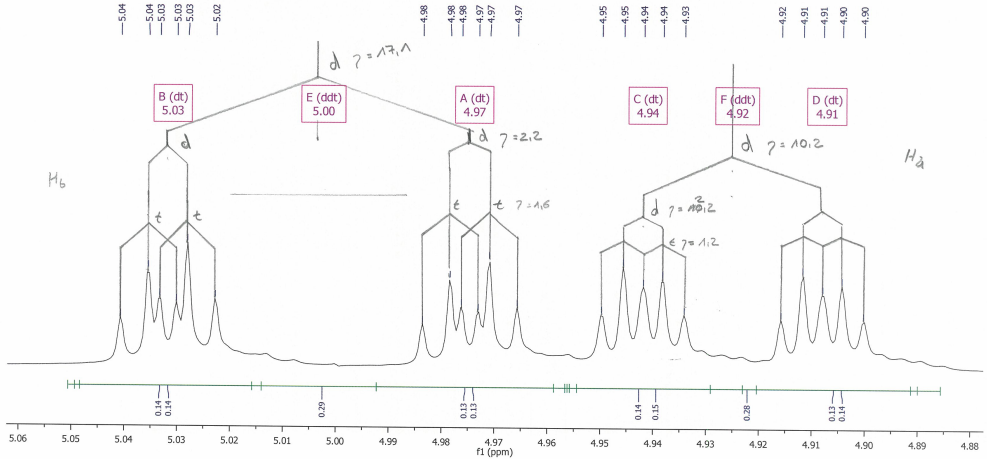

(b) PHIP proton H_b and strongly coupled H_a

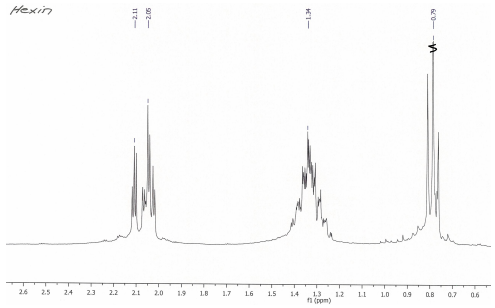

(c) remaining thermally polarized protons

Figure 7.3: High resolution spectra of 1-Hexene at 7 Tesla (for structure of molecule see 3.2 on page 30).

7.2.3 deTSE-Sequence

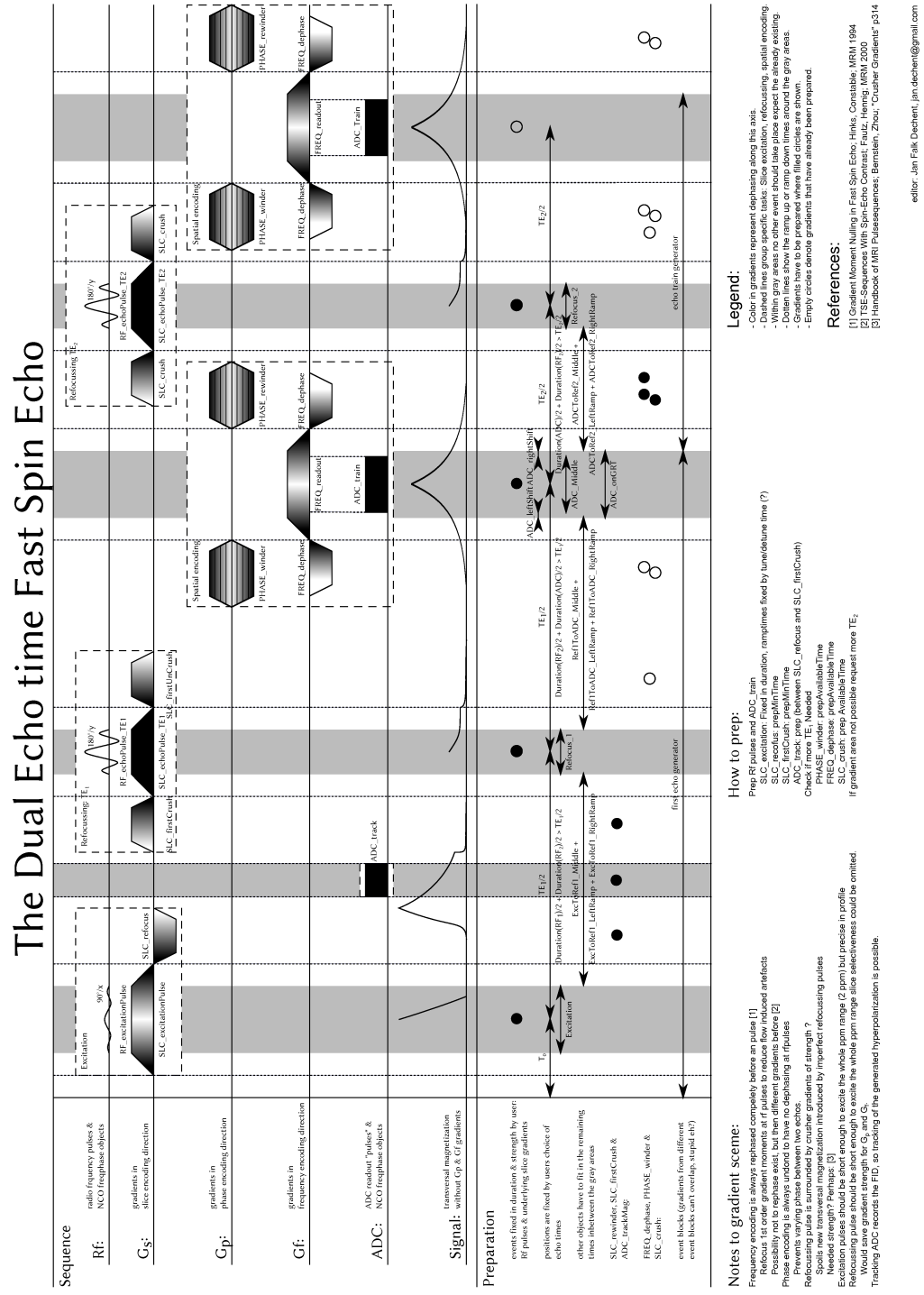

Figure 7.4: Sequence diagramm for deTSE as implemented for the experiments.

7.3 Declaration